ulm university universität ulm

Batf defines a differentiation checkpoint limiting hematopoietic stem cell self renewal in response to DNA damage

Vom Fachbereich der naturwissenschaftlichen Fakultät der

Universität Ulm zur Erlangung des Grades

Doktor der Naturwissenschaften

Dr. rer. nat.

genehmigte Dissertation

von

M.Sc. Genetics Jianwei Wang

geboren am 27.11.1979 in Tianjin, China

August 2011

Amtierender Dekan: Prof. Dr. Axel Groß

1. Gutachter: Prof. Dr. Karl Lenhard Rudolph

2. Gutachter: Prof. Dr. Michael Kühl

3. Gutachter: Prof. Dr. Christopher Baum

Tag der Promotion: 09-02-2012

Acknowledgements

I would like to express my reverence for my supervisor, Prof. Karl Lenhard Rudolph, his passion in science, his devotion to explore mechanism behind natural phenomenon, and his patience to nurture a novice, encourage me to finish my project.

I would like to thank all of the colleagues in our lab, their contribution and discussion accelerate my achievement.

I would like to thank my wife and son, their understanding and support excite me to pursue in science.

I would like to appreciate my parents for their nurturance.

Abstract

There is growing evidence that the accumulation of DNA damage and telomere dysfunction contributes to declines in stem cell function and tissue maintenance during aging and in response to chronic disease. Checkpoint responses that mediate the decline in stem cell function in response to DNA damage remain yet to be delineated. Here we conducted a functional genomic in vivo screen to identify genes impairing the function of hematopoietic stem cells in the context of chronic DNA damage induced by telomere dysfunction. Screening a shRNA library of 1000 cancer related genes revealed that shRNA mediated knock down of the transcription factor Batf was most potent to rescue the function of telomere dysfunctional stem cells. Specifically, Batf knockdown was 500fold enriched in telomere dysfunctional HSCs compared to wildtype HSCs when transplanted into lethally irradiated recipients. Our study shows that Batf is strongly upregulated in HSCs in response to telomere dysfunction or gamma-irradiation induced DNA damage and during mouse aging. Upregulation of Batf in HSCs in response to DNA damage was G-CSF/Stat3 dependent. shRNA-mediated knockdown of Batf rescued the repopulation capacity of telomere dysfunctional stem cells in transplanted recipients. This rescue in HSC function was associated with impaired induction of lymphocyte differentiation markers, cell cycle inhibitors (p53, p21, p16), and apoptosis in telomere dysfunctional or gamma-irradiated HSCs. Irradiation experiments revealed that lymphoid competent HSCs (CD150lowCD34-KSL) were most sensitive to DNA damage induced stem cell depletion, which was rescued by shRNA mediated knockdown of Batf. Together, this study provides the first experimental evidence that DNA damage leads to induction of a Batf-dependent differentiation checkpoint limiting the repopulation capacity of HSCs and the self-renewal of lymphoid

competent HSCs. It is conceivable that this molecular circuit contributes to the age-dependent skewing of HSC characterized by impairments in lymphopoiesis and increases myelopoiesis.

Zusammenfassung

Durch DNA-Schädigung aktivierte Kontrollmechanismen limitieren die Selbsterneuerung von Stammzellen und schützen so vor der Entstehung von Krebs, können aber gleichsam die Gewebealterung vorantreiben. Die molekularen Mechanismen, welche auf Stammzellebene durch DNA Schäden aktiviert werden, sind allerdings nur in Ansätzen charakterisiert. Hier haben wir in einem in vivo RNAi screen den Transkriptionsfaktor BATF (basic leucine zipper transcription factor, ATF-like) als einen wichtigen Faktor identifiziert, der die Selbsterneuerung von hämatopoetischen Stammzellen (HSZ) als Antwort auf Fehlfunktion von Telomeren und Bestrahlung limitiert. DNA Schäden induzieren BATF in Abhängigkeit von G-CSF und STAT3, was zu lymphoider Differenzierung von hämatopoetischen Stammzellen führt. Der Verlust von BATF verbessert die Funktion von HSZ sowie die Fähigkeit zur Selbsterneuerung nach Telomerverkürzung und Bestrahlung, führt aber gleichermaßen zu Akkumulation von DNA Schäden. Die Knochenmarkanalyse von Patienten mit Myelodysplastischem Syndrom legt den Schuss nahe, dass eine DNA-Schaden-abhängige Induktion von BATF auch in menschlichen HSZ konserviert ist. Zusammengefasst zeigen die vorgelegten Experimente, dass ein BATF-abhängiger Differenzierungs-Kontrollmechanismus existiert, welcher die Selbsterneuerung von HSZ als Antwort auf DNA Schäden limitiert.

Contents

1 Introduction

An age-dependent decline in stem cell function has been demonstrated in various tissues of model organisms including mammals and it is conceivable that this decline contributes to impairments in the maintenance of tissue homeostasis and function during aging (Rando 2006, Sharpless and DePinho 2007). Aging is also associated with alterations of the immune system including impairments in T- and B-lymphopoiesis and it has been hypothesized that these impairments contribute to immunosenescene in the elderly (Linton PJ et al., 2004). An altered differentiation capacity of hematopoietic stem cells (HSCs) has been causally linked to a reduction in lymphopoiesis during aging in mice and implied for in man (Sudo K et al., 2000; Warren LA et al., 2009; Geiger H et al., 2002; Geiger H et al., 2009). Whole genome expression analyses indicated that HSC intrinsic alterations in gene expression contribute to this phenotype (Rossi DJ et al., 2005; Chambers SM et al., 2007; Song Z et al., 2010). Novel studies recently revealed that the pool of HSCs comprises different HSC subpopulations that are biased towards myeloid or lymphoid differentiation (Dykstra B et al., 2007; Sieburg HB et al., 2006; Wilson A et al., 2008; Challen GA et al., 2010). There is emerging experimental evidence that upon aging myeloid biased HSCs are maintained, whereas lymphoid biased HSCs get lost (Cho RH et al., 2008; Roeder I et al., 2008). These findings provide a novel and interesting concept for the imbalance in myelo-lymphopoiesis occurring with aging. The molecular causes of this age-associated selection of HSC subpopulations remain to be delineated.

Accumulation of DNA damage has been associated with aging of HSCs in both mice and man (Rossi DJ et al., 2007; Rübe CE et al., 2011). In addition, there is experimental evidence that the accumulation of DNA damage can accelerate aging in DNA repair deficient mouse mutants modeling human progeria syndromes (Hoeijmakers 2009). Although still under debate, these findings suggest that DNA damage accumulation can contribute to human aging. In agreement with this hypothesis, an age-dependent accumulation of DNA damage is seen in various tissues including stem cell compartments, such as HSCs (Rossi et al. 2007, Rübe et al. 2011). Moreover, studies on telomerase knockout mice ($Terc^{-/-}$) mice revealed evidence that chronic DNA damage signaling in response to telomere dysfunction leads to enhanced hematopoietic skewing with a strong decrease in lymphopoiesis involving both cell intrinsic checkpoints as well as alterations in the blood circulatory

environment (Song Z et al., 2010; Choudhury AR et al., 2007; Ju Z et al., 2007).

1.1 Clonal diversity model of HSCs aging

A decrease in lymphopoiesis has long been recognized as a hallmark phenotype of the aged hematopoietic system (Sudo K et al., 2000) and it has been shown that this decline correlates with impaired generation of early lymphoid progenitor cells that are known as common lymphoid progenitor cells (CLPs) (Min H et al., 2006). The classical clonal succession model of HSC aging implies that the entire population of HSCs experiences age-associated changes that limit the lymphoid differentiation capacity of HSCs, whereas myeloid differentiation capacities remain intact (Rossi DJ et al., 2008). However, this is so far accepted paradigm of HSC aging shifted recently. It was shown that HSCs consist of different subpopulation of stem cells that have different capacities to undergo myeloid or lymphoid differentiation (Dykstra B et al., 2007; Sieburg HB et al., 2006; Wilson A et al., 2008; Challen GA et al., 2010). Moreover, it was recognized that aging does not lead to a general shift in the HSC potential but selects for a subpopulation of HSCs that have low lymphoid but a high myeloid differentiation potential (Challen GA et al., 2010; Cho RH et al., 2008; Roeder I et al., 2008). These findings have led to the hypothesis that HSC aging follows a selection model rather than a population shift model (Roeder I et al., 2008; Rossi DJ et al., 2008). Recent studies have identified markers (CD150, side population) that can be used to purify different subpopulation of HSCs in mice (Challen GA et al., 2010; Morita Y et al., 2010; Beerman I et al., 2010) and it has been confirmed that aging selects for subpopulations of HSCs that carry a specific marker population and an increased capacity to differentiate into myeloid cells (Challen GA et al., 2010). Together, these data indicate that myeloid competent HSCs have a higher self-renewal capacity compared to lymphoid competent HSCs. The molecular mechanisms that restrict the self-renewal capacity of lymphoid competent HSCs remain to be defined. Since recent studies reported an accumulation of DNA damage in HSCs during aging of mice and man (Rossi DJ et al., 2007; Rübe CE et al., 2011), one hypothesis indicates that the DNA damage response could contribute to this process.

1.2 Influence of DNA damage and telomere dysfunction on HSC aging

Studies on mouse models and human hematopoietic disorders support the

concept that DNA damage can contribute to HSC aging (Lieber MR et al., 2004; Nalapareddy K et al., 2008). This concept is support by publications indicating that mutations in genes related to DNA repair and DNA damage checkpoint are associated with human premature aging syndromes (Lieber MR et al., 2004). It suggests that maintenance of DNA integrity plays a pivotal role in preventing tissue aging. Mice with mutations in DNA repair enzymes develop progressive failure of the hematopoietic system, which is associated with DNA damage accumulation and reduced HSC function (Nijnik A et al., 2007; Rossi DJ et al., 2007). Whether DNA repair capacities become limiting in normal physiological aging is currently unknown.

Several mechanisms could contribute to the accumulation of DNA damage in aging stem cells, including oxidative stress and telomere dysfunction (Choudhury AR et al., 2007; Ito K et al., 2004; Liu J et al., 2009). Telomere shortening limits the proliferative capacity of cells to a finite number of cell division (Bodnar AG et al., 1998). Telomeres shorten due to the end replication problem of DNA polymerase and due to processing of telomeres during S-phase. Of note, telomeres also shorten in human CD34+ HSCs during aging, although these cells have low levels of active telomerase – the enzyme that can synthesize telomeres *de novo*. A current concept states that this low-level telomerase activity is sufficient to ensure long-term survival of HSCs but it is not sufficient to prevent aging-associated telomere shortening, which may become limiting at advanced age.

In response to critical shortening, telomeres lose capping function at the chromosome ends and 4-5 dysfunctional telomeres are sufficient to induce a DNA response leading to cell cycle arrest (senescence) or apoptosis (Zou Y et al., 2004; Lee HW et al., 1998). Studies on telomerase knockout mice have shown that telomere dysfunction limits the self-renewal, colony formation and repopulation capacity of HSCs (Lee HW et al., 1998; Allsopp RC et al., 2003; Choudhury AR et al., 2007). Knockout experiments on human fibroblasts have provided experimental evidence that p21 induces replicative senescence in cell culture (Brown JP et al., 1997). Studies on telomerase/ p21 double mutant mice revealed *in vivo* evidence that this checkpoint represent a cell intrinsic mechanism limiting self-renewal and repopulation capacity of HSCs in response to telomere dysfunction (Choudhury AR et al., 2007). In addition, telomere dysfunctional mice exhibited alterations in the stem cell environment that led to impairments in stem cell differentiation and

engraftment (Ju Z et al., 2007; Min H et al., 2006). The relative contribution of cell intrinsic checkpoints and environmental alterations (niche or circulatory environment) with respect to impaired HSC function during human aging remain to be elucidated. Studies on bone marrow transplantation in humans have revealed evidences that both the donor and the recipient age impact on the success of stem cell engraftment and clinical outcome, indicating that similar to mouse, both stem cell intrinsic and environmental alteration might contribute to human HSC aging (Song Z et al., 2009).

In light of the novel clonal succession model of stem cell aging, it is of particular interest to determine the contribution of cell intrinsic mechanisms and environmental alteration in promoting aging-associated changes in the composition of the HSC pool in response tot DNA damage or telomere dysfunction. Of note, it has recently been shown that environmental alteration in the hematopoietic niche can induce a severe skewing toward increased myelopoiesis and impairments in lymphopoiesis (Omatsu Y et al., 2010). It is thus tempting to speculate that both intrinsic as well as extrinsic mechanisms might contribute to clonal selection of HSC subpopulations upon aging.

1.3 Age-dependent skewing and decline in B-lymphopoiesis

One of the hallmark features of mouse and human aging is the decline in B-lymphopoiesis in bone marrow. This age dependent impairment in B-lymphopoiesis is not only associated with reduced differentiation of HSCs in CLPs, but also with impaired maturation of pro-B cells to pre-B-cells. In addition, it was also noted that CLPs from aged mice present a reduced proliferation capacity and an impaired responsiveness to Il7 induced B-lymphopoiesis coinciding with an increased rate of apoptosis (Min H et al., 2006; Allman D et al., 2003; Van der Put E et al., 2003). As outlined above, aging of the hemato-lymphopoietic system appears to be induced at HSC levels by a selective survival of myeloid competent HSCs and a depletion of lymphoid competent HSCs. It is conceivable that this process significantly contributes to the impairments in B-lymphopoiesis during aging. In agreement with this hypothesis, the transplantation of myeloid-competent HSCs that accumulate during aging resulted in a significant increase in myelopoiesis and defective lymphopoiesis in recipient mice (Challen GA et al., 2010; Morita Y et al., 2010; Beerman I et al., 2010). Studies on telomerase deficient mice demonstrated

that telomere dysfunction accelerates hemato-lymphopoietic skewing, which is characterized by the reduction in B-lymphopoiesis and increased myeolpoiesis (Ju Z et at., 2007). Impairments in B-lymphopoiesis in response to telomere dysfunction were induced by alteration in the circulatory environment as well as HSC intrinsic alterations that persisted after transplantation into wild-type mice (Song Z et al., 2010). It remains to be seen whether telomere dysfunction and DNA damage signaling contributes to an impaired maintenance of lymphoid-competent HSCs and whether this mechanism contributes to impaired B-lymphopoiesis in human aging.

1.4 Thymic involution and age-dependent reduction in T-lymphopoiesis

While age-associated impairments in T-lymphopoiesis in wild-type mice have been associated with defects in the thymic epithelium (Aw D et al., 2008; Mackall CL et al., 1997), studies on telomerase knockout mice ($Terc^{-/-}$) revealed that alterations in the systemic, circulatory environment represent the main cause of impaired T-lymphopoiesis in the context of telomere dysfunction induced aging (Song Z et al., 2010). Together, these studies indicate that alterations in the systemic environment and in the thymic niche can represent causal factors of impaired T-lymphopoiesis during aging, which is characterized by alterations in apoptosis and proliferation of T-lymphocyte progenitor cells (Andrew D et al., 2001; Aw D et al., 2010). Of note, thymic involution in aging mice can be partially rescued by deletion of p16 in CD4/CD8-double-negative (DN) T-lymphocyte progenitor cells (Liu Y et al., 2011; Eshraghi P and Rudolph KL, 2011) indicating that environmental alteration induce thymic involution by activating T-cell intrinsic expression of inhibitory genes. The relative contribution of cell intrinsic and environmental factors to thymic involution during human aging is unknown.

Despite the pronounced involution of the aging thymus, it has been shown that low rates of naive T-lymphocytes are produced up to an advanced age (Douek DC et al., 1998; Mitchell WA et al., 2010). It is tempting to speculate that the age-dependent decrease in lymphoid competent HSCs contributes to a reduction in thymic output at advanced age. Fate mapping studies indicate that T-lymphopoiesis stems from Il7R-positive early lymphoid progenitor cells (Schlenner SM et al., 2010). It is conceivable that an age associated selection of HSC sub-populations contributes to the age-dependent reduction in early lymphopoietic progenitor cells, e.g. common lymphoid progenitor cells (CLPs), which is observed during aging (Min

H et al., 2006). It remains an open question, whether this process could become limiting for the low level thymic output, which persists up to an advanced age.

1.5 short hairpin RNA screening to identify novel checkpoints limiting self-renewal of HSCs with DNA damage

Unbiased, functional genomic approaches have been conducted at stem cell level (Hope et al. 2010) and could also help to identify checkpoint responses in stem cells. Studies on carcinogenesis demonstrated the power of such approaches to discover novel tumor suppressor checkpoints (Zender et al. 2008). Of note, tumor suppressor checkpoints can also limit the regenerative capacity of tissues during aging, e.g. p53, p16, p21 (Signer et al. 2008, Janzen et al. 2006, Liu et al. 2011, Molofsky et al. 2006, Nishino et al. 2008, Choudhury et al. 2007, Sharpless and DePinho 2007). This dual role of checkpoint genes in cancer protection and aging stands in agreement with the concept of antagonistic pleiotropy indicating that some genes can have beneficial functions in early life but contribute to impairments in cellular and organismal function at late age (Rose and Graves 1989). This concept could also be relevant for checkpoint responses induced by DNA damage at stem cell level (Pelicci 2004, Beausejour and Campisi 2006, Sharpless and DePinho 2007). It is possible that DNA damage checkpoints that protect from stem cell derived cancer could contribute to impairments in stem cell function and tissue maintenance during aging. Telomere shortening represents a cell intrinsic mechanism contributing to the accumulation of DNA damage in aging cells (d'Adda di Fagagna et al. 2003, Takai et al. 2003, Shay and Wright 1992). Critically short telomeres lose capping function at chromosome ends and induce DNA damage responses that lead to induction of cell cycle arrest or apoptosis (Blasco et al. 1997, Lee et al. 1998, Wright and Shay. 1992). Studies on late generation telomerase knockout mice (G3 mTerc-/-) revealed the first experimental evidence that telomere dysfunction induced DNA damage checkpoints can limit self-renewal and the repopulation capacity of HSCs in aging mice (Choudhury et al. 2007). Following this line of argumentation, we reasoned that functional genetic screening could be used to identify novel checkpoints limiting the self-renewal of adult stem cells in the context of DNA damage.

2. Materials and methods

2.1 Antibodies

Actin antibody	Sigma
Batf antibody	Abcam
Batf antibody	Abnova
Biotin conjugated anti-mouse B220	eBioscience
Biotin conjugated anti-mouse CD11b	eBioscience
Biotin conjugated anti-mouse Gr1	eBioscience
Biotin conjugated anti-mouse CD3	eBioscience
Biotin conjugated anti-mouse CD4	eBioscience
Biotin conjugated anti-mouse CD5	eBioscience
Biotin conjugated anti-mouse CD8	eBioscience
Biotin conjugated anti-mouse Ter119	eBioscience
B220-Fitc conjugate anti-mouse	BD Pharmingen
CD4-Fitc conjugated anti-mouse	BD Pharmingen
CD8-APC conjugated anti-mouse	BD Pharmingen
CD11b-APC conjugated anti-mouse	BD Pharmingen
cKit-APC conjugated	BD Pharmingen
HRP conjugated anti-mouse	Zymed
HRP conjugated anti-rabbit	Zymed
Pho-p53	Cell Signaling

2.2 Chemicals

Agarose (Electrophoresis grade)	Gibco
Aquatex (water based mounting medium)	Merck
Ammonium chloride	Sigma
Ammonium persulphate	Fluka
5’-bromo-2’-deoxyuridine (BrdU)	Amersham
Bromophenol blue	Serva
BSA (bovine serum albumin)	PAA
Chemiluminescence reagent	Perkin elmer
Collagenase A	Sigma
Complete mini (protein stabiliser)	Roche

Chloroform	J.T.Baker
Citric acid	Merck
3, 3'-diaminobenzidine tetra-hydrochloride	Roche
Deoxycholic acid	Applichem
dNTP´s	Invitrogen
EDTA	Sigma
Ethanol	J.T.Baker
Ethidiumbromide	Sigma
Formaldehyde	Merck
Hemalum solution	Merck
Hydrochloric acid	Merck
Hydrogen peroxide	Merck
Isopropanol	J.T.Baker
Kanamycin	Sigma
Mayer´s Haematoxylin solution	Sigma
Methanol	J.T.Baker
Mounting medium for fluorescence	Vectashield
Mounting medium with DAPI	Vectashield
NNN´N´ tetramethylethylenediamine	Sigma
Paraformaldehyde	Merck
PBS (phosphate buffered saline)	PAA
Potassium bicarbonate	Sigma
Propidium Iodide	Sigma
Roti-Phenol/Chloroform	Roth
Sodium hydroxide	Merck
Sodium chloride	Merck
Sodium dodecylsulphate (SDS)	Sigma
Tris (Tris-(hydroxymethyl)-aminomethane)	Applichem
Tween 20	Sigma
Triton 100	Sigma

2.3 Laboratory Equipment

0.20µm filter	Nalgene
0.45µM PVDF membrane	Millipore

Abc (animal blood counter)	Scil animal care company
Desktop centrifuge	Eppendorf
Electrophoresis-Apparatus Labtech,	Pharmacia Biotech
Electrophoresis apparatus for PAGE	Bio-Rad
LSRII FACS Machine	Beckton Dickinson
Aria II sorter	Beckton Dickinson
Cell viability analyzer Vi-Cell XR Beckman coulter	Eppendorf
FACS tubes	Falcon
Fluorescence microscope	Olympus
Gel doc	Syngene
Heat block	Eppendorf
Nylon net (60µm)	Fishcher scientific
PCR master cycler	Eppendorf
PCR soft tubes	Biozym
Power-Supply	Biometra
Spectrophotometer	Eppendorf
Vortex	Omnilab
Western blotting chamber	Biorad

2.4 Mice

Mice were fed with a standard diet and maintained in a pathogen-free environment in the animal facilities of University Ulm. C57BL/6 congenic mice expressing CD45.1 or CD45.2 on leukocytes were used for transplantation experiments. G3mTerc$^{-/-}$ or mTerc$^{+/+}$ mice (CD45.2) were used as donor, and 2-3 months old wildtype mice (CD45.1) were used as recipient for bone marrow transplantation.

2.5 Bone marrow transplantation

Bone marrow cells from 12 month old G3mTerc$^{-/-}$ or mTerc$^{+/+}$ (CD45.2) mice were isolated by flushing both tibias and femurs with sterile PBS, and intravenously injected into lethally irradiated (12 Gy) 2-3 months old wildtype mice (CD45.1).

2.6 Competitive transplantation

Bone marrow cells from 2-3 month old wild-type mice were transplanted into

sub-lethally irradiated 3month old wild-type mice (ly5.2) or G3mTerc$^{-/-}$ mice. At 9 months after transplantation, the donor derived cells (ly5.1) were recaptured for cell cycle analysis. Also donor derived cell (100 CD34-/LSK cells) were retransplanted into wild type mice (ly5.2) with 2*10^5 competator cells (ly5 het: CD45.1+&CD45.2+). Chimerism was analyzed every month after transplantation in white blood cells collected from retroorbital bleeding.

2.7 Flow cytometry

Mice were sacrificed at the respective time points and bone marrow was flushed from both the hind limbs with sterile PBS and pelleted down. After RBC lysis (ammoniumchloride-0.15M, potassium bicarbonate-10mM, EDTA-0.1mM) for 3 minutes at roomtemperature the cells were spun down and re-suspended in 1ml staining medium (PBS with 2% FBS and 0.02% sodium azide). The cells were counted in Neubauer chamber and 1 million cells were used for B-cell and myeloid cell compartment staining and 3 million cells were used for analysing stem cell compartment. For B-cell staining the cells were pelleted down and re-suspended in 50µl staining medium and added antibodies conjugated with respective fluorescent colors (B220 PE conjugated, IgD-FITC conjugated, IgM-APC conjugated, CD43 biotinylated which is again stained with Streptavadin conjugated to PercP antibody) and took the cells for FACS. For myeloid cells CD11b APC conjugated antibody and for dendritic cells CD11c PE or FITC conjugated antibodies were used. For stem cell staining, cells were first treated with biotinylated lineage antibodies (Gr-1, Mac-1, B220-1:300 dilution, Ter119, CD3-1:200 dilution, CD4, CD8, CD5 -1:300 dilution in staining medium) and incubated for 15 minutes on ice in dark and washed with staining medium and then added ckit antibody conjugated to APC and Sca1-FITC conjugated antibody and streptavadin linked PercP-Cy5.5 for all lineage antibodies. For Annexin staining after staining with B220 FITC conjugated, CD11b–APC conjugated for 15 minutes. The cells were washed and stained for apoptosis with Annexin V–PE conjugated 1:20 dilution and 7AAD (7AAD excludes dead cells) 1:20 dilution in binding buffer provided by the kit and incubated at room temperature for 15 minutes in dark and added 500µl of binding buffer and cells were took for FACS. After FACS the data was analysed with Flowjo software.

2.8 Cell cycle analysis

Five million BM cells were collected as described above. Antibodies used for hematopoietic stem cells staining as describe above. Fix the cells with 750 µl 3% PFA for 10 min at 37°C, Permeabilize the cells with 700µl staining media + 0,5% saponin (=saponin-buffer) for 30 min on ice, add anti-ki67 antibody (1:100 dilution) for 1 hour on ice. Data acquisition was performed on FACS LSRII, cell sorting were performed on FACS Aria. Data were analyzed on the Diva6.1 software.

2.9 Protein preparation

Whole cell extracts of mouse ear fibroblasts were obtained by resuspending the pellet in RIPA lysis buffer (50mM Tris-HCl (pH 8.0) 150mM Nacl, 1% NP-40, 0.5% deoxycholic acid, 0.1% SDS, 1mM Sodium meta vanadate, 1mM DTT, 1mM PMSF and finally protease inhibitor) for 20 minutes on ice and then centrifuged at 13,200rpm for 15minutes and collected the supernatant. The protein was quantified by adding Bio-Rad reagent to the protein (protein 5µl, distilled water 795µl and Bio rad reagent 200µl), incubated at room temperature for 10 minutes and OD was measured at 595 nm in spectrophotometer. 20µg of protein is treated with loading buffer (0.5MTris Hcl pH 6.8, SDS powder-640mg, 100% glycerol-3.2ml, ß-mercaptoethanol-1.6ml, bromophenol blue -0.001gm dissolved in distilled water 2.14ml) and heated at 95°C for 10 minutes.

2.10 Protein separation through SDS-PAGE and Western blotting

Protein was subjected to SDS-PAGE (Acrylamid:bis acrylamide 30:0.8, 1.5M Tris pH.8.8, distilled water, 10% ammonium persulphate, TEMED, in 1x running buffer Tris, Glycine and SDS pH8.8 at 60V for 2-3hrs) and blotted on the PVDF membrane using semidry western transfer apparatus using western transfer buffer for 20-30 minutes at 25V, 300mA (Western transfer buffer-Glycine-2.9gms, Tris-5.8gms, SDS-0.37gms, methanol-200ml all of them made up to one litre with distilled water). After blotting the membrane was blocked in 5% milk powder in TBS-Tween (Tris, borate, saline and 0.1% Tween 20 pH 7.6) for 1 hour and then the required protein was detected using antibody against Batf (1:1000 dilution, Abcam and Abnova), phospho-p53-Ser15 (1:1000 dilution, Cell Signalling) and against ß-Actin (1:10000 dilution, Sigma) over night incubation at 4°C and used HRP conjugated secondary antibodies (Anti rabbit 1:2000 dilution, Zymed, Antimouse 1:2000 dilution depending upon the host in which primary antibodies were raised)

and then developed the membrane with chemiluminescence reagent on the Chemiluminescence films in the developing machine.

2.11 Plasmid and lentiviral vector construction

SF-LV-shRNA-EGFP: to impove vector performance in somatic and especially hematopoietic cells, we inserted a spleen-focus forming promoter (SFFV) driven GFP expression cassette into the lentiviral GIPZ (Open Biosystems, Huntsville, USA) vector. The SFFV-GFP cassette was flanked by *XbaI* / *NheI* and *NotI* sites (Schambach et al. 2006) and cloned as an *XbaI* / *NotI* fragment into pGIPZ to form SFFV-pGIPz vector which still has IRES-puromycin cassette inside. To remove IRES-puromycin cassette from SFFV-pGIPz vector, the following primers were used to amplify the 120bp fragment harboring the 5'mir30 sequence: 5'mir30 5'-AGCGGCCGCAAATTCCGGTTTGTTTGAATGAGGCTTCAGTACTT-3' and 3'mir30 5'-TACCTCGACTCGAGCCTTCTGTT-3'. The amplified fragment was inserted in the target vector (SFFV-pGIPz, flanked by XhoI and NotI) to create the final vector SF-LV-shRNA-EGFP. The resulting SF-LV-shRNA-EGFP vector directly drives the GFP cassette followed by the mir30 embedded shRNA cassette and the woodchuck hepatitis virus posttranscriptional regulatory element (PRE).

SF-LV-cDNA-EGFP: to express cDNA by using the same backbone we used for shRNA expression (SF-LV-shRNA-EGFP), SFFV-pGIPz was flanked by *AgeI* and *KpnI* restriction sites, a multiple cloning site including *AgeI*, *PacI*, *XhoI*, *HpaI NotI* was inserted inside. Fragment flanked by *NotI* and *MluI* was purified from SF91 vector (Hildinger et al. 1999, Schambach et al. 2000) and inserted into SFFV-pGIPz to form SF-LV-cDNA-EGFP vector. The resulting vector directly drives inserted cDNA expression followed by IRES and EGFP cassette and the woodchuck hepatitis virus posttranscriptional regulatory element (PRE).

2.12 Lentivirus production

The human embryonic kidney cell line 293T was cultured in Dulbecco's modified Eagle's medium (DMEM) supplemented with 10 % fetal bovine serum, 100 U/ml penicillin and 100 µg/ml streptomycin. Twenty microgram shRNA plasmid, 15 µg pCMVΔR8.91 helper plasmid and 6 µg pMD.G (Schambach et al. 2006) were co-transfected using standard calcium phosphate transfection. Medium was replaced with fresh medium twelve hours after transfection. To harvest viral particles,

supernatants were collected 48 hours after transfection, filtered through 0.22 μm-pore-size filters, and concentrated at 25,000rpm for 2.5 hours, 4 °C, virus pellet was resuspended in sterile PBS. Virus was stored at -80 °C.

2.13 cDNA clone

Batf cDNA was amplified by using the following primers (forward frimer: ACTGCTCGAGGCCACCATGCCTCACAGCTCCG and reverse primer: CAGTGCGGCCGCAACTATCCACCCCCTGC) and flanked by *NotI* and *XhoI*, then inserted into SF-LV-cDNA-EGFP flanked by *NotI* and *XhoI*. The insert was verified by sequencing.

2.14 shRNA Recovery, Identification, and Determination of Representation

Genomic DNA was isolated from lineage negative bone marrow cells (Gentra Puregene Blood Kit, Qiagen) and the integrated proviral sequences were amplified with primers flanking the mir30 cassette (for details see Zender et al. 2008).

2.15 RNA isolation

Total RNA was isolated from freshly isolated and sorted HSCs by using MagMAX 96 total RNA isolation Kit (Ambion) due to the manufactors protocol.

2.16 Quantitative real-time PCR

Quantitative real-time PCR was performed with an ABI 7300 Real-Time PCR System (Applied Biosystems) in duplicates from at least 3 biological samples. The superscript III kit (Invitrogen) was used for cDNA synthesis total RNA from HSCs. Primer sets for the detection of single genes are listed in supplement (Suppl. Table 4). The quantitative PCR was done in a volume of 25μl by using the iTaq SYBR Green supermix with Rox (Bio-Rad).

2.17 Statistics

SPSS 11.5 was used for statistical analyses. Unpaired Student's *t* test was used to generate *P* values for all of the datasets.

2.18 Mathematical modeling

We considered two groups of HSCs, one with $CD150^{hi}$ and the other with

$CD150^{lo}$ in our mathematical models. Delay-differential equations were used to model changes of the $CD150^{hi}$ and $CD150^{lo}$ cell numbers (see Suppl. Text_1 for details) and integrated numerically (Mathematica V8, Wolfram Research). Functions for effects of proliferation and apoptosis were fitted to data from the experiments. Differentiation is modeled as occurring within a specific time frame. Rates for the strength of the respective cellular processes and delays for differentiation were inferred by fitting the curves of resulting functions to the numbers of cells measured in the experiments using least-squares. Ten separate runs with random starting values for initializing parameters were performed for each model fit. The result with lowest error was utilized. Data sets for $CD150^{hi}$ and $CD150^{lo}$ HSC populations including the fractions of cells expressing apoptosis and proliferation markers were available for five time points (0 h, 6 h, 12 h, 18 h and 24 h), each in triplicate. This generates 3^5=243 possible combinations for time courses. We fitted models including differentiation and simplified models without differentiation to each combination. The distributions of errors for both modeling approaches were compared using a Wilcoxon test.

3. Result

3.1 *In vivo* RNAi screening identifies a set of target genes rescuing the repopulation capacity of telomere dysfunctional stem cells.

To identify novel checkpoint components limiting the self-renewal of HSCs in response to telomere dysfunction, we conducted an *in vivo* RNAi screen. c-KIT-positive, Sca1-positive, lineage-negative (KSL) cells enriched for HSCs were freshly isolated from bone marrow of 3 month old mice with dysfunctional telomeres (third generation telomerase knockout: G3 *mTerc*$^{-/-}$) and from wildtype mice with long telomere reserves (*mTerc*$^{+/+}$, n= 24 donors per group, Figure 1).

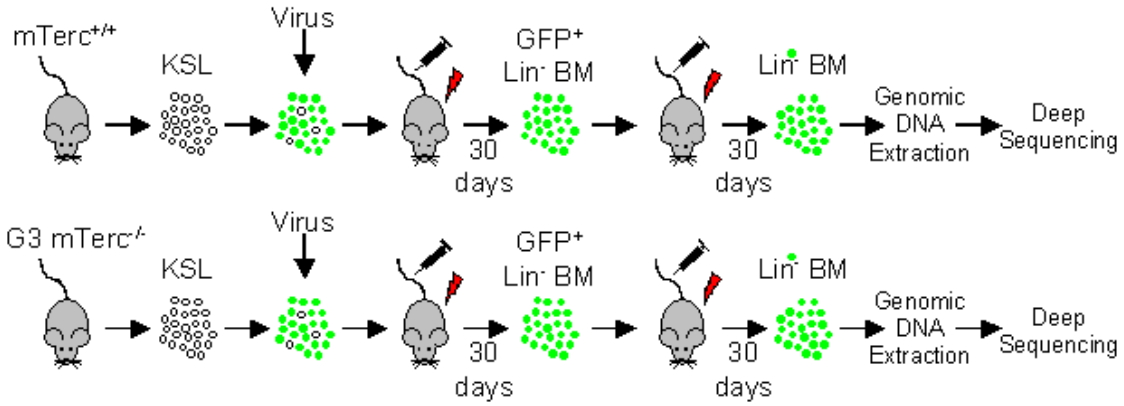

Figure 1: **Experimental procedure: Freshly isolated KSL cells from bone marrow of 3 month old *mTerc*$^{+/+}$ and G3 *mTerc*$^{-/-}$ mice (n=24 mice per group) were infected with a pool of lentiviruses targeting putative human tumor suppressor genes or oncogenes (n= 1772 shRNA constructs). Infected KSL cells were transplanted into lethally irradiated recipients (n=24 mice per group) together with non-infected KSL cells from the same culture. One month after transplantation, GFP^{+} Lin^{-} BM cells were isolated and transplanted into lethally irradiated, secondary recipients. One month later, Lin^{-} BM cells were collected for deep sequencing analysis of integrated shRNA constructs.**

The library used for the screen was derived from a recently published set of shRNAs “Cancer 1000” targeting genes compiled from microarray expression data and literature mining (Bric et al. 2009). The list contained potential tumor suppressors, as well as oncogenes. A subset of 1772 shRNAs targeting 947 genes was transferred into a lentiviral backbone (Figure 2, Table 1).

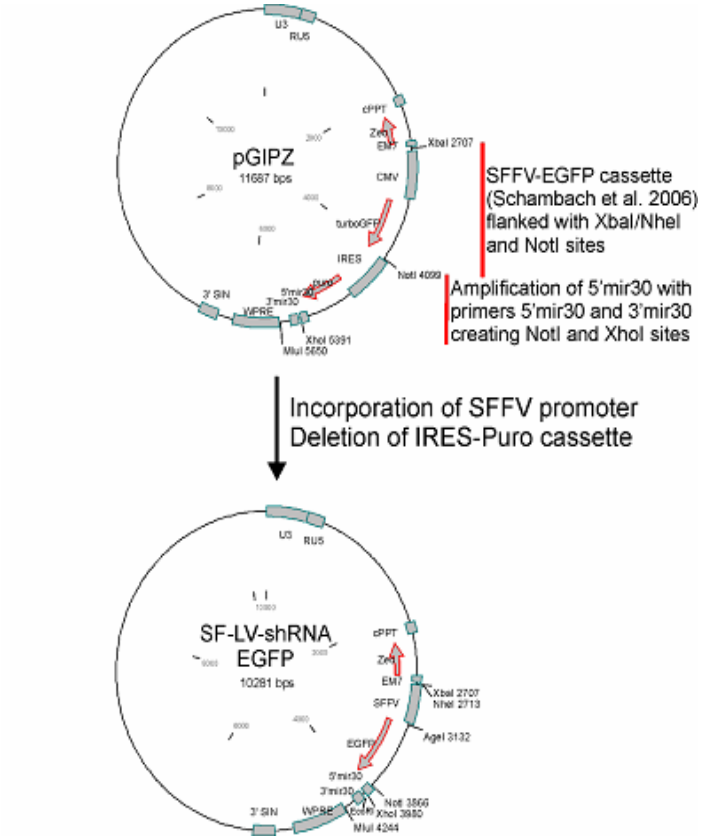

Figure 2: Figure is showing the cloning strategy to modify pGIPz lentiviral vector. We named the final vector: SF-LV-shRNA-EGFP. The SFFV-GFP cassette was flanked by *XbaI / NheI* and *NotI* retriction sites and cloned as an *XbaI / NotI* fragment into pGIPZ to form SFFV-pGIPz vector. The 120bp fragment harboring 5'mir30 sequence was amplified from pGIPz vector (primer sequence are listed in the experimental procedures) and flanked by *XhoI/NotI* and inserted into SFFV-pGIPz flanked by *XhoI / NotI* to create the final lentiviral vector SF-LV-shRNA-EGFP. Short hairpin RNAs are cloned into SF-LV-shRNA-EGFP at XhoI and EcoRI site in between 5'mir30 and 3'mir30.

All shRNAs were based on the miR30 design, where sequence homologous to the targeted gene are inserted into a natural microRNA structure and thus are efficiently incorporated into the RNAi pathway and capable of potent knockdown when integrated at single copy in the genome (Dickins et al., 2005; Silva et al., 2005). KSL cells were infected with a pool of lentiviruses expressing all short hairpin RNAs. The transduction efficiency of KSL cells was 82-84%. The screening setup was established in a way that each shRNA was infected in at least 500 KSL cells to avoid unspecific loss of shRNAs during cell transplantation. Virally transduced KSL cells were transplanted for two consecutive rounds into lethally irradiated recipient mice. Four weeks after the second transplantation, hematopoietic cells (Lin-negative) were isolated from secondary recipients for deep sequencing analysis of integrated shRNAs. This analysis revealed that the vast majority of shRNAs that were used for virus production, were also present in hematopoietic cells derived from secondary recipients transplanted with virally transduced *mTerc*$^{+/+}$ or G3 *mTerc*$^{-/-}$ HSCs (Figure 3).

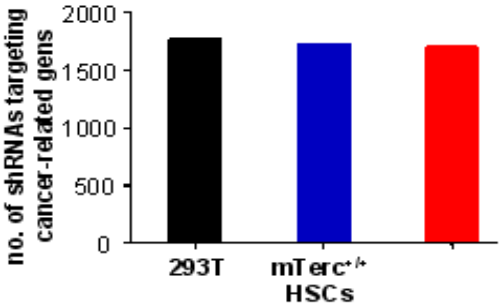

Figure 3: **The histogram depicts the numbers of shRNAs that were detected by deep sequencing analysis in virus producer cells and Lin$^-$ bone marrow cells from secondary recipients transplanted with virally targeted *mTerc*$^{+/+}$ or G3 *mTerc*$^{-/-}$ hematopoietic cells. Note that a very small percentage of shRNA constructs was lost during the experimental time course.**

These data indicated that imbalances in the prevalence of individual shRNA constructs in secondary recipients did not occur because of the random loss of shRNA constructs in the experimental groups.

Twelve mice of each group were subjected to deep sequencing analysis and showed highly reproducible and strong enrichment of seven shRNAs that were strongly (>35fold) selected in recipients transplanted with G3 *mTerc*$^{-/-}$ HSCs compared to recipients transplanted with *mTerc*$^{+/+}$ HSCs (Figure 4, Table 1).

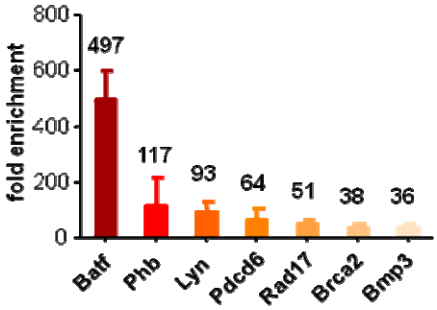

Figure 4: **Histogram showing the strongest selected shRNAs in G3 *mTerc*$^{-/-}$ Lin$^-$ BM compared to *mTerc*$^{+/+}$ Lin$^-$ BM after 2 rounds of transplantation. The enrichment was calculated based on the number of sequence reads of individual constructs per total number of reads in each cohort.**

To validate positive effects of selected shRNAs on the repopulation capacity of telomere dysfunctional HSCs, freshly isolated *mTerc*$^{+/+}$ and G3 *mTerc*$^{-/-}$ KSL cells were infected with single shRNA constructs or a scrambled shRNA followed by transplantation into lethally irradiated mice. In primary recipients transplanted with G3 *mTerc*$^{-/-}$ hematopoietic cells, four out of seven candidate shRNAs were positively selected compared to non-infected cells (shRNA – *Batf*: p= 0.007 and 0.012 for shRNA1 and shRNA2, respectively; shRNA – *Lyn*: p=0.001; shRNA – *Pdcd6*: p=0.001; shRNA - *Bmp3*: p=0.015; n= 3 recipients per group, Figure 5-8).

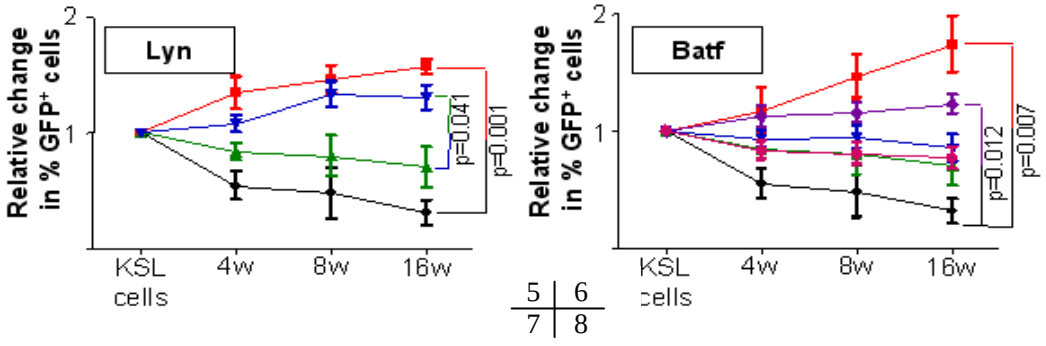

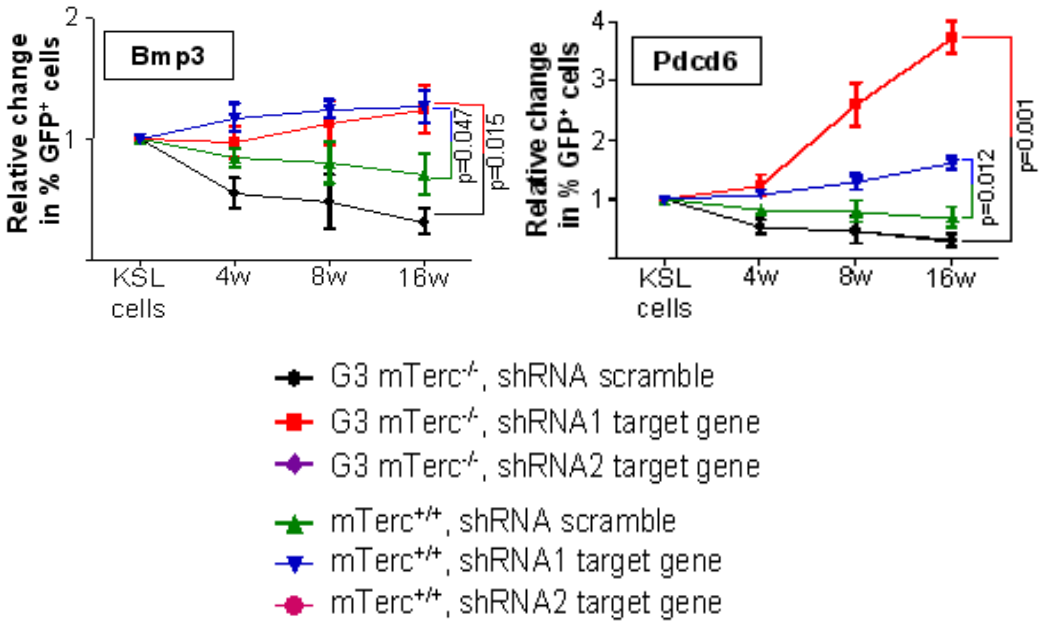

Figure 5-8: **Freshly isolated KSL cells from mTerc$^{+/+}$ or G3 mTerc$^{-/-}$ mice (n= 8 donors per group) were infected with single shRNA constructs targeting candidate genes or with a scrambled shRNA control. The infection rate was 22-50 % and was normalized to 1 for each experiment. Infected cells were transplanted into lethally irradiated recipients along with non-infected cells from the same culture (n= 3 recipients for each group). The histograms depict changes in peripheral blood chimerism of infected cells (GFP-positive) in primary recipients at the indicated time point after transplantation.**

All of these shRNAs exhibited a good knockdown efficiency of target genes on mRNA level (61.5-88.5% knockdown, Figure 9, Table 2). Three of the shRNAs also showed a positive selection in primary recipients transplanted with *mTerc*$^{+/+}$ hematopoietic cells (shRNA *Pdcd6*: p= 0.012, shRNA *Lyn*: p= 0.041, shRNA *BMP3*: p= 0.047). However, this selection was less pronounced compared to the selection of the shRNAs in recipient of G3 *mTerc*$^{-/-}$ hematopoietic cells (Figure 6-8). It is possible that proliferative stress induces DNA damage in transplanted hematopoietic cells, which could explain why selected shRNAs also referred a growth advantage to *mTerc*$^{+/+}$ HSCs.

The top candidate in the list of positively selected shRNAs in G3 *mTerc*$^{-/-}$ hematopoietic cells was an shRNA targeting “Basic leucine zipper transcription factor, ATF-like”, also known as *Batf* (Dorsey et al. 1995), which was 497-fold enriched in recipients transplanted with G3 *mTerc*$^{-/-}$ *vs*. *mTerc*$^{+/+}$ hematopoietic cells (Figure 4). Two independent shRNAs targeting *Batf* had no measurable effect on *mTerc*$^{+/+}$ hematopoietic cells but were strongly selected in transplanted G3 *mTerc*$^{-/-}$

hematopoietic cells (Figure 5). Of note, the shRNA with the better knockdown efficiency (shRNA1-*Batf*, Figure 9) was stronger selected compared to the less efficient shRNA2 targeting *Batf* (Figure 5).

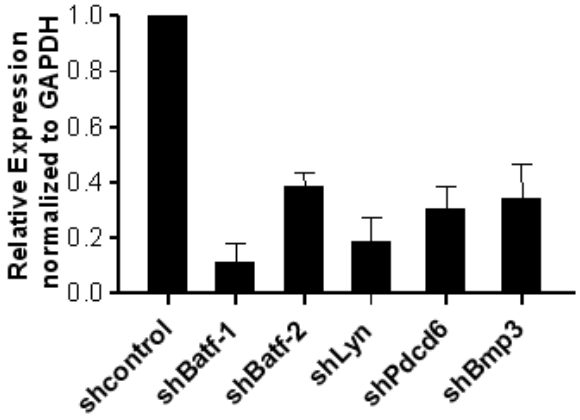

Figure 9: **Histogram showing mRNA expression levels (normalized to GAPDH) of *Batf*, *Lyn*, *Pdcd6* and *Bmp3* in *mTerc*$^{+/+}$ hematopoietic cells (Lin negative) infected by *Batf* shRNA-1 lentivirus, *Batf* shRNA-2 lentivirus, *Lyn* shRNA lentivirus, *Pdcd6* shRNA lentivirus, *Bmp3* shRNA lentivirus compared to scrambled shRNA lentivirus. Values are shown as mean±SD, n=3 per group.**

The shRNA-mediated knockdown of *Batf* was also strongly selected in serially transplanted G3 *mTerc*$^{-/-}$ hematopoietic cells (Figure 10) suggesting that it improved the repopulation and self-renewal capacity of telomere dysfunctional HSCs.

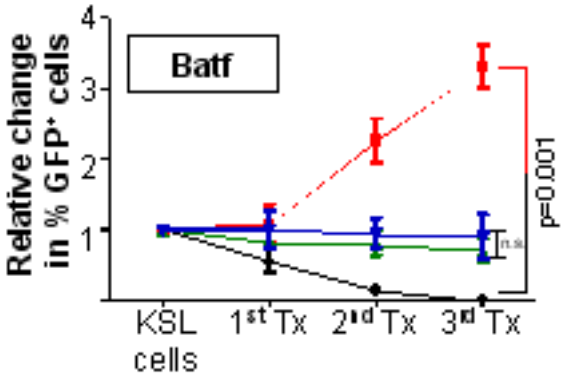

Figure 10: **The histogram shows changes in peripheral blood chimerism 1 month after transplantation at the indicated round of serial transplantation.**

3.2 *Batf* knockdown impairs lymphoid lineage differentiation of HSCs but improves self-renewal and myeloid potential of telomere dysfunctional HSCs.

In previous studies, it was shown that BATF regulates differentiation of distinct subsets of peripheral T- and B-lymphocytes (Betz et al. 2010, Schraml et al. 2009). However, BATF has not been shown to affect the self-renewal of HSCs or differentiation of early hematopoietic progenitor cells and it has not been associated with telomere dysfunction signaling.

To analyze consequences of *Batf* knockdown at early stages of hematolymphopoiesis in the context of functional *vs*. dysfunctional telomeres, bone

marrow of primary recipients were analyzed 16 weeks after transplantation of *mTerc*$^{+/+}$ or G3 *mTerc*$^{-/-}$ HSCs targeted with shRNA-*Batf* or scrambled shRNA. In agreement with previous publications (Choudhury et al. 2007), the self-renewal of G3 *mTerc*$^{-/-}$ HSCs (CD34^{-} KSL) was reduced compared to *mTerc*$^{+/+}$ HSCs (p=0.009, Figure 11).

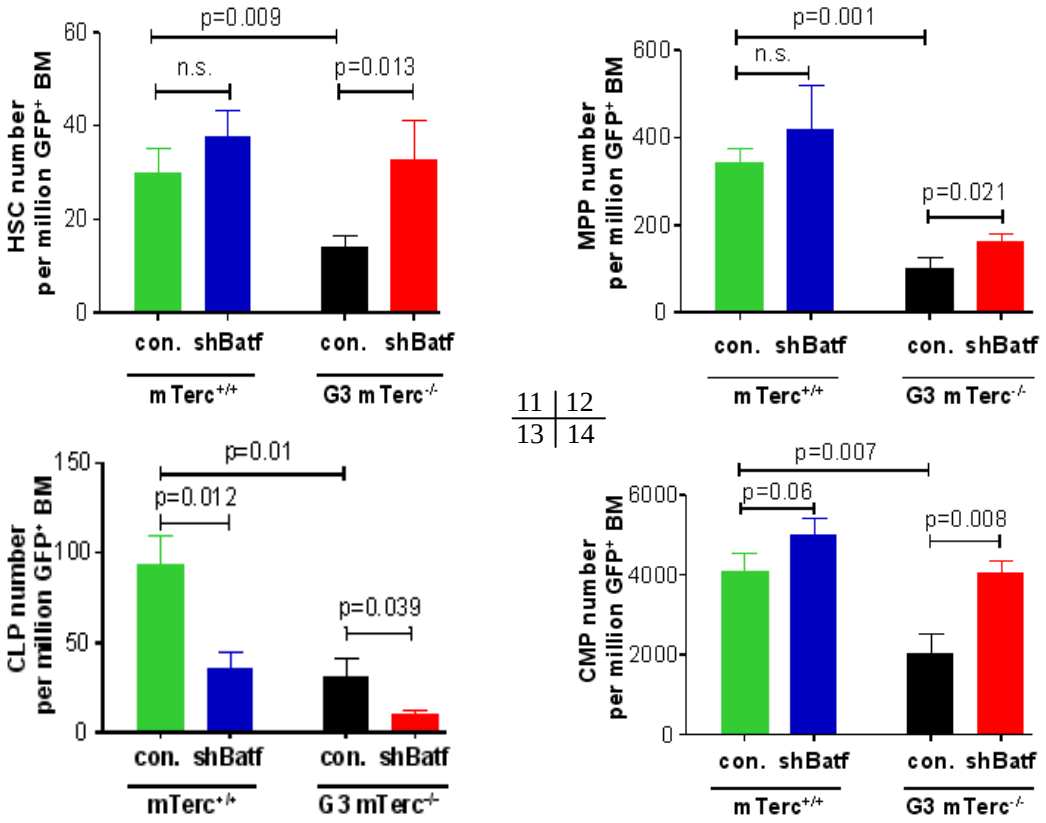

Figure 11-14: **Hematopoietic cells (KSL) of *mTerc*$^{+/+}$ or G3 *mTerc*$^{-/-}$ mice were infected with lentiviruses expressing scrambled shRNA (control = con.) or shRNA-*Batf* (=sh*Batf*). Viruses co-expressed GFP. Virally transduced HSCs were transplanted along with non-infected cells into lethally irradiated mice. Infection efficiencies were 22-50 %. Hematopoiesis was analyzed in GFP^{+} cells of long-term reconstituted recipients at 16 weeks after transplantation. (11-14) The histograms show the numbers of (Figure 11) HSCs (CD34^{-} KSL cells), (Figure 12) multipotent potent progenitor cell (MPPs), (Figure 13) common lymphoid progenitor cells (CLPs), and (Figure 14) common myeloid progenitor cells (CMPs) in GFP^{+} bone marrow cells of recipient mice transplanted with HSCs of the indicated genotypes.**

In addition, G3 *mTerc*$^{-/-}$ HSCs compared to *mTerc*$^{+/+}$ HSCs exhibited a significantly reduced potential to generate multipotent progenitor cells (MPPs, p=0.001, Figure 12), common lymphoid progenitor cells (CLPs, p=0.01, Figure 13), or common myeloid progenitors (CMPs, p=0.007, Figure 14).

The rescue in the repopulation capacity of G3 *mTerc*$^{-/-}$ HSCs in response to

Batf-knockdown correlated with an improvement in HSC self-renewal (Figure 11,15) and improved generation of MPPs and CMPs in recipients transplanted with shRNA-*Batf vs*. scrambled-shRNA targeted G3 *mTerc*$^{-/-}$ HSCs (Figure 12,14,15).

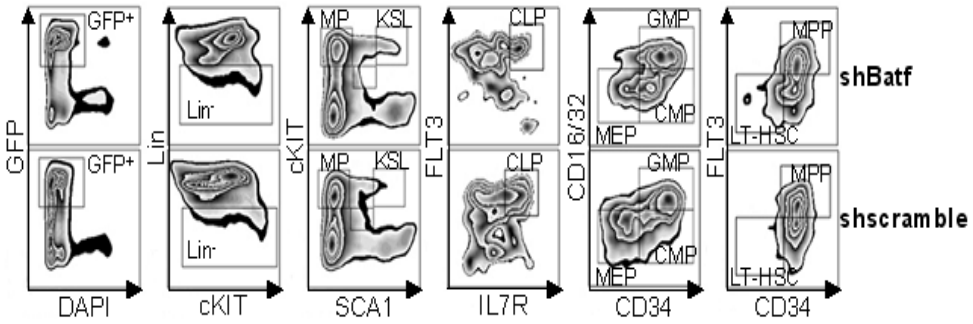

Figure 15: **Representative blots from flow cytometry analysis of freshly isolated bone marrow from recipient mice, 16 weeks after transplantation of shRNA *Batf* or scrambled shRNA transduced KSL cells from G3 *mTerc*$^{-/-}$ mice.**

Batf knockdown did not affect HSC self renewal and the generation of MPPs or CMPs in *mTerc*$^{+/+}$ HSC recipients (Figure 11,12,14).

In contrast to the improvements in the repopulation capacity of G3 *mTerc*$^{-/-}$ HSC, *Batf*-knockdown impaired the formation of CLPs in recipients of both *mTerc*$^{+/+}$ and G3 *mTerc*$^{-/-}$ HSCs (Figure 13,15). In agreement with the inhibitory effects of *Batf*-knockdown on CLP generation, recipients of shRNA-*Batf* infected HSCs exhibited a skewing in HSC differentiation resulting in increased myelopoiesis and decreased lymphopoiesis compared to recipients of scrambled shRNA infected HSCs (Figure 16-18).

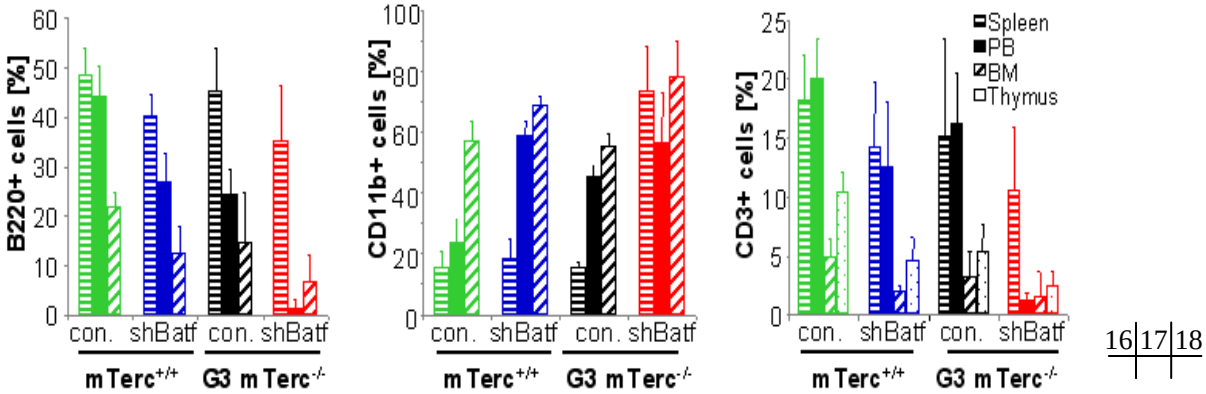

Figure 16-18: **The histograms show the percentage of the indicated cell types in GFP^{+} cells from spleen, peripheral blood (PB), bone marrow (BM), and thymus of recipient mice transplanted with HSCs of the indicated genotypes: (16) B-cells (B220^{+}), (17) myeloid cells (CD11b^{+}) and (18) T lymphocytes (CD3^{+}).**

Because *Batf*-knockdown rescued CMP formation in the context of telomere dysfucntion, the skewing in response to *Batf*-knockdown was more pronounced in recipients of G3 *mTerc*$^{-/-}$ HSCs compared to *mTerc*$^{+/+}$ HSCs.

Together, these experiments showed that BATF controls HSC differentiation into CLPs independent of telomere status. In addition, BATF limits self-renewal and the repopulation capacity of HSCs in response to telomere dysfunction. These data suggested that DNA damage may lead to BATF-dependent differentiation limiting the maintenance of HSCs.

3.3 *Batf* is upregulated in HSC in response to aging and DNA damage and *Batf* overexpression impairs HSC function.

To directly test whether *Batf* was upregulated in HSCs in response to DNA damage, mRNA was extracted from purified long term HSCs (CD34$^-$, FLT3$^-$, KSL), short term HSC (CD34$^+$, FLT3$^-$, KSL), MPP (CD34$^+$, FLT3$^+$, KSL), CMP (Lin$^-$, SCA1$^-$, cKIT$^+$, CD34$^+$, CD16/32^{lo}) and CLP (Lin$^-$, SCA1^{lo}, cKIT^{lo}, IL7R$^+$, FLT3$^+$) from 3 and 12 month old *mTerc*$^{+/+}$ and G3 *mTerc*$^{-/-}$ mice. There was an upregulation of *Batf* mRNA expression in different populations of hematopoietic progenitor cells (Figure 19) and in long-term HSCs (Figure 20) of G3 *mTerc*$^{-/-}$ mice compared to *mTerc*$^{+/+}$ mice.

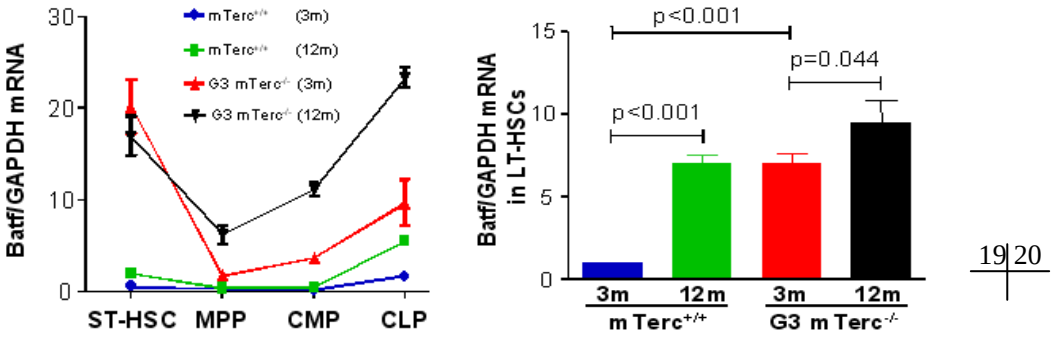

Figure 19-20: **The histograms show the mRNA expression of *Batf* relative to *Gapdh* in the indicated, purified progenitor cell fractions from freshly isolated bone marrow of 3 and 12 month old *mTerc*$^{+/+}$ and G3 *mTerc*$^{-/-}$ mice: (19) short term hematopoietic stem cells (=ST-HSC, CD34$^+$ FLT3$^-$ KSL), multipotent progenitor cells (MPP), common myeloid progenitor cells (CMP), common lymphoid progenitor cells (CLP); (20) long-term HSCs (CD34$^-$ FLT3$^-$ KSL), (n=3 mice per group; data are shown as mean; error bar represent SEM).**

In both cohorts there was an age dependent induction of *Batf* levels in HSCs (Figure 20) possibly reflecting increasing levels of DNA damage in HSCs during mouse aging (Rossi et al. 2007). On protein level, increased expression of BATF was seen

in hematopoietic progenitor cells (KSL) and HSCs (CD34$^-$ KSL) of G3 *mTerc*$^{-/-}$ mice compared to *mTerc*$^{+/+}$ mice (Figure 21,22). Again, there was an age-dependent increase in both cohorts (Figure 21).

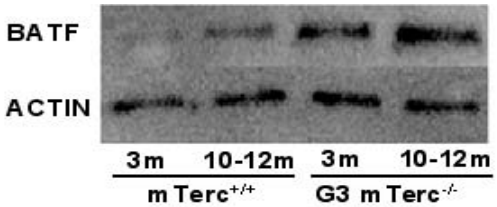

Figure 21: **Representative western blot showing expression of BATF in freshly isolated hematopoietic progenitor cells (KSL) of 10-12 month old and 3 month old G3 *mTerc*$^{-/-}$ and *mTerc*$^{+/+}$ mice (n= 3 mice per group, β-ACTIN was used as loading control).**

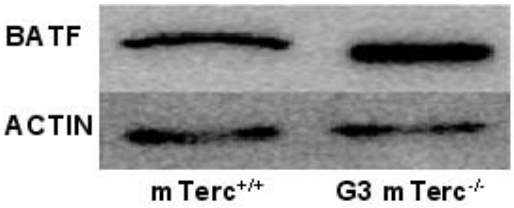

Figure 22: Representative western blot showing expression of BATF in freshly isolated hematopoietic stem cells (CD34$^-$ KSL) from bone marrow of 10-12 month old G3 *mTerc*$^{-/-}$ and *mTerc*$^{+/+}$ mice (n= 5 mice per group, β-ACTIN was used as loading control).

To analyze whether other types of DNA damage would also induce *Batf* in hematopoietic cells, *Batf* mRNA expression was measured in freshly isolated HSCs from *mTerc*$^{+/+}$ mice at different time points after 4 Gy whole body irradiation (IR). There was a significant induction of *Batf* expression from 6-48 h after IR (Figure 23, n= 3 mice per group). Irradiation induced BATF expression was confirmed on protein level in freshly isolated HSCs from irradiated (6h after IR) compared to non-irradiated (NIR) mice (Figure 24).

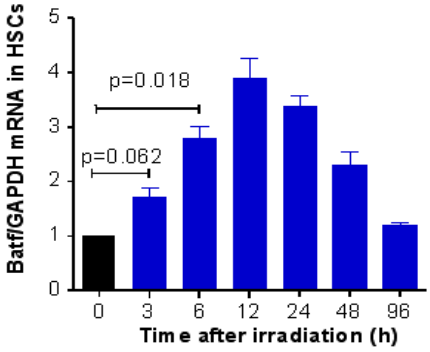

Figure 23: **The histogram shows the mRNA expression of *Batf* relative to *Gapdh* in freshly isolated HSCs (CD34$^-$ KSL) from bone marrow of 3 month old *mTerc*$^{+/+}$ mice at the indicated time points after whole body γ-irradiation (4 Gy, n= 3 mice per time point).**

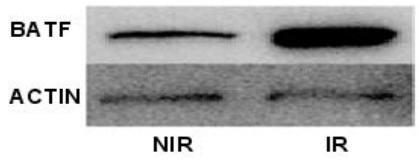

Figure24: Representative western blot showing expression of Batf in freshly isolated hematopoietic stem cells (CD34$^-$ KSL) from bone marrow of 10-12 month old mTerc$^{+/+}$ mice with or without γ-irradiation (4Gy, 12 h before HSC isolation, n= 5 mice per group, β-ACTIN was used as loading control).

Together, these data indicated that DNA damage (gamma-irradiation or telomere dysfunction) induces *Batf* expression in HSCs and hematopoietic progenitor cells. To test the hypothesis that the upregulation of *Batf* contributes to impairments in

HSC function in response to DNA damage, freshly isolated KSL cells from *mTerc*$^{+/+}$ or G3 *mTerc*$^{-/-}$ mice were infected with a *Batf*–cDNA expressing lentivirus or a control lentivirus (empty vector, Figure 25,26). The infection rate was 40-50% and was normalized to 1 (Figure 27).

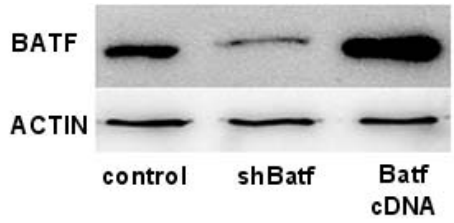

Figure 25: **Representative western blot showing expression of BATF in freshly isolated, GFP^{+} hematopoietic cells (Lin^{-}) from bone marrow of recipient mice, 5 weeks after transplantation of shRNA-*Batf*, cDNA-*Batf* or scrambled shRNA transduced KSL cells from *mTerc*$^{+/+}$ mice.**

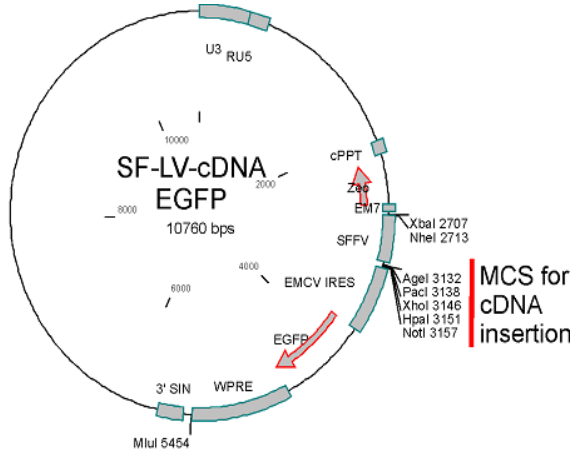

Figure 26: This vector is used to express cDNA. cDNA can be cloned into SF-LV-cDNA-EGFP at multiple cloning sites: AgeI, PacI, XhoI, HpaI and NotI. It is drived under SFFP promoter followed by IRES and EGFP cassette.

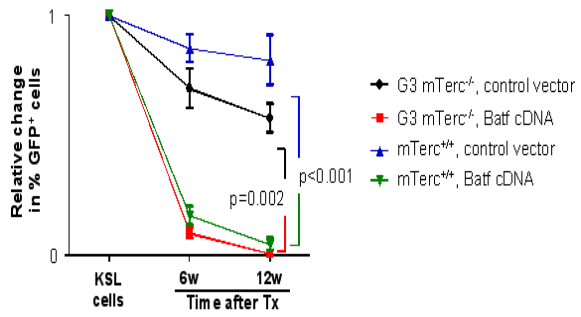

Figure 27: **KSL cells of *mTerc*$^{+/+}$ mice were infected with a lentivirus expressing the *Batf*-cDNA or with an empty vector. KSL cell were transplanted along with non-infected cells. The infection efficiency was 40-50 % and was normalized to 1. The histogram depicts changes in peripheral blood chimerisms of infected cells (GFP-positive) in primary recipients at the indicated time points after transplantation (n= 3 recipients per group; data are shown as mean; error bar represent SEM).**

Infected cells were transplanted together with non-infected cells into lethally irradiated recipients. Overexpression of *Batf* significantly impaired the repopulation capacity of HSCs of both genotypes compared to empty vector infected HSCs (n=3 mice per group, p<0.001 for G3 *mTerc*$^{-/-}$ mice, p= 0.002 for *mTerc*$^{+/+}$ mice).

3.4 G-CSF/STAT3-dependent but p53-independent upregulation of BATF in HSCs in response to DNA damage

The classical checkpoint response to dysfunctional telomeres or gamma-irradiation involves the activation of p53 and its downstream targets, such as p21 and PUMA (Chin et al. 1999, Choudhury et al. 2007, Schaetzlein et al. 2007,

Kuerbitz et al. 1992). An analysis of BATF protein expression in freshly isolated Lin$^-$ cells of gamma -irradiated (4Gy) and non-irradiated *Trp53* knockout mice (*Trp53*$^{-/-}$) revealed that the upregulation of BATF in response to gamma-irradiation was p53-independent (Figure 28).

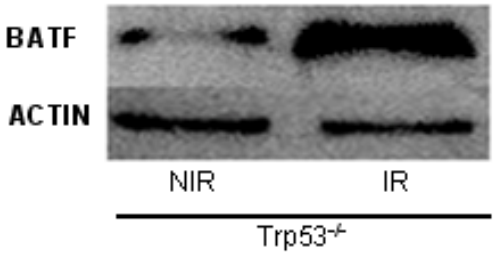

Figure 28: Representative western blot showing the expression of BATF in freshly isolated hematopoietic progenitor cells (Lin$^-$) from bone marrow of *Trp53*$^{-/-}$ mice with and without whole body γ-irradiation (4 Gy, 6 h after irradiation, n= 2 mice per group, β-ACTIN was used as loading control).

Previous studies suggested that STAT3 dependent upregulation of BATF induces differentiation of murine leukemia cell lines in response to leukemia inhibitory factor (LIF) treatment (Senga et al. 2002, Liao et al 2011). STAT3 belongs to the STAT family of latent transcription factors that are activated by cytokines and growth factor signaling (Zhong et al. 1994). In hematopoietic cells, G-CSF has been shown to activate STAT3 (Tian et al. 1994). To analyze whether G-CSF/STAT3 signaling contributed to the activation of BATF in HSCs in response to DNA damage, BATF protein expression was determined in Lin$^-$ cells of non-irradiated and irradiated *G-Csf* knockout mice (*G-Csf*$^{-/-}$) and control mice (*G-Csf*$^{+/-}$). These experiments revealed that the induction of BATF in response to gamma-irradiation was strongly G-CSF dependent (Figure 29).

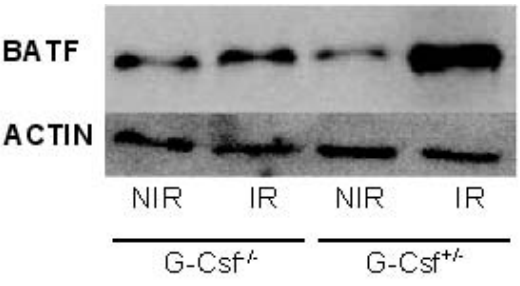

Figure 29: Representative western blot showing the expression of BATF in freshly isolated hematopoietic progenitor cells (Lin$^-$) from bone marrow of *G-Csf*$^{-/-}$ and *G-Csf*$^{+/-}$ mice with and without whole body γ-irradiation (4 Gy, 6 h after irradiation, n= 3 mice per group, β-ACTIN was used as loading control).

Cell culture experiments provided direct evidence that stimulation with G-CSF induced BATF protein levels in freshly isolated hematopoietic cells (Lin$^-$) from wildtype mice and this induction was strongly STAT3 dependent (Figure 30,31).

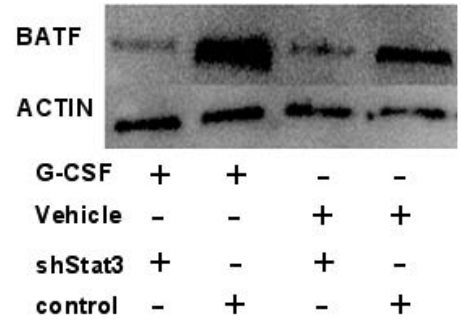

Figure 30: **Representative western blot showing the expression of BATF in primary cultures of hematopoietic progenitor cells (Lin$^-$) that were infected with an shRNA against *Stat3* or a scrambled shRNA. GFP positive cells were purified and exposed for 3 days to G-CSF (10 ng/ml) or vehicle control (n= 2 repeat experiments).**

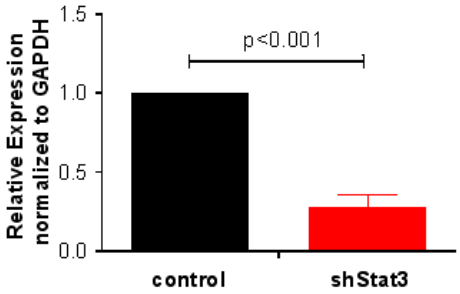

Figure 31: **Histogram is showing mRNA expression levels (normalized to GAPDH) of Stat3 mRNA in mTerc+/+ hematopoietic cells (Lin negative) infected by Stat3 shRNA lentivirus compared to scrambled shRNA lentivirus. Values are shown as mean±SD, n=3 per group.**

To directly test the functional influence of G-CSF/STAT3 signaling on HSC function in the context of DNA damage, shRNA-transduced G3 *mTerc*$^{-/-}$ KSL cells (scramble shRNA or shRNA *Stat3*) were transplanted along with non-infected into lethally irradiated recipients. These experiments showed that *Stat3* knockdown rescued the repopulation capacity of G3 *mTerc*$^{-/-}$ HSCs (Figure 32, p<0.001).

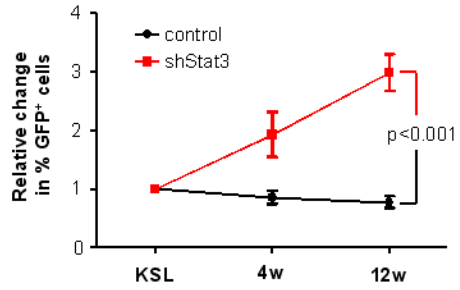

Figure 32: **Freshly isolated KSL cells from *mTerc*$^{+/+}$ or G3 *mTerc*$^{-/-}$ mice (n= 3 donors per group) were infected with a shRNA targeting *Stat3* or with a scrambled shRNA control. The infection rate was 24-35 % and was normalized to 1 for both groups. Infected cells were transplanted into lethally irradiated recipients along with non-infected cells from the same culture (n= 3 recipients for each group). The histogram depicts changes in peripheral blood chimerism of infected cells (GFP-positive) in primary recipients at the indicated time point after transplantation. Values are shown as mean±SEM, n= 3 mice per group.**

Together, these data provided experimental evidence that BATF is upregulated in HSCs in response to DNA damage in G-CSF/STAT3 dependent manner and this signaling pathways limits the repopulation capacity of telomere dysfunctional HSCs.

3.5 DNA damage induces BATF-dependent lymphoid differentiation of HSCs.

The above results showed that BATF has a functional role in lymphocytic differentiation of HSCs but BATF-upregulation impairs the self-renewal of HSCs in

the context of DNA damage. To analyze whether BATF induction in response to DNA damage would induce lymphoid differentiation of HSCs, the mRNA expression of lymphoid and myeloid marker genes was measured in purified HSCs ($CD34^-$ KSL) from 10-12 month old *mTerc*$^{+/+}$ and G3 *mTerc*$^{-/-}$ mice (Figure 33-35, Table 3).

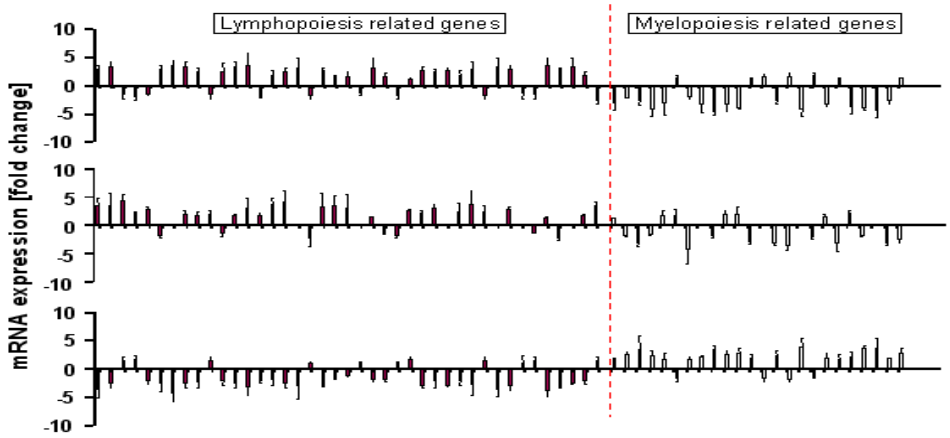

Figure 33-35: The histograms show fold changes in the mRNA expression of lymphopoiesis and myelopoiesis-related genes (Table 3) in freshly isolated HSCs ($CD34^-$ KSL) from bone marrow of, Figure 33: 8-10 month old G3 *mTerc*$^{-/-}$ vs. *mTerc*$^{+/+}$ mice, Figure 34: 2 month old, non-irradiated *vs.* irradiated *mTerc*$^{+/+}$ mice (4 Gy, cells were extracted 12 h after IR), Figure 35: recipient mice, 16 weeks after transplantation of shRNA-*Batf* vs. scrambled shRNA targeted hematopoietic cells from G3 *mTerc*$^{-/-}$ mice. (A-C) n= 3 mice per group; data are shown as mean; error bars represent SD.

Telomere dysfunction was associated with an induction of lymphoid differentiation markers and an inhibition of myeloid differentiation markers in HSCs (Figure 33, n=3 mice per group). Similarly, gamma-irradiation induced DNA damage activated the expression of lymphoid differentiation marker genes in HSCs from *mTerc*$^{+/+}$ mice (Figure 34, n=3 mice per group). To test whether the induction of lymphoid differentiation in response to DNA damage was BATF-dependent, freshly isolated G3 *mTerc*$^{-/-}$ HSCs were transduced with an shRNA- *Batf* or scrambled shRNAs. Targeted HSCs were transplanted into wildtype recipients and re-isolated 4 months after transplantation. qPCR revealed that the knockdown of *Batf* reverted the induction of lymphoid differentiation markers in G3 *mTerc*$^{-/-}$ HSCs (Figure 35).

Knockin Interleukin-7-receptor (IL7R) mice represent another experimental system to analyze induction of lymphoid differentiation in early stem and progenitor cells (Kondo et al. 1997, Schlenner et al. 2010). In these mice, Cre-recombinase is expressed under the endogenous IL7R promotor. When crossed to Cre-inducible reporter mice (e.g. Rosa-lox-stop-lox-RFP), activation of IL7R marks the induction of lymphoid differentiation by inducing reporter gene expression. It was shown that

IL7R-reporter gene is not induced at HSC level but gets activated in response to lymphoid differentiation at CLP level (Schlenner et al. 2010). Here, we tested whether DNA damage would lead to an induction of lymphoid differentiation at HSC level. A significant induction of IL7R-reporter activity was detected 12 h after 4Gy gamma-irradiation in CD34^{-} KSL cells compared to non-irradiated control mice (Figure 36).

To test, which subpopulation of HSCs was most sensitive to induction of lymphoid differentiation in response to DNA damage, SLAM marker (CD150) was included into the analysis of *Il7r* mice. CD150 staining can subdivide CD34^{-} KSL into (i) myeloid biased HSCs (expressing high levels of CD150 = CD150^{hi}) and (ii) lymphoid competent HSCs (expressing low levels of CD150= CD150^{lo}) (Morita et al. 2010, Beerman et al. 2010). Analyzing HSCs in response to irradiation revealed a significant induction of IL7-reporter activity in CD150^{lo} HSCs but not in CD150^{hi} HSCs (Figure 37,38) suggesting that lymphoid competent HSCs may be more sensitive to DNA damage induced lymphoid differentiation. To test whether this phenotype was BATF dependent, IL7-reporter HSCs were infected with lentiviruses expressing *Batf*- or scrambled shRNAs and transplanted into recipient mice. Four Gy gamma-irradiation of recipient mice (18 weeks after transplantation) revealed that the DNA damage dependent induction of IL7-reporter activity in HSCs (12 h after IR) was strongly BATF dependent and was almost completely abolished in shRNA *Batf* expressing HSCs (Figure 39,40).

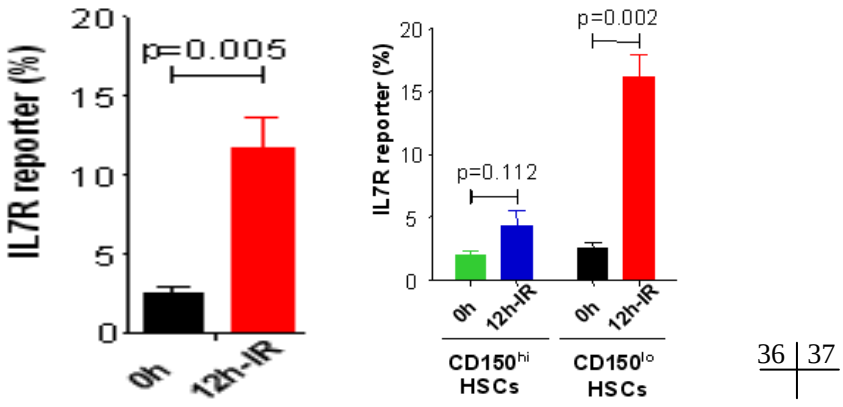

Figure 36, 37: Mice were transplanted with total bone marrow from Il7-receptor reporter mice (Schlenner et al. 2010). 6 week after transplantation, IL7R-reporter activity (RFP) was analyzed in freshly isolated HSCs of non-irradiated vs. irradiated recipients (12 h after 4 Gy IR): (Figure 38-39) The histograms show the percentage of IL7R-reporter^{+} cells in (Figure 38) HSCs (CD34^{-} KSL), (Figure 39) in myeloid competent HSCs (CD150^{hi}) and in lymphoid competent HSCs

(CD150^{lo}).

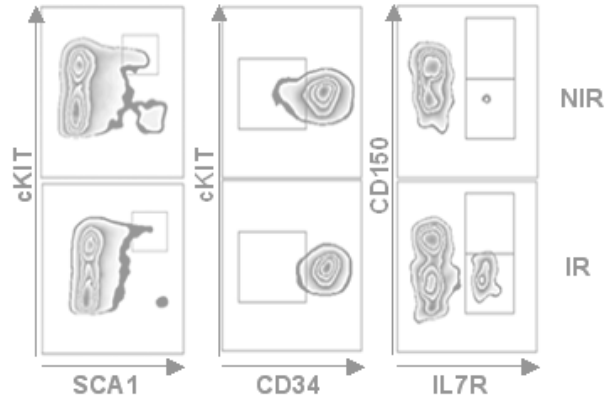

Figure 38: Representative FACS analysis of IL7R-reporter induction in irradiated vs. non-irradiated mice: gates in left panel indicates KSL cells, gates in middle panel indicate CD34^{-} KSL cells, gates in right panel show IL7R-reporter positive cells in CD150^{hi} (upper gates) and CD150^{lo} (lower gates) HSCs. Note that irradiation induced reporter activity is restricted to CD150^{lo} HSCs.

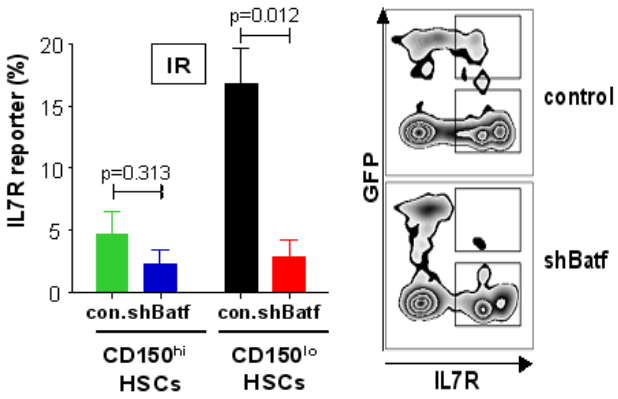

Figure 39,40: Hematopoietic cells from IL7R-reporter mice were infected with shRNA *Batf* or a scrambled shRNA and transplanted into recipient mice. Long-term reconstituted mice (16 weeks after Tx) were irradiated and the induction of IL7R-reporter activity was determined in CD150^{hi} and CD150^{lo} HSCs at 12 h after IR: Figure 39, Histogram showing the percentage of IL7R-reporter^{+} HSCs. Note that BATF knockdown rescues induction of IL7R-acticvity in CD150^{lo} HSCs in response to IR (n=3 mice per group); Figure 40, Representative FACS blots showing IL7R-reporter activity in CD150^{lo} HSCs from irradiated mice. Note that the induction of IL7R activity is rescued in sh*Batf* infected HSCs (GFP^{+}, upper gate in lower panel) compared to scrambled RNA infected HSCs (GFP^{+}, upper gate in lower panel).

Together, these data on IL7-reporter mice indicated that DNA damage induces BATF-dependent lymphoid differentiation at HSC level.

3.6 BATF dependent differentiation contributes to the depletion of myeloid and lymphoid competent HSCs in response to irradiation.

The data on selective induction of IL7-reporter activity in HSC in response to gamma-irradiation suggested that lymphoid competent (CD150^{lo}) HSCs were more sensitive to DNA damage induced differentiation than CD150^{hi} HSCs (Figure 37). However, an analysis of absolute HSC numbers at different time points after gamma-irradiation revealed a significant reduction in the number of both CD150^{lo} and CD150^{hi} HSCs (Figure 41).

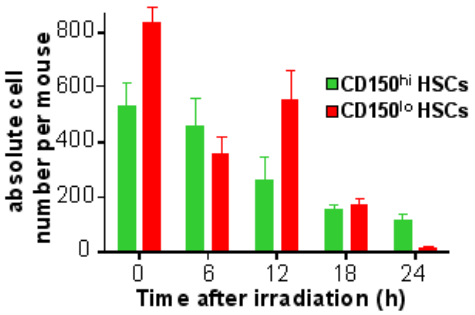

Figure 41: Histogram showing the absolute number of CD150^{hi} and CD150^{lo} HSCs (CD34^{-} KSL) in bone marrow of 2 month old *mTerc*$^{+/+}$ mice at the indicated time points after 4 Gy γ-irradiation.

The percentage of apoptotic and proliferating HSC was low in both compartments at these early time points after gamma-irradiation suggesting that other factors were involved in the observed changes in cell number in response to IR. Previous studies on single cell transplantations suggested that CD150^{hi} HSCs can differentiate into CD150^{lo} HSCs (Morita et al. 2010). A possible explanation for the observed changes in HSC numbers in response to gamma-irradiation in our experiments was that DNA damage led to differentiation of CD150^{hi} HSCs into CD150^{lo} HSCs, followed by lymphoid differentiation induced depletion of CD150^{lo} HSCs (Figure 37). In agreement with this interpretation, we observed a transient increase in the number CD150^{lo} HSCs from 6 to 12 h after gamma-irradiation paralleling the reduction in the total number of CD150^{hi} HSCs (Figure 39). Mathematical modeling revealed an improvement of model fitness for the observed kinetics of gamma-irradiation induced changes in cell numbers when (i) differentiation of CD150^{hi} to CD150^{lo} HSCs and (ii) differentiation induced depletion of CD150^{lo} HSCs were included in the equation (Figure 42). Plain models (Figure 43) that were solely based on the rates of HSC proliferation (Figure 44) and apoptosis (Figure 45), exhibited significantly higher error values as they were fitted to the observed data when compared to models that included DNA damage induced differentiation (Figure 46). Altogether, these analyses supported the concept that differentiation contributed to the depletion of HSCs in response to gamma-irradiation induced DNA damage.

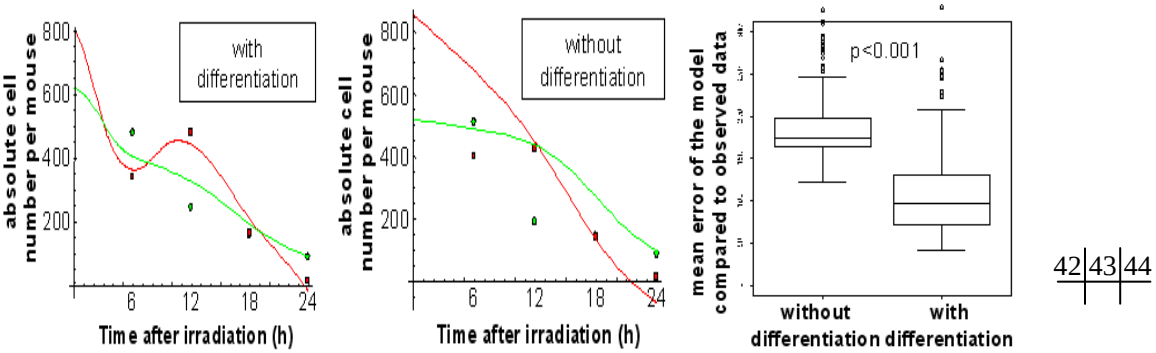

Figure 42-44: **Mathematical modeling of the observed changes in cell number in response to**

irradiation: Figure 42, Model without DNA damage induced differentiation, solely based on changes of cell numbers by cell death and proliferation; Figure 43, DNA damage induced differentiation was included in the delay-differential equations assuming that CD150^{hi} HSCs differentiated into CD150^{lo} HSCs and CD150^{lo} HSCs were depleted from the stem cell pool by induction of lymphocyte differentiation; Figure 44, Box blot showing the mean error of cell numbers in mathematical models compared to the observed data. Modeling of the DNA damage induced changes in cell number was significantly improved in models that included DNA damage induced differentiation in the equations.

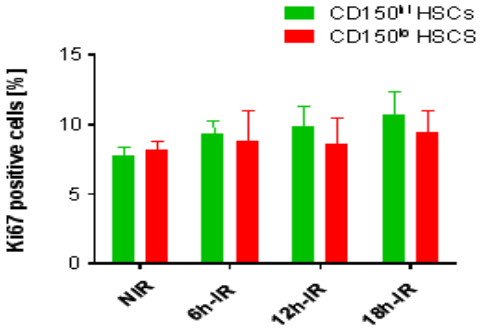

Figure 45: Histogram showing the percentage of Ki67 positive CD150^{hi} HSCs and CD150^{lo} HSCs from 8 weeks old mTerc$^{+/+}$ mice with whole body γ-irradiation (4Gy) at indicated time points. Values are shown as mean±SD, n=3 mice per group.

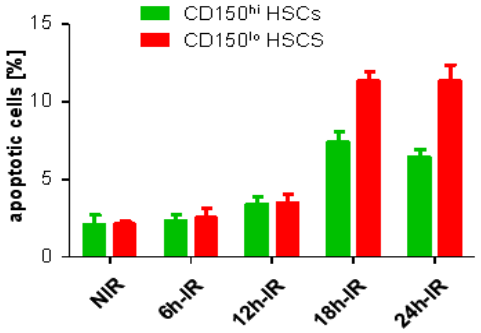

Figure 46: Histogram showing the percentage of apoptosis (Annexin V^{+}) CD150^{hi} HSCs and CD150^{lo} HSCs from 8 weeks old mTerc$^{+/+}$ mice with whole body γ-irradiation (4Gy) at indicated time points. Values are shown as mean±SD, n=3 mice per group.

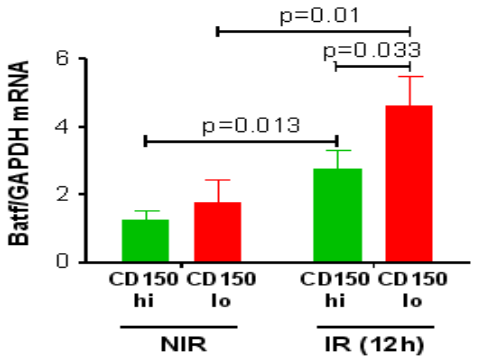

Figure 47: Histogram is showing mRNA expression level (normalized to GAPDH) of Batf in CD150^{hi} and CD150^{lo} HSCs isolated from whole body γ-irradiated mice (12 h after IR). Values are shown as mean±SD, n=3 per group.

From the previous results, it was conceivable that DNA damage induced G-CSF/BATF expression contributed to the induction of differentiation in CD150^{hi} and CD150^{lo} HSCs. In agreement with this assumption, mRNA expression of *Batf* was significantly induced in freshly isolated HSCs of gamma-irradiated mice (12 h after IR) in both CD150^{hi} and CD150^{lo} HSCs (Figure 47, n=3 mice per group). To test the functional role of DNA damage induced BATF expression in the depletion of

HSC subpopulations, gamma-irradiation was applied to (i) mice that were long-term reconstituted with *Batf*- or scrambled shRNA infected HSCs (IR was applied 18 weeks after transplantation) and (ii) to *G-Csf*$^{+/+}$ mice and *G-Csf*$^{-/-}$ mice (Figure 48,49).

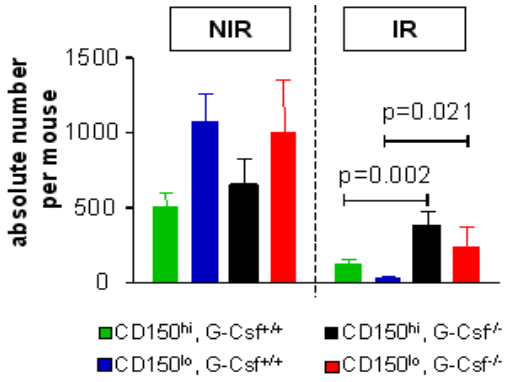

Figure 48: **Histogram showing absolute number of CD150^{hi} and CD150^{lo} HSCs (CD34^{-} KSL) in *G-Csf*$^{-/-}$ and *G-Csf*$^{+/-}$ mice at 24 h after 4 Gy γ-irradiation compared to none irradiated mice (n= 4 mice per group). Note that G-CSF deletion partially rescued the decrease in HSC number in response to IR.**

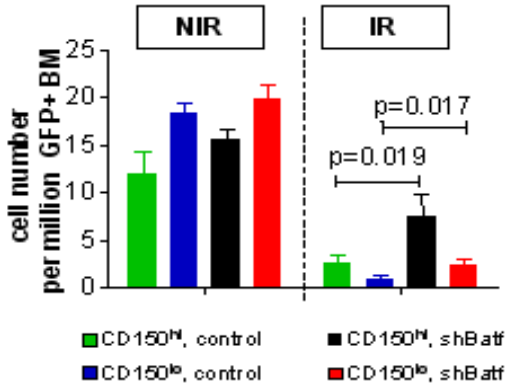

Figure 49: **Hematopoietic cells were infected with shRNA *Batf* or scrambled shRNA viruses and transplanted into lethally irradiated mice. One group of recipient mice received 4 Gy γ-irradiation 24 h before bone marrow analysis. The histogram shows absolute number of CD150^{hi} and CD150^{lo} HSCs (CD34^{-} KSL) per 10^{6} infected (GFP^{+}) bone marrow cells in irradiated compared to non-irradiated recipients (n= 3 mice per group). Note that BATF knockdown partially rescued the decrease in HSC numbers in response to IR.**

G-Csf$^{-/-}$ mice showed a partial rescue in gamma-irradiation induced depletion of CD150^{lo} HSCs (p=0.021) and CD150^{hi} HSCs (p=0.002) compared to *G-Csf*$^{+/+}$ mice (n=3 mice per group, Figure 48). Similarly, the knockdown of *Batf* significantly rescued the number of CD150^{lo} HSCs (p=0.019) and CD150^{hi} HSCs (p=0.017) in irradiated recipients of shRNA *Batf* infected HSCs compared to recipients of scrambled shRNA infected HSCs (n= 3 mice per group, Figure 49). FACS analysis did not reveal a significant influence of *Batf* knockdown or *G-Csf* knockout on the number of CD150^{lo} or CD150^{hi} HSCs in non-irradiated recipients (n=3 mice per group, Figure 48,49). Together, these data indicated that BATF-dependent differentiation contributed to the depletion of both CD150^{lo} and CD150^{hi} HSCs in response to irradiation. The relative increase in the percentage of CD150^{hi} HSCs compared to CD150^{lo} HSCs at 24 h after irradiation may reflect that CD150^{hi} HSC are more resistant to DNA damage induced activation of lymphoid differentiation programs allowing a higher percentage of these cells to survive sublethal doses of

irradiation compared to CD150^{lo} HSCs.

3.7 BATF induction contributes to activation of DNA damage signals in HSCs

Restrictions in self-renewal and induction of differentiation of stem cells are associated with an activation of p53 and cell cycle inhibitors (e.g. p21, p16) in various organs including the hematopoietic system (Kastan et al. 1991, Cordenonsi et al. 2003, Topley et al. 1999, Takubo et al. 2010, Lacroix et al. 2010, Akala et al. 2008). Previous studies revealed an upregulation of p21 in HSCs of telomere dysfunctional mice and deletion of p21 rescued the maintenance and repopulation capacity of G3 *mTerc*$^{-/-}$ HSCs (Choudhury et al. 2007). To test whether BATF contributed to the induction of these inhibitors of stemness in response to DNA damage, p16 and p21 mRNA expression and p53 phosphorylation were analyzed in recipient mice of *Batf*-shRNA vs. scrambled-shRNA infected G3 *mTerc*$^{-/-}$ HSCs four months after transplantation. This analysis revealed a significant rescue in the over-expression of p16 and p21 in CD34^{-} G3 *mTerc*$^{-/-}$ HSCs infected with *Batf*-compared to scrambled shRNA (Figure 50,51).

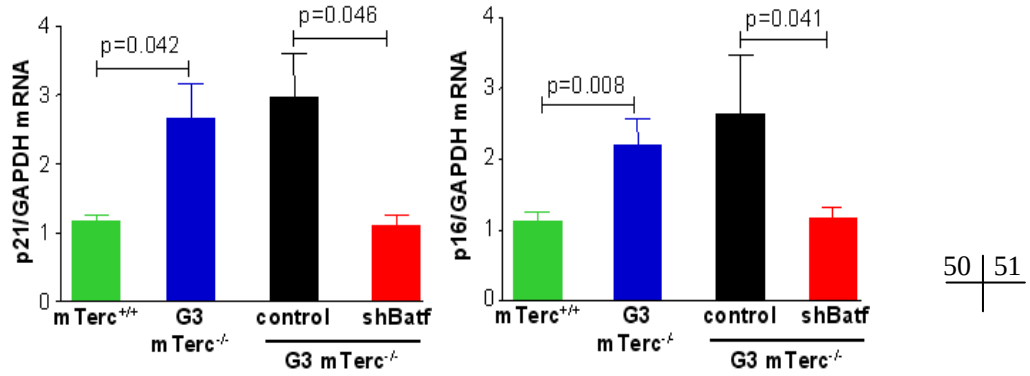

Figure 50,51: Histograms showing mRNA expression of p21 (Figure 50) and p16 (Figure 51) relative to GAPDH in freshly isolated HSCs (CD34^{-} KSL) from 8-10 month old *mTerc*$^{+/+}$ and G3 *mTerc*$^{-/-}$ mice, and from long-term reconstituted mice, 16 weeks after transplantation of hematopoietic cells from G3 *mTerc*$^{-/-}$ that were transduced with a *Batf* shRNA or a scrambled shRNA.

Western blot analysis showed that the induction of p53 in hematopoietic cells (Lin^{-} cells) in response to telomere dysfunction or gamma-irradiation was BATF dependent (Figure 52,53). Together, these data indicated that upregulation of BATF contributes to the induction of DNA damage signals that can limit self-renewal and induce differentiation of HSCs.

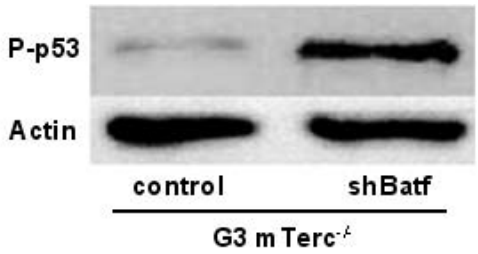

Figure 52: Representative western blot showing the expression of phospho-p53 in freshly isolated Lin$^-$ cells from bone marrow of long-term reconstituted mice, 16 weeks after transplantation of shRNA-*Batf* or scrambled shRNA transduced G3 *mTerc*$^{-/-}$ hematopoieti c cells (n= 3 mice per group).

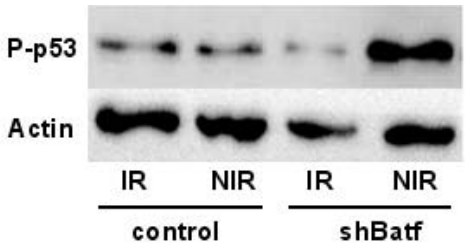

Figure 53: Hematopoietic cells from *mTerc*$^{+/+}$ mice were transduced with shRNA-*Batf* or scrambled shRNA and transplanted into lethally irradiated recipients. Two months after transplantation one group of the recipients was irradiated with 4 Gy γ-irradiation. Representative western blot showing the expression of phospho-p53 in freshly isolated Lin$^-$ cells from bone marrow of non-irradiated and irradiated recipients (6 h after IR, n= 3 mice per group). Note that shRNA knockdown of *Batf* impaired γ-irradiation induced p53 phosphorylation.

3.8 Activation of BATF in human HSCs correlates with telomere shortening and activation of DNA damage signals in patients with myelodyplastic syndromes (MDS).

MDS are aging associated diseases of the hematopoietic system leading to bone marrow failure, skewing of hematopoiesis with increased myelopoiesis, and a sharply increased risk of leukemia formation (Tefferi and Vardiman 2009). On the molecular level, MDS have been characterized by increases in HSC proliferation and telomere shortening (Ohyashiki et al. 1994). To determine whether BATF induction in response to DNA damage was conserved in human HSCs, we analyzed the expression of *Batf* mRNA, telomere length, and the expression of p21 (a downstream of p53, induced by DNA damage) in freshly isolated CD34$^+$ HSCs from bone marrow biopsies of patients with MDS. There was a significant inverse correlation between telomere length and *p21* mRNA expression indicating that telomere shortening was associated with an activation of DNA damage responses in these samples (Figure 54). Moreover, there was a direct association of BATF expression levels with p21 expression (p=0.021) and an inverse association of BATF expression with telomere length (p= 0.002, Figure 55,56). These data indicated that increases in BATF expression represent a conserved response to DNA damage in murine and human HSCs.

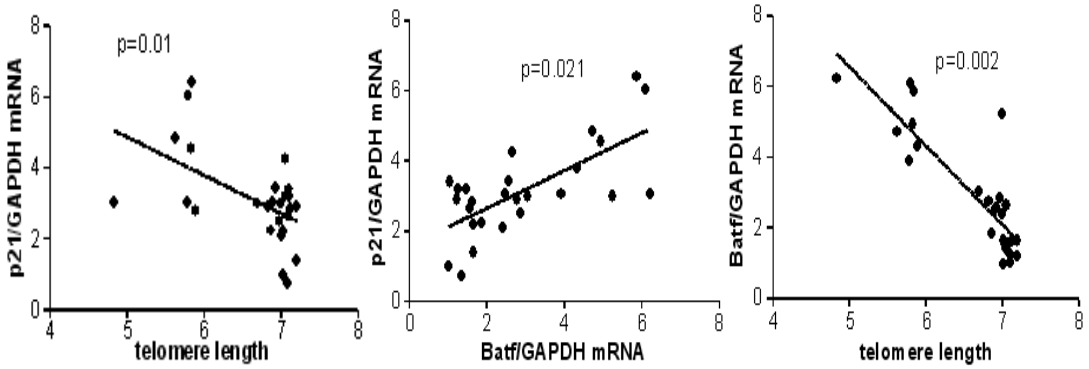

54 55 56

Figure 54-56: Telomere length and the mRNA expression of p16 and *Batf* (relative to *Gapdh*) was measured in CD34$^+$ human HSCs from patients with myelodysplastic syndromes (MDS, n= 26): The histograms show, Figure 54: the correlation between p21 mRNA level and telomere length, Figure 55: p21 mRNA level and *Batf* mRNA level, and Figure 56: Batf mRNA level and telomere length. Note that telomere shortening and the induction of p21 correlates with induction of *Batf* in human CD34$^+$ HSCs.

4. Discussion

My studies provide the first experimental evidence for a differentiation checkpoint limiting self-renewal of HSCs in response to telomere dysfunction or gamma-irradiation induced DNA damage. This checkpoint is BATF independent and involves the newly defined role of this transcription factor in regulating differentiation of HSCs into early hematopoietic progenitor cells.

4.1 BATF controls early lymphoid commitment of HSCs.

Early stages of lymphoid differentiation are still under investigation and only a few genetic components have been identified that regulate the formation of early lymphoid progenitor cells (Bell and Bhandoola 2010, Urbänek et al. 1994, Arinobu et al. 2007). This study shows that BATF contributes to the induction of early stages of lymphopoiesis. Previous studies revealed that germline deletion of BATF impairs formation of subpopulations T-helper cells (Betz et al. 2010, Schraml et al. 2009) as well as differentiation of peripheral B-lymphocytes (Betz et al. 2010). However, a role of BATF in differentiation of HSC into early hematopoietic progenitor cells was not shown in these studies. A possible explanation is that other AP1 transcription factors (e.g. BATF3, JUND or FOSB, Hess et al. 2004) compensate the function of BATF in early stages of hemato-lymphopoiesis in *Batf* germline knockout mice. The current study provides direct evidence that the knockdown of BATF in adult HSC impairs the formation of CLPs but not the formation of MPPs or CMPs. These data indicate that the formation of CLPs represent a step in hematolymphopoiesis, which partially depends on BATF.

4.2 BATF–dependent differentiation limits self-renewal of HSC in response to DNA damage.

Differentiation of melanocytic stem cell in the hair buldge occurs in response to gamma-irradiation induced DNA damage (Inomata et al. 2009). The current data provide experimental evidence that DNA damage induces a differentiation checkpoint in HSCs. These data support the hypothesis that differentiation in response to DNA damage may represent a general response of tissue stem cells to DNA damage. In this study we decipher the first molecular pathway controlling stem cell differentiation in response to genotoxic stress. Specifically, the study shows that DNA damage leads to G-CSF/STAT3 dependent upregulation of BATF in

HSCs, which in turn limits self-renewal and repopulation capacity of HSCs by induction of lymphoid differentiation. Thus, DNA damage leads to amplification of a differentiation pathway, which also contributes to differentiation of undamaged HSC into lymphoid progenitor cells. It remains to be seen whether the same concept applies to other stem cell compartments. It is tempting to speculate that genotoxic stress enhances tissue specific differentiation pathways in stem cells depending on the genetic and epigenetic programs controlling natural differentiation of stem cells in the respective tissue.

4.3 Stem cell differentiation checkpoints: implication for cancer protection?

Stem cell differentiation could represent an additional checkpoint mechanism to prevent survival of damaged stem cells and the initiation of stem cell derived cancers. The current study shows that classical checkpoint responses (such as cell cycle arrest and apoptosis) only partially account for the decrease in stem cell numbers in response to irradiation induced DNA damage. Instead, mathematical modeling revealed that differentiation represents a major component limiting maintenance of HSCs in response to DNA damage.

Mathematical models were validated by *in vivo* experiments in genetic mouse models showing that the knockdown or the knockout of components of this differentiation pathway (G-CSF/STAT3/BATF) can rescue the induction of differentiation and improves the maintenance of HSCs in response to DNA damage or telomere dysfunction. It remains elusive, why this additional checkpoint layer developed in the hematopoietic system. It is conceivable that the extreme quiescence of HSCs selected for an additional checkpoint layer protecting from accumulation of genetic damage. Recent studies showed that HSCs enter the cell cycle only once every 3-4 months (Wilson et al. 2008). It is conceivable that cell cycle arrest does not represent an efficient checkpoint response to prevent aberrant DNA repair in quiescent stem cells. Along these lines, it was recently shown that quiescent HSCs rely on error-prone non-homologues end joining for DNA repair (Mohrin et al. 2010). Since quiescent cells are also more resistant to DNA damage induced cell death (Sullivan et al. 1987), it is conceivable that apoptosis checkpoints could also fail to prevent the survival of quiescent HSCs harboring DNA damage. In quiescent stem cell compartments, induction of differentiation could thus represent a failsafe mechanism eliminating stem cells with high loads of genotoxic damage.

4.4 Stem cell differentiation checkpoints: implication for aging?

A current concept indicates that DNA damage checkpoints have a dual role preventing cancer formation but promoting tissues aging in the context of DNA damage. There is experimental evidence that deletion of DNA damage checkpoints can improve tissue integrity and lifespan in model system of accelerated aging, e.g. in the context of telomere dysfunction (Choudhury et al. 2007, Schaetzlein et al. 2007). The current study has identified a novel checkpoint limiting self-renewal and function of HSCs in response to DNA damage. This checkpoint was identified in an in vivo RNAi screen on oncogenes and tumor suppressor genes that also included a large set of shRNA targeting well known checkpoint genes limiting cell proliferation and survival in response to DNA damage, e.g. *Atm*, *Trp53*, *Gadd45a* and *Gadd45g*, *Caspase 3*, *Rad17*, a.o. (Table 4). Of note, *Batf* knockdown was by far the most strongly selected shRNA among these gene knockdowns indicating that BATF represents a major pathway limiting HSC function in response to DNA damage. It is conceivable that this newly defined pathway affects aging of the hematopoietic system since there is growing evidence that DNA damage accumulates in HSCs during aging in mice and humans (Rossi et al. 2007, Rübe et al. 2011).

Impaired replication potential and skewing of differentiation represent the most prominent aging phenotypes of the hematpoietic system. Studies on the cellular composition of bone marrow derived HSC in mice have revealed evidence that the HSC pool consists of distinct subpopulations that are biased to undergo myeloid differentiation or lymphoid differentiation (Challen et al. 2010). Aging associated skewing of hematopoiesis (reduction in lymphopoiesis and increase in myleopoiesis) was recently associated with an increased survival of myeloid competent HSCs in aging mice supporting a population shift model of HSC aging (Cho et al. 2008, Beerman et al. 2010). According to this model myeloid competent HSCs are selected and outcompete lymphoid competent HSCs during aging. The molecular mechanisms that control this selection process during aging are unknown. This study shows that BATF-dependent differentiation limits the repopulation capacity and self-renewal of HSCs in response to telomere dysfunction or gamma-irradiation. Lymphoid competent HSCs ($CD150^{lo}$) were more sensitive to BATF-induced HSC differentiation and were almost completely depleted in response to gamma-irradiation. These data indicate that BATF upregulation could represent a molecular pathway enhancing the ablation of lymphoid competent HSCs thereby

increasing skewing of hematopoiesis in response to aging associated DNA damage accumulation.

DNA damage dependent induction of BATF appears to be maintained in human HSCs since telomere shortening and activation of DNA damage signaling (p21) significantly associated with BATF upregualtion in human $CD34^+$ HSCs from aged patients with myelodysplastic syndromes. MDS patients show a progressive development of bone marrow failure and a strongly increased risk in the development of myeloid leukemia. It is tempting to speculate that the BATF-dependent depletion of lymphoid competent HSCs contributes to the preferential development of myeloid leukemia in this premalignant disease stage.

In summary, the current study has identified a novel BATF-dependent pathway controlling early lymphoid differentiation of HSCs. The study provides evidence that the same pathway functions as a differentiation checkpoint limiting self-renewal of HSCs in response to DNA damage or telomere dysfunction. These data support a new concept indicating that DNA damage limits stem cell self-renewal by activating pathways that control natural differentiation of undamaged stem cells. The newly discovered differentiation checkpoint appears to be conserved in human HSCs and could impact on age-associated changes in stem cell differentiation and transformation in the hematopoietic system.

5. Supplementary Data

5.1 Table 1: shRNAs targeting cancer related genes

The table is showing 1772 shRNA sequences targeting mouse orthologs of human cancer related genes compiled from microarray expression data and literature mining (Bric et al. 2009).

Gene Symbol	Gene Description	Ratio of enrichment in G3 mTerc-/- to mTerc+/+
Aass	aminoadipate-semialdehyde synthase	0,2381
Abcb11	ATP-binding cassette, sub-family B (MDR/TAP), member 11	1,8262
Abcb4	ATP-binding cassette, sub-family B (MDR/TAP), member 4	2,2727
Abcb6	ATP-binding cassette, sub-family B (MDR/TAP), member 6	2,4629
Abcb8	ATP-binding cassette, sub-family B (MDR/TAP), member 8	3,1111
Abcc1	ATP-binding cassette, sub-family C (CFTR/MRP), member 1	0,076
Abcc3	ATP-binding cassette, sub-family C (CFTR/MRP), member 3	0,0823
Abcg1	ATP-binding cassette, sub-family G (WHITE), member 1	0,1046
Abcg2	ATP-binding cassette, sub-family G (WHITE), member 2	0,1071
Abhd12	abhydrolase domain containing 12	5,0398
Abhd6	predicted gene 1833; abhydrolase domain containing 6	3,0827
Accn5	amiloride-sensitive cation channel 5, intestinal	2,6188
Acox3	acyl-Coenzyme A oxidase 3, pristanoyl	3,5367
Acss2	acyl-CoA synthetase short-chain family member 2	0,5627
Acss3	acyl-CoA synthetase short-chain family member 3	1,5985
Acta1	actin, alpha 1, skeletal muscle	3,5
Actb	actin, beta	1,9816
Actg1	predicted gene 8543; actin-like 8; predicted gene 7505; predicted gene 12715; predicted gene 12003; predicted gene 8399; predicted gene 6375; actin, gamma, cytoplasmic 1; similar to gamma-actin; predicted gene 4667; similar to cytoplasmic beta-actin; predicted gene 16385	0,3797
Actr8	ARP8 actin-related protein 8 homolog (S. cerevisiae)	0,4486
Actrt1	actin-related protein T1	0,3459
Adad1	adenosine deaminase domain containing 1 (testis specific); similar to Tenr protein	8,1875
Adss	adenylosuccinate synthetase, non muscle	11,6381
Ahr	aryl-hydrocarbon receptor	0,519
Aif1	allograft inflammatory factor 1	0,3683
Akr1b7	aldo-keto reductase family 1, member B7	0,0991
Akr1b8	aldo-keto reductase family 1, member B8	0,1591
Akr1c12	aldo-keto reductase family 1, member C12	0,2458
Akt3	thymoma viral proto-oncogene 3	6,6604
Alb	albumin	17,1667
Alpl	alkaline phosphatase, liver/bone/kidney	0,2658
Alx1	ALX homeobox 1	0,3976
Ankfy1	ankyrin repeat and FYVE domain containing 1	8,122
Ap1s2	adaptor-related protein complex 1, sigma 2 subunit	3,7983
Ap4b1	adaptor-related protein complex AP-4, beta 1	4,3788
Apaf1	apoptotic peptidase activating factor 1	2,2621

Apbb3	amyloid beta (A4) precursor protein-binding, family B, member 3	0,71
Apc	similar to adenomatosis polyposis coli; adenomatosis polyposis coli	6,3
Apoa1	apolipoprotein A-I	1,639
Apod	apolipoprotein D	1,6451
App	amyloid beta (A4) precursor protein	0,6957
Appbp2	amyloid beta precursor protein (cytoplasmic tail) binding protein 2	3,2195
Araf	v-raf murine sarcoma 3611 viral oncogene homolog	0,2669
Areg	amphiregulin	0,3107
Arf4	ADP-ribosylation factor 4	13,6571
Arg2	arginase type II	2,6282
Arhgap4	Rho GTPase activating protein 4	1,3111
Arhgdia	Rho GDP dissociation inhibitor (GDI) alpha	0,8136
Arl4c	similar to ADP-ribosylation factor-like protein 7; ADP-ribosylation factor-like 4C	1,0752
Arpc1a	actin related protein 2/3 complex, subunit 1A	20,8372
Arpc3	actin related protein 2/3 complex, subunit 3	21,0167
Arpc5	predicted gene 16372; actin related protein 2/3 complex, subunit 5	2,216
Asb6	ankyrin repeat and SOCS box-containing 6	1,0089
Ate1	arginyltransferase 1	3,9778
Atm	ataxia telangiectasia mutated homolog (human)	10,2
Atp6v0a1	ATPase, H+ transporting, lysosomal V0 subunit A1	1,1165
Atp9b	ATPase, class II, type 9B	1,7338
Atr	ataxia telangiectasia and Rad3 related	6,5
Bag1	BCL2-associated athanogene 1	0,1746
Baiap2	brain-specific angiogenesis inhibitor 1-associated protein 2	0,3151
Bak1	BCL2-antagonist/killer 1	0,1342
Batf	basic leucine zipper transcription factor, ATF-like	497,5
Bax	BCL2-associated X protein	2,5
Bcar1	breast cancer anti-estrogen resistance 1	2,4444
Bcar3	breast cancer anti-estrogen resistance 3	2,8768
Bcas1	breast carcinoma amplified sequence 1	4,6995
Bcas2	breast carcinoma amplified sequence 2	6,7847
Bcl2	predicted gene 3655; B-cell leukemia/lymphoma 2	8,2
Bcl2l2	BCL2-like 2	0,582
Bcl9	B-cell CLL/lymphoma 9	1,8047
Birc5	baculoviral IAP repeat-containing 5	0,7745
Bloc1s1	biogenesis of lysosome-related organelles complex-1, subunit 1; predicted gene 7936	0,7959
Bmi1	Bmi1 polycomb ring finger oncogene	0,828
Bmp1	bone morphogenetic protein 1	1,7891
Bmp10	bone morphogenetic protein 10	1,913
Bmp15	bone morphogenetic protein 15	2,3475
Bmp3	bone morphogenetic protein 3	36,525
Bmp5	bone morphogenetic protein 5	0,2826
Brca1	breast cancer 1	28
Brca2	breast cancer 2	30
Btc	betacellulin, epidermal growth factor family member	0,652
Bub1b	budding uninhibited by benzimidazoles 1 homolog, beta (S. cerevisiae)	10,152
Cadm2	cell adhesion molecule 2	0,0863

Capn11	calpain 11	19
Car2	carbonic anhydrase 2	0,0995
Car9	carbonic anhydrase 9	0,2468
Cartpt	CART prepropeptide	1,0813
Casp2	caspase 2	10,2
Casp3	caspase 3	1,4
Cast	calpastatin	23,1525
Cat	catalase	0,9172
Ccar1	cell division cycle and apoptosis regulator 1	2,0016
Ccdc101	coiled-coil domain containing 101	6,4675
Ccdc106	coiled-coil domain containing 106	0,3342
Ccdc124	coiled-coil domain containing 124	1,3779
Ccdc132	coiled-coil domain containing 132	1,5288
Ccdc15	coiled-coil domain containing 15	1,5686
Ccdc77	coiled-coil domain containing 77	6,8217
Ccdc85b	coiled-coil domain containing 85B	0,0551
Ccl12	chemokine (C-C motif) ligand 12; similar to monocyte chemoattractant protein-5	0,0554
Ccl20	chemokine (C-C motif) ligand 20	0,2338
Ccl24	chemokine (C-C motif) ligand 24	0,275
Ccna2	cyclin A2	2,4
Ccnb1	predicted gene 8416; predicted gene 5593; cyclin B1; similar to cyclin B1; predicted gene 4870	9,1144
Ccnb2	cyclin B2	0,9724
Ccnc	cyclin C	1,3803
Ccnd1	cyclin D1	1,3
Ccnd2	cyclin D2	0,2833
Ccnd3	similar to Cyclin D3; cyclin D3	1,3919
Ccne2	cyclin E2	0,3242
Ccnf	cyclin F	0,3568
Cd177	CD177 antigen	1,0912
Cd209c	similar to SIGNR2; CD209c antigen	0,2216
Cd22	CD22 antigen; hypothetical protein LOC100047973	2,0541
Cd27	CD27 antigen	3,3505
Cd34	CD34 antigen	1,3056
CD44	CD44 antigen	5,6
Cd84	CD84 antigen	0,2317
Cd8b1	CD8 antigen, beta chain 1	0,1708
Cdc25a	cell division cycle 25 homolog A (S. pombe)	0,0974
Cdc25c	cell division cycle 25 homolog C (S. pombe)	0,1103
Cdc42	cell division cycle 42 homolog (S. cerevisiae); predicted gene 7407	0,2525
Cdc42ep3	CDC42 effector protein (Rho GTPase binding) 3	0,6329
Cdc5l	predicted gene 9040; predicted gene 9046; predicted gene 9029; predicted gene 9048; cell division cycle 5-like (S. pombe); predicted gene 9049; predicted gene 9044; predicted gene 9030; predicted gene 9045	1,799
Cdc6	cell division cycle 6 homolog (S. cerevisiae); predicted gene 9430; similar to cell division cycle 6 homolog	14,4
Cdc7	cell division cycle 7 (S. cerevisiae)	1,26
Cdh1	cadherin 1	18,0909
Cdh10	cadherin 10	0,6767
Cdh15	cadherin 15	2,1295

Cdh2	cadherin 2; similar to N-cadherin	2,6026
Cdh3	cadherin 3	2,9774
Cdh7	cadherin 7, type 2	3,0376
Cdh8	cadherin 8	6,9686
Cdk10	cyclin-dependent kinase (CDC2-like) 10; predicted gene 6473	0,7208
Cdk2	cyclin-dependent kinase 2	8,2
Cdk4	similar to Cell division protein kinase 4 (Cyclin-dependent kinase 4) (PSK-J3) (CRK3); cyclin-dependent kinase 4	1,1429
Cdk5	cyclin-dependent kinase 5	1,1239
Cdk6	cyclin-dependent kinase 6	1,3469
Cdk7	cyclin-dependent kinase 7 (homolog of Xenopus MO15 cdk-activating kinase)	2,3492
Cdk8	predicted gene 7107; cyclin-dependent kinase 8	2,9462
Cdkn2b	similar to Cyclin-dependent kinase 4 inhibitor B (p14-INK4b) (p15-INK4b); cyclin-dependent kinase inhibitor 2B (p15, inhibits CDK4)	5,2159
Cdkn3	cyclin-dependent kinase inhibitor 3	4,2478
Cdx2	caudal type homeo box 2	0,4707
Cebpg	CCAAT/enhancer binding protein (C/EBP), gamma	1,2
Chd5	chromodomain helicase DNA binding protein 5	0,2765
Chek1	checkpoint kinase 1 homolog (S. pombe)	1,4
Chek2	CHK2 checkpoint homolog (S. pombe)	2,1
Chn2	chimerin (chimaerin) 2	1,4901
Chodl	chondrolectin	0,0229
Chst5	carbohydrate (N-acetylglucosamine 6-O) sulfotransferase 5	0,0843
Ckap4	cytoskeleton-associated protein 4	0,4477
Cklf	chemokine-like factor	0,3507
Cks1b	predicted gene 10124; predicted gene 6340; CDC28 protein kinase 1b	28,7516
Clca2	chloride channel calcium activated 2	19,381
Clca5	chloride channel calcium activated 5	32,8925
Cldn1	claudin 1	1,1144
Cldn11	claudin 11	1,2416
Cldn4	claudin 4	4,2871
Clec4a3	C-type lectin domain family 4, member a3	0,1479
Clns1a	chloride channel, nucleotide-sensitive, 1A	0,214
Cnga3	cyclic nucleotide gated channel alpha 3	0,4359
Cog3	component of oligomeric golgi complex 3	4,2059
Col11a1	collagen, type XI, alpha 1	1,2903
Col17a1	collagen, type XVII, alpha 1	1,2584
Col4a1	collagen, type IV, alpha 1	16,6319
Col4a4	collagen, type IV, alpha 4	0,344
Col4a6	collagen, type IV, alpha 6	0,4286
Col5a1	collagen, type V, alpha 1	12,6307
Col5a2	collagen, type V, alpha 2	32,425
Col6a3	collagen, type VI, alpha 3	1,135
Col9a1	collagen, type IX, alpha 1	0,4845
Col9a3	collagen, type IX, alpha 3	0,7568
Cope	coatomer protein complex, subunit epsilon	5,6962
Cox6a2	cytochrome c oxidase, subunit VI a, polypeptide 2	0,0574
Cpa2	carboxypeptidase A2, pancreatic	0,255
Cpb1	carboxypeptidase B1 (tissue)	0,2855

Cpne3	copine III	14,2644
Crabp2	cellular retinoic acid binding protein II	2,6723
Crebbp	CREB binding protein	20,1831
Crkl	v-crk sarcoma virus CT10 oncogene homolog (avian)-like	0,1733
Cryba1	crystallin, beta A1	0,1388
Cse1l	chromosome segregation 1-like (S. cerevisiae)	0,4947
Csf1	colony stimulating factor 1 (macrophage)	0,7193
Csf2	colony stimulating factor 2 (granulocyte-macrophage)	4,1899
Csn2	casein beta	0,1881
Csnk1e	casein kinase 1, epsilon	0,3886
Csrp2	cysteine and glycine-rich protein 2	5,4052
Ctgf	connective tissue growth factor	12,6729
Ctnnb1	catenin (cadherin associated protein), beta 1	0,3425
Ctsb	cathepsin B	0,8468
Ctsc	cathepsin C	1,8456
Ctsd	cathepsin D	4,4355
Ctse	cathepsin E	0,3471
Ctsg	cathepsin G	0,6044
Ctsh	cathepsin H	2,8717
Ctsk	cathepsin K	4,4717
Ctso	cathepsin O	12,6557
Ctsz	cathepsin Z	0,2007
Cxcl3	chemokine (C-X-C motif) ligand 3	0,3234
Cxcl5	similar to LPS-induced CXC chemokine; chemokine (C-X-C motif) ligand 5	0,7717
Cyct	cytochrome c, testis	0,1184
Cyp17a1	cytochrome P450, family 17, subfamily a, polypeptide 1	0,5918
Cyp19a1	cytochrome P450, family 19, subfamily a, polypeptide 1	0,7107
Cyp1a1	cytochrome P450, family 1, subfamily a, polypeptide 1	0,162
Cyp1a2	cytochrome P450, family 1, subfamily a, polypeptide 2	0,25
Cyp1b1	cytochrome P450, family 1, subfamily b, polypeptide 1	0,4778
Cyp24a1	cytochrome P450, family 24, subfamily a, polypeptide 1	6,6596
Cyp2b23	cytochrome P450, family 2, subfamily b, polypeptide 23	0,8659
Cyp2c29	cytochrome P450, family 2, subfamily c, polypeptide 29	0,8904
Cyp2c37	similar to cytochrome P450; CYP2C37; cytochrome P450, family 2. subfamily c, polypeptide 37	0,1823
Cyp2c44	cytochrome P450, family 2, subfamily c, polypeptide 44	1,383
Cyp2c55	cytochrome P450, family 2, subfamily c, polypeptide 55	0,491
Cyp2d22	cytochrome P450, family 2, subfamily d, polypeptide 22	1,038
Cyp2g1	cytochrome P450, family 2, subfamily g, polypeptide 1	2,7973
Cyp2j8	cytochrome P450, family 2, subfamily j, polypeptide 8	3,1172
Cyp2s1	cytochrome P450, family 2, subfamily s, polypeptide 1	3,7325
Cyp3a11	cytochrome P450, family 3, subfamily a, polypeptide 11	25,9512
Cyp3a41a	cytochrome P450, family 3, subfamily a, polypeptide 41A; cytochrome P450, family 3, subfamily a, polypeptide 41B	26,2338
Cyp3a44	cytochrome P450, family 3, subfamily a, polypeptide 44	1,2056
Cyp4v3	cytochrome P450, family 4, subfamily v, polypeptide 3	0,1129
Cyr61	cysteine rich protein 61	6,25
Cysltr1	cysteinyl leukotriene receptor 1	0,0571
Cytl1	cytokine-like 1	0,1913

D16Ertd472e	DNA segment, Chr 16, ERATO Doi 472, expressed	1,9326
Dap3	death associated protein 3	1,1135
Dapk2	death-associated protein kinase 2	3,0766
Dcc	deleted in colorectal carcinoma	6,3125
Dcn	decorin	3,8953
Dcp2	DCP2 decapping enzyme homolog (S. cerevisiae)	0,7398
Dctd	dCMP deaminase	0,4817
Dctn3	dynactin 3	1,4371
Ddr2	discoidin domain receptor family, member 2	0,6809
Ddx11	DEAD/H (Asp-Glu-Ala-Asp/His) box polypeptide 11 (CHL1-like helicase homolog, S. cerevisiae)	1,0882
Des	desmin	0,4982
Dhfr	dihydrofolate reductase	0,6516
Dimt1	DIM1 dimethyladenosine transferase 1-like (S. cerevisiae)	0,6745
Dll1	delta-like 1 (Drosophila)	0,128
Dnahc11	dynein, axonemal, heavy chain 11	1,6082
Dnahc14	dynein, axonemal, heavy chain 14	6,1688
Dnajb9	predicted gene 6568; DnaJ (Hsp40) homolog, subfamily B, member 9	0,6578
Dnajc12	DnaJ (Hsp40) homolog, subfamily C, member 12	2,7923
Dnajc4	DnaJ (Hsp40) homolog, subfamily C, member 4	0,6887
Dnm1	dynamin 1	1,5987
Dnmt1	DNA methyltransferase (cytosine-5) 1	0,7396
Dnmt3b	DNA methyltransferase 3B	0,9338
Dpm2	dolichol-phosphate (beta-D) mannosyltransferase 2	1,4173
Dtx1	deltex 1 homolog (Drosophila)	0,4744
Dysf	dysferlin	0,385
E2f2	E2F transcription factor 2	0,0751
E2f4	E2F transcription factor 4	0,1246
E2f6	E2F transcription factor 6	0,3989
Ear1	eosinophil-associated, ribonuclease A family, member 8; eosinophil-associated, ribonuclease A family, member 1	6,279
Ebf4	early B-cell factor 4	1,9919
Ecel1	endothelin converting enzyme-like 1	5,5991
Eef1a1	predicted gene 5869; predicted gene 7161; predicted gene 7105; predicted gene 5822; similar to eukaryotic translation elongation factor 1 alpha 1; predicted gene 6192; predicted gene 6392; predicted gene 6767; predicted gene 6170; predicted gene 6548; predicted gene 6789; eukaryotic translation elongation factor 1 alpha 1	2,3
Efna2	ephrin A2	6,6543
Efnb1	ephrin B1	28,782
Egf	epidermal growth factor	30,5668
Egfbp2	epidermal growth factor binding protein type B; kallikrein 1-related petidase b26; similar to EGF-binding protein	3,0186
Egfr	epidermal growth factor receptor	3,2993
Egr2	early growth response 2	3,8589
Ehbp1l1	EH domain binding protein 1-like 1	3,8973
Eif1ay	eukaryotic translation initiation factor 1A, Y-linked	2
Eif2ak2	eukaryotic translation initiation factor 2-alpha kinase 2	2,3901
Eif3e	eukaryotic translation initiation factor 3, subunit E	2,5439
Eif3h	eukaryotic translation initiation factor 3, subunit H; predicted gene 6552	0,0697
Eif4e	hypothetical LOC630527; eukaryotic translation initiation factor 4E; similar to eukaryotic translation initiation factor 4E	7,8734
Elf3	E74-like factor 3	0,9681

Elf5	E74-like factor 5	1,8853
Elk3	ELK3, member of ETS oncogene family	4,2302
Emp1	epithelial membrane protein 1	0,2271
Eno2	enolase 2, gamma neuronal	6,001
Eno3	enolase 3, beta muscle	6,246
Ep300	E1A binding protein p300	6,5
Epgn	epithelial mitogen	0,3833
Eps8	epidermal growth factor receptor pathway substrate 8	0,1884
Erbb2	v-erb-b2 erythroblastic leukemia viral oncogene homolog 2, neuro/glioblastoma derived oncogene homolog (avian)	0,3064
Erbb3	v-erb-b2 erythroblastic leukemia viral oncogene homolog 3 (avian)	0,3573
Erbb4	v-erb-a erythroblastic leukemia viral oncogene homolog 4 (avian)	0,2
Ercc1	excision repair cross-complementing rodent repair deficiency, complementation group 1	2,6
Ercc3	excision repair cross-complementing rodent repair deficiency, complementation group 3	0,91
Ercc4	excision repair cross-complementing rodent repair deficiency, complementation group 4	8,3
Ercc5	excision repair cross-complementing rodent repair deficiency, complementation group 5	6,3
Ercc6	excision repair cross-complementing rodent repair deficiency, complementation group 6	1,8
Erf	Ets2 repressor factor	0,8138
Esr1	estrogen receptor 1 (alpha)	0,6562
Etv6	ets variant gene 6 (TEL oncogene)	0,6782
Ewsr1	predicted gene 6627; Ewing sarcoma breakpoint region 1	2,3524
Exo1	exonuclease 1	2,1
Extl1	exostoses (multiple)-like 1	0,0222
F2r	coagulation factor II (thrombin) receptor	0,0246
F3	coagulation factor III	31,3256
F7	coagulation factor VII	1,3361
F8	coagulation factor VIII	1,7227
Fabp3	fatty acid binding protein 3, muscle and heart; similar to mammary-derived growth inhibitor	0,1309
Fabp7	fatty acid binding protein 7, brain	0,2453
Fadd	Fas (TNFRSF6)-associated via death domain	0,0832
Fads2	fatty acid desaturase 2	0,706
Fap	fibroblast activation protein	0,5243
Fasl	Fas ligand (TNF superfamily, member 6)	0,1209
Fasn	fatty acid synthase	12,8897
Fbl	similar to Fibrillarin; fibrillarin	0,3559
Fbxo4	F-box protein 4	22,1905
Fgf10	fibroblast growth factor 10	10,2
Fgf12	fibroblast growth factor 12	0,415
Fgf13	fibroblast growth factor 13	5,0919
Fgf14	fibroblast growth factor 14	13,3811
Fgf15	fibroblast growth factor 15	17,1973
Fgf16	fibroblast growth factor 16	0,932
Fgf18	fibroblast growth factor 18	0,8155
Fgf2	fibroblast growth factor 2	1,6691
Fgf23	similar to FGF23; fibroblast growth factor 23	0,3342
Fgf4	fibroblast growth factor 4	3,5217
Fgf5	fibroblast growth factor 5	0,0624
Fgf6	fibroblast growth factor 6	0,0818

Fgf7	fibroblast growth factor 7	0,098
Fgfr2	fibroblast growth factor receptor 2	0,1342
Fgfr4	fibroblast growth factor receptor 4	0,5249
Fgr	Gardner-Rasheed feline sarcoma viral (Fgr) oncogene homolog	1,8943
Fhit	fragile histidine triad gene	5,5976
Fkbp4	FK506 binding protein 4	1,5039
Fkbpl	FK506 binding protein-like	1,8137
Fmnl1	formin-like 1	3,9383
Fn1	fibronectin 1	0,5408
Fndc4	fibronectin type III domain containing 4	1,0125
Fos	FBJ osteosarcoma oncogene	18,1252
Fosl1	fos-like antigen 1	5,4136
Foxn3	forkhead box N3	2,9492
Frk	fyn-related kinase	0,2117
Fxyd3	FXYD domain-containing ion transport regulator 3	21,7788
Fyn	Fyn proto-oncogene	0,1892
Fzd2	frizzled homolog 2 (Drosophila)	15,7778
Fzd7	frizzled homolog 7 (Drosophila)	17,192
Fzd9	frizzled homolog 9 (Drosophila)	21,3368
G3bp1	Ras-GTPase-activating protein SH3-domain binding protein 1	2,1739
Gabra2	gamma-aminobutyric acid (GABA) A receptor, subunit alpha 2; similar to Gamma-aminobutyric-acid receptor subunit alpha-2 precursor (GABA(A) receptor subunit alpha-2)	0,6384
Gabra3	gamma-aminobutyric acid (GABA) A receptor, subunit alpha 3	0,7472
Gabrb2	gamma-aminobutyric acid (GABA) A receptor, subunit beta 2	0,758
Gadd45a	growth arrest and DNA-damage-inducible 45 alpha	13,2
Gadd45g	growth arrest and DNA-damage-inducible 45 gamma	9,8
Galnt2	UDP-N-acetyl-alpha-D-galactosamine:polypeptide N-acetylgalactosaminyltransferase 2	2,557
Gas8	growth arrest specific 8	6,4741
Gata3	GATA binding protein 3	2,6552
Gck	glucokinase	0,0982
Gdap2	ganglioside-induced differentiation-associated-protein 2	0,7612
Gjb2	gap junction protein, beta 2	1,7238
Gli2	GLI-Kruppel family member GLI2	0,0583
Gli3	GLI-Kruppel family member GLI3	0,0783
Glo1	glyoxalase 1	3,6145
Glra4	glycine receptor, alpha 4 subunit	2,5922
Glul	predicted gene 4949; glutamate-ammonia ligase (glutamine synthetase)	0,1704
Gm1096	predicted gene 1096	1,3244
Gm270	hypothetical LOC667488	8,307
Gng3	guanine nucleotide binding protein (G protein), gamma 3	0,1334
Gng7	guanine nucleotide binding protein (G protein), gamma 7	0,1512
Gpd1	glycerol-3-phosphate dehydrogenase 1 (soluble)	2,4377
Gpnmb	glycoprotein (transmembrane) nmb	2,7789
Gpr34	G protein-coupled receptor 34	0,2893
Gprc2a-rs5	vomeronasal 2, receptor 61; G protein-coupled receptor, family C, group 2, member A, related sequence 5; vomeronasal 2, receptor, pseudogene 60; vomeronasal 2, receptor, pseudogene 57; vomeronasal 2, receptor 60	0,1426
Gpx2	glutathione peroxidase 2	0,7683

Grb10	growth factor receptor bound protein 10	0,7774
Grb2	growth factor receptor bound protein 2; predicted gene 12791	2,3
Grb7	growth factor receptor bound protein 7	0,1067
Gstm1	similar to Glutathione S-transferase Mu 1 (GST class-mu 1) (Glutathione S-transferase GT8.7) (pmGT10) (GST 1-1); predicted gene 5562; glutathione S-transferase, mu 1	0,4141
Gstp1	glutathione S-transferase, pi 2; glutathione S-transferase, pi 1; similar to glutathione S-transferase pi class A; predicted gene 3934	2,0833
Gstt2	glutathione S-transferase, theta 2	2,2344
Gtf2b	general transcription factor IIB	0,0507
Guk1	guanylate kinase 1	0,2065
Gulo	gulonolactone (L-) oxidase	0,3047
Hat1	histone aminotransferase 1	22
Hbs1l	similar to Hbs1l protein; predicted gene 9923; Hbs1-like (S. cerevisiae)	1,3533
Hck	hemopoietic cell kinase	17,0242
Hdac2	histone deacetylase 2	2,2065
Hdac3	histone deacetylase 3	2,6517
Heatr5b	HEAT repeat containing 5B; similar to CG2747-PB, isoform B	4,1947
Hecw1	HECT, C2 and WW domain containing E3 ubiquitin protein ligase 1	5,8686
Hepacam	hepatocyte cell adhesion molecule	0,1041
Hgf	hepatocyte growth factor	0,1336
Hif1a	hypoxia inducible factor 1, alpha subunit	11,1204
Hltf	helicase-like transcription factor	15,9231
Hmgb1	high-mobility group (nonhistone chromosomal) protein 1-like 1;	15,4
Hmha1	histocompatibility (minor) HA-1	1,9069
Hmmr	hyaluronan mediated motility receptor (RHAMM)	6,4625
Hmx1	H6 homeo box 1	3,3476
Hnrnpa1	heterogeneous nuclear ribonucleoprotein A1-like 2	0,4555
Hoxb6	homeo box B6	4,2627
Hoxb7	homeo box B7	4,7649
Hpca	hippocalcin	0,7544
Hrg	histidine-rich glycoprotein	1,8872
Ibsp	similar to Integrin binding sialoprotein; integrin binding sialoprotein	0,7202
Id1	inhibitor of DNA binding 1	0,0791
Id2	inhibitor of DNA binding 2	0,0881
Ier2	immediate early response 2	11,5625
Ier5	immediate early response 5	17,6436
Ifna13	interferon alpha 13	3,3992
Ifna4	interferon alpha 4	0,1132
Ifng	interferon gamma	0,2168
Igf1	insulin-like growth factor 1	0,0662
Igf1r	insulin-like growth factor I receptor	0,622
Igf2	insulin-like growth factor 2	0,0686
Igfbp3	insulin-like growth factor binding protein 3	0,0741
Igfbp4	insulin-like growth factor binding protein 4	0,0973
Igfbp5	insulin-like growth factor binding protein 5	0,1419
Igfbp7	insulin-like growth factor binding protein 7	0,1921
Ikbkap	inhibitor of kappa light polypeptide enhancer in B-cells, kinase complex-associated protein	0,1681
Il10	interleukin 10	0,4086
Il11	interleukin 11	0,4514

Il13	interleukin 13	0,7289
Il19	interleukin 19	1,843
Il1b	interleukin 1 beta	0,2481
Il20	interleukin 20	1,9776
Il3	interleukin 3	2,2106
Il6	interleukin 6	5,0311
Il7	interleukin 7	0,2656
Ilk	integrin linked kinase; predicted gene 6263	1,239
Ins1	insulin I	0,2213
Ins2	insulin II	1,7878
Insl5	insulin-like 5	0,7236
Insl6	insulin-like 6	0,0262
Insr	insulin receptor	0,0772
Ints4	integrator complex subunit 4	0,7055
Irs1	insulin receptor substrate 1	0,1659
Isca1	iron-sulfur cluster assembly 1 homolog (S. cerevisiae)	0,2718
Isoc1	isochorismatase domain containing 1	0,3646
Itga6	integrin alpha 6	6,475
Itgav	integrin alpha V	9,3141
Itgax	integrin alpha X	12,9647
Itgb3	integrin beta 3	18,8459
Itgb4	integrin beta 4	1,104
Ivd	isovaleryl coenzyme A dehydrogenase	0,4874
Ivns1abp	influenza virus NS1A binding protein	0,0608
Jag1	jagged 1	0,6163
Jag2	jagged 2	0,8919
Jun	Jun oncogene	1,2169
Jup	junction plakoglobin	2,8745
Kcnj12	potassium inwardly-rectifying channel, subfamily J, member 12	5,2011
Kifc3	kinesin family member C3	0,1942
Klk1	kallikrein 1	3,2549
Klk10	kallikrein related-peptidase 10	0,1648
Klk1b1	kallikrein 1-related peptidase b1	3,6098
Klk1b11	kallikrein 1-related peptidase b11	6,5326
Klk1b21	kallikrein 1-related peptidase b21	6,5412
Klk1b22	kallikrein 1-related peptidase b22	6,779
Klk1b24	kallikrein 1-related peptidase b24	8,822
Klk1b26	epidermal growth factor binding protein type B; kallikrein 1-related petidase b26; similar to EGF-binding protein	3,9466
Klk1b4	kallikrein 1-related pepidase b4	3,5497
Klk1b5	kallikrein 1-related peptidase b5	9,3642
Klk1b9	kallikrein 1-related peptidase b9	0,1833
Klk6	kallikrein related-peptidase 6	0,1935
Klk7	kallikrein related-peptidase 7 (chymotryptic, stratum corneum)	0,2039
Klri2	killer cell lectin-like receptor family I member 2; similar to killer cell lectin-like receptor family I member 2	0,0791
Kri1	KRI1 homolog (S. cerevisiae)	0,2801
Krit1	KRIT1, ankyrin repeat containing	0,2937
Krt13	keratin 13	0,205

Krt15	keratin 15	0,2805
Krt17	keratin 17	0,3372
Krt18	keratin 18	0,5651
Krt19	keratin 19	8,4766
Krt75	keratin 75	0,7562
Krt76	keratin 76	0,0527
L2hgdh	L-2-hydroxyglutarate dehydrogenase; predicted gene 7842	0,3017
Lama1	laminin, alpha 1	0,4744
Lamb1-1	laminin B1 subunit 1	0,3534
Lancl3	LanC lantibiotic synthetase component C-like 3 (bacterial)	0,5523
Lasp1	LIM and SH3 protein 1	15,7643
Lefty1	left right determination factor 1	1,3474
Lep	leptin	1,5547
Lgals1	lectin, galactose binding, soluble 1	1,7209
Lgals4	lectin, galactose binding, soluble 6; hypothetical protein LOC100044254; lectin, galactose binding, soluble 4	1,9666
Lgals6	lectin, galactose binding, soluble 6; hypothetical protein LOC100044254; lectin, galactose binding, soluble 4	0,4209
Lgals9	lectin, galactose binding, soluble 9	0,5872
Lgi4	leucine-rich repeat LGI family, member 4	7,851
Lif	leukemia inhibitory factor	10,7277
Lima1	LIM domain and actin binding 1	15,8542
Lmbrd2	LMBR1 domain containing 2	18,1595
Lrrc20	leucine rich repeat containing 20	1,9103
Lrrc32	leucine rich repeat containing 32	2,2727
Lrrc8d	leucine rich repeat containing 8D	4,2199
Lum	lumican	19,9925
Lyn	Yamaguchi sarcoma viral (v-yes-1) oncogene homolog	94
Mafg	similar to mafG; v-maf musculoaponeurotic fibrosarcoma oncogene family, protein G (avian)	1,6439
Mamld1	mastermind-like domain containing 1	0,0561
Man2b1	mannosidase 2, alpha B1	27,2886
Man2c1	mannosidase, alpha, class 2C, member 1	28,3391
Map2k1	mitogen-activated protein kinase kinase 1	2,0538
Map2k2	mitogen-activated protein kinase kinase 2	2,1481
Map2k3	mitogen-activated protein kinase kinase 3	2,1817
Map2k4	mitogen-activated protein kinase kinase 4	2,7184
Map2k5	mitogen-activated protein kinase kinase 5	3,5377
Map2k6	mitogen-activated protein kinase kinase 6	3,7077
Map2k7	predicted gene 14378; similar to transforming growth factor, beta receptor III (betaglycan, 300kDa); mitogen-activated protein kinase kinase 7	1,783
Map3k10	mitogen-activated protein kinase kinase kinase 10	3,712
Map3k2	mitogen-activated protein kinase kinase kinase 2	6,0606
Map4k5	mitogen-activated protein kinase kinase kinase kinase 5	8,0505
Mapk1	mitogen-activated protein kinase 1	0,1162
Mapk11	mitogen-activated protein kinase 11	0,399
Mapk12	mitogen-activated protein kinase 12	5,6
Mapk3	mitogen-activated protein kinase 3	0,0961
Mapk4	mitogen-activated protein kinase 4	0,4299
Mapk6	similar to Mitogen-activated protein kinase 6 (Extracellular signal-regulated kinase 3) (ERK-3); predicted gene 2587; mitogen-activated protein kinase 6; similar to Mapk6 protein	2,2243

Mapk8	mitogen-activated protein kinase 8	1,3154
Mapk9	mitogen-activated protein kinase 9	1,7377
Mapre3	microtubule-associated protein, RP/EB family, member 3	3,8101
Mark4	MAP/microtubule affinity-regulating kinase 4	0,5674
Max	similar to Myn protein; Max protein	2,2297
Mbip	MAP3K12 binding inhibitory protein 1	0,0555
Mc3r	melanocortin 3 receptor	0,3488
Mcam	melanoma cell adhesion molecule	0,3547
Mcc	mutated in colorectal cancers	4,188
Mcm10	minichromosome maintenance deficient 10 (S. cerevisiae)	23,1
Mcm3	minichromosome maintenance deficient 3 (S. cerevisiae)	2,5
Mcm7	minichromosome maintenance deficient 7 (S. cerevisiae)	2,2
Mcph1	microcephaly, primary autosomal recessive 1	3,7006
Mdga2	MAM domain containing glycosylphosphatidylinositol anchor 2	24,8693
Met	met proto-oncogene	0,5053
Mfge8	milk fat globule-EGF factor 8 protein	4,021
Mgp	matrix Gla protein	0,091
Mkl2	MKL/myocardin-like 2	8,7316
Mllt11	myeloid/lymphoid or mixed-lineage leukemia (trithorax homolog, Drosophila); translocated to, 11	0,3426
Mmp13	matrix metallopeptidase 13	0,0931
Mmp14	matrix metallopeptidase 14 (membrane-inserted)	0,1101
Mmp17	matrix metallopeptidase 17	0,1129
Mmp19	matrix metallopeptidase 19	0,1516
Mmp1a	matrix metallopeptidase 1a (interstitial collagenase)	0,8753
Mmp1b	matrix metallopeptidase 1b (interstitial collagenase)	0,9423
Mmp25	matrix metallopeptidase 25	1,1279
Mmp9	matrix metallopeptidase 9	0,2179
Mobkl2c	MOB1, Mps One Binder kinase activator-like 2C (yeast)	11,6196
Mobkl3	MOB1, Mps One Binder kinase activator-like 3 (yeast)	22,3288
Mpp6	membrane protein, palmitoylated 6 (MAGUK p55 subfamily member 6)	0,4037
Mras	muscle and microspikes RAS	1,5097
Mrpl2	mitochondrial ribosomal protein L2	8,7651
Mrpl32	mitochondrial ribosomal protein L32	10,5604
Mrps30	mitochondrial ribosomal protein S30	0,1266
Mst1r	macrophage stimulating 1 receptor (c-met-related tyrosine kinase)	20,3481
Mt3	metallothionein 3	1,4458
Mthfs	5, 10-methenyltetrahydrofolate synthetase; predicted gene 2372; predicted gene 2382	3,0854
Muc1	mucin 1, transmembrane	1,2625
Mxd1	MAX dimerization protein 1	0,2827
Myb	myeloblastosis oncogene	0,2312
Myc	myelocytomatosis oncogene	0,2786
Mycbp	c-myc binding protein	0,0234
Mylk	myosin, light polypeptide kinase	0,6599
Myom2	myomesin 2	0,4275
Nans	N-acetylneuraminic acid synthase (sialic acid synthase)	0,7983
Nbl1	neuroblastoma, suppression of tumorigenicity 1	0,1028
Ncf4	neutrophil cytosolic factor 4	2,8343

Ncoa2	nuclear receptor coactivator 2	1,9316
Ncoa4	predicted gene 6768; nuclear receptor coactivator 4	2,8105
Ndufa5	NADH dehydrogenase (ubiquinone) 1 alpha subcomplex, 5	1,2515
Nefl	neurofilament, light polypeptide	0,1467
Nek4	NIMA (never in mitosis gene a)-related expressed kinase 4	11,7674
Nek7	NIMA (never in mitosis gene a)-related expressed kinase 7	26,1854
Neurod4	neurogenic differentiation 4	1,2281
Nhedc1	Na+/H+ exchanger domain containing 1	0,7831
Nhlrc3	NHL repeat containing 3	3,1149
Nme1	similar to Nucleoside diphosphate kinase A (NDK A) (NDP kinase A) (Tumor metastatic process-associated protein) (Metastasis inhibition factor NM23) (NDPK-A) (nm23-M1); non-metastatic cells 1, protein (NM23A) expressed in	0,1411
Nme2	predicted gene 7730; non-metastatic cells 2, protein (NM23B) expressed in; predicted gene 5566; predicted gene 5425; similar to Nucleoside diphosphate kinase B (NDK B) (NDP kinase B) (P18)	3,0662
Nol3	nucleolar protein 3 (apoptosis repressor with CARD domain)	0,2431
Nox4	NADPH oxidase 4	0,7063
Nphs1	nephrosis 1 homolog, nephrin (human)	0,0731
Npy2r	neuropeptide Y receptor Y2	1,2568
Nr0b1	nuclear receptor subfamily 0, group B, member 1	5,3374
Nr0b2	nuclear receptor subfamily 0, group B, member 2	0,1034
Nr1d1	nuclear receptor subfamily 1, group D, member 1	0,3238
Nr1h3	nuclear receptor subfamily 1, group H, member 3	0,3442
Nr1h4	nuclear receptor subfamily 1, group H, member 4	0,6048
Nr1i3	nuclear receptor subfamily 1, group I, member 3	0,6138
Nr2c1	nuclear receptor subfamily 2, group C, member 1	0,317
Nr2e1	nuclear receptor subfamily 2, group E, member 1	0,4045
Nr2e3	nuclear receptor subfamily 2, group E, member 3	0,4046
Nr2f1	nuclear receptor subfamily 2, group F, member 1	0,6322
Nr3c1	nuclear receptor subfamily 3, group C, member 1	0,7326
Nr3c2	nuclear receptor subfamily 3, group C, member 2	0,7922
Nr4a1	nuclear receptor subfamily 4, group A, member 1	1,7294
Nr4a2	nuclear receptor subfamily 4, group A, member 2	0,1354
Nr4a3	nuclear receptor subfamily 4, group A, member 3	0,1525
Nr6a1	nuclear receptor subfamily 6, group A, member 1	0,1947
Nrg1	neuregulin 1	0,0741
Nrip1	nuclear receptor interacting protein 1	3,8598
Nt5dc1	5'-nucleotidase domain containing 1	3,7104
Nt5e	5' nucleotidase, ecto	1,5748
Ntsr1	similar to neurotensin receptor type 1; neurotensin receptor 1	2,6258
Nubp2	nucleotide binding protein 2	0,5461
Nudt19	nudix (nucleoside diphosphate linked moiety X)-type motif 19	0,5864
Nudt2	nudix (nucleoside diphosphate linked moiety X)-type motif 2	1,6641
Nudt4	nudix (nucleoside diphosphate linked moiety X)-type motif 4; similar to Nudt4 protein	7,0753
Nupr1	nuclear protein 1	6,9
Odz1	odd Oz/ten-m homolog 1 (Drosophila); similar to odd Oz/ten-m homolog 1 (Drosophila)	0,197
Ofd1	oral-facial-digital syndrome 1 gene homolog (human)	2,0683
Ogt	O-linked N-acetylglucosamine (GlcNAc) transferase (UDP-N-acetylglucosamine:polypeptide-N-acetylglucosaminyl transferase)	0,9298
Olfml2a	olfactomedin-like 2A	0,318

Olfr1085	hypothetical protein LOC100044199; olfactory receptor 1083; olfactory receptor 1085	10,2569
Olfr1093	olfactory receptor 1093	0,3542
Olfr1106	olfactory receptor 1106	0,5871
Olfr113	olfactory receptor 113	0,6965
Olfr1132	olfactory receptor 1132	2,757
Olfr114	olfactory receptor 114	3
Olfr116	olfactory receptor 116	3,7562
Olfr1161	olfactory receptor 1161	5,3375
Olfr1179	olfactory receptor 1179	5,9832
Olfr125	olfactory receptor 125	7,0163
Olfr127	olfactory receptor 127	11,437
Olfr1350	olfactory receptor 1350	0,2315
Olfr1356	olfactory receptor 1356	0,2729
Olfr1366	olfactory receptor 1366	0,3191
Olfr1426	olfactory receptor 1426	0,327
Olfr1495	olfactory receptor 1495	0,6982
Olfr295	olfactory receptor 295	1,3464
Olfr297	olfactory receptor 297	1,7258
Olfr301	olfactory receptor 301; olfactory receptor 302	0,2731
Olfr305	olfactory receptor 305	0,3879
Olfr307	olfactory receptor 307	0,6339
Olfr311	olfactory receptor 311	1,2767
Olfr312	olfactory receptor 312	1,6906
Olfr419	olfactory receptor 419	2,4088
Olfr502	olfactory receptor 502	2,6092
Olfr531	olfactory receptor 531	8,309
Olfr692	olfactory receptor 692	0,0824
Olfr701	olfactory receptor 701	0,2548
Olfr761	olfactory receptor 761	0,2795
Olfr95	olfactory receptor 95	0,2878
Opn4	opsin 4 (melanopsin)	1,1753
Opn5	opsin 5	1,2611
Orc1l	origin recognition complex, subunit 1-like (S.cereviaiae)	2,1099
Orc2l	origin recognition complex, subunit 2-like (S. cerevisiae)	9,5097
Orc3l	origin recognition complex, subunit 3-like (S. cerevisiae)	3,4455
Orc4l	origin recognition complex, subunit 4-like (S. cerevisiae)	1,915
Orc5l	origin recognition complex, subunit 5-like (S. cerevisiae)	0,5441
Orc6l	origin recognition complex, subunit 6-like (S. cerevisiae)	0,1343
Osm	oncostatin M	0,9674
Oxct1	3-oxoacid CoA transferase 1	1,2036
Oxtr	oxytocin receptor	0,2044
Paip1	polyadenylate binding protein-interacting protein 1; similar to poly(A) binding protein interacting protein 1	0,2721
Pam	peptidylglycine alpha-amidating monooxygenase	0,8994
Parn	poly(A)-specific ribonuclease (deadenylation nuclease)	0,0875
Parp1	poly (ADP-ribose) polymerase family, member 1	7,4
Pax3	paired box gene 3	0,2395
Pcna	proliferating cell nuclear antigen; similar to proliferating cell nuclear antigen (DNA polymerase delta auxiliary protein)	0,78

Pcnt	pericentrin (kendrin)	2,2633
Pcsk1n	proprotein convertase subtilisin/kexin type 1 inhibitor	0,0227
Pdcd1	programmed cell death 1	13,4242
Pdcd10	programmed cell death 10	0,0742
Pdcd2	programmed cell death 2	0,0913
Pdcd4	programmed cell death 4	0,0955
Pdcd5	predicted gene 3837; programmed cell death 5	0,1051
Pdcd6	programmed cell death 6	64,525
Pdpn	podoplanin	3,2686
Pea15a	phosphoprotein enriched in astrocytes 15A	0,0738
Pecam1	platelet/endothelial cell adhesion molecule 1	0,2974
Pglyrp1	peptidoglycan recognition protein 1; similar to peptidoglycan recognition protein	3,3876
Pglyrp4	peptidoglycan recognition protein 4	3,6786
Pgr	progesterone receptor	10,8333
Phb	prohibitin; predicted gene 4773; RIKEN cDNA 1700071K01 gene	117,475
Phka2	phosphorylase kinase alpha 2	0,0849
Phlda3	pleckstrin homology-like domain, family A, member 3	2,255
Picalm	phosphatidylinositol binding clathrin assembly protein	16,4228
Pign	phosphatidylinositol glycan anchor biosynthesis, class N	16,761
Pip	prolactin induced protein	0,2775
Pip5k1b	phosphatidylinositol-4-phosphate 5-kinase, type 1 beta; similar to phosphatidylinositol 4-phosphate 5-kinase type I-alpha	16,9097
Pja2	praja 2, RING-H2 motif containing	24,0417
Pla2g4a	phospholipase A2, group IVA (cytosolic, calcium-dependent)	0,0535
Plat	plasminogen activator, tissue	0,2908
Plaur	plasminogen activator, urokinase receptor	1,9291
Plek2	pleckstrin 2	0,0667
Plg	plasminogen	0,1027
Pltp	phospholipid transfer protein	0,0549
Pnrc1	proline-rich nuclear receptor coactivator 1	1,9297
Polb	polymerase (DNA directed), beta	6,4
Pole3	polymerase (DNA directed), epsilon 3 (p17 subunit)	1,9979
Polr2b	polymerase (RNA) II (DNA directed) polypeptide B	3
Polr2j	polymerase (RNA) II (DNA directed) polypeptide J	3,5477
Polr3a	polymerase (RNA) III (DNA directed) polypeptide A	4,5415
Polr3b	polymerase (RNA) III (DNA directed) polypeptide B	4,6684
Pparg	peroxisome proliferator activated receptor gamma	10,0426
Ppid	peptidylprolyl isomerase D (cyclophilin D); similar to peptidylprolyl isomerase D; predicted gene 5551	1,0238
Ppm1j	protein phosphatase 1J	3,183
Ppp2r4	protein phosphatase 2A, regulatory subunit B (PR 53)	5,1765
Prdx1	peroxiredoxin 1; predicted gene 7204	3,0117
Prdx3	peroxiredoxin 3	3,7975
Prkca	protein kinase C, alpha	0,5925
Prkcd	protein kinase C, delta	0,6035
Prkcdbp	protein kinase C, delta binding protein	0,7383
Prkce	RIKEN cDNA 9630025F12 gene; protein kinase C, epsilon	2,1335
Prkch	protein kinase C, eta	0,8009
Prkci	protein kinase C, iota	0,8863

Prkcq	protein kinase C, theta	0,9085
Prkd1	protein kinase D1	1,1216
Prkd3	protein kinase D3	1,8357
Prkdc	protein kinase, DNA activated, catalytic polypeptide	6,8
Prl	prolactin	0,2345
Prlr	prolactin receptor	0,4986
Prph	peripherin	2,4466
Prps2	phosphoribosyl pyrophosphate synthetase 2	0,0817
Psg16	pregnancy specific glycoprotein 16	2,875
Psg17	pregnancy specific glycoprotein 17	3,1225
Psg18	pregnancy specific glycoprotein 18	3,131
Psg19	pregnancy specific glycoprotein 19	5,2698
Psg23	pregnancy-specific glycoprotein 23	6,2857
Psg29	pregnancy-specific glycoprotein 29	7,1034
Psip1	PC4 and SFRS1 interacting protein 1	2,9575
Psmb8	proteasome (prosome, macropain) subunit, beta type 8 (large multifunctional peptidase 7)	3,4
Psmd9	proteasome (prosome, macropain) 26S subunit, non-ATPase, 9	0,4973
Psme2	protease (prosome, macropain) 28 subunit beta B, pseudogene;	0,115
Pstpip2	proline-serine-threonine phosphatase-interacting protein 2	1,6383
Ptch1	patched homolog 1	0,2636
Pten	phosphatase and tensin homolog	15,6429
Ptgfr	prostaglandin F receptor	3,1031
Ptk2b	PTK2 protein tyrosine kinase 2 beta	7,2727
Ptn	pleiotrophin	3,2
Ptpn1	protein tyrosine phosphatase, non-receptor type 1	5,9231
Ptprf	protein tyrosine phosphatase, receptor type, F	6,3571
Ptprm	protein tyrosine phosphatase, receptor type, M	6,5727
Pwp1	PWP1 homolog (S. cerevisiae)	10,6975
Pygm	muscle glycogen phosphorylase	2,4359
Rab31	RAB31, member RAS oncogene family	14,8635
Rab35	RAB35, member RAS oncogene family	23,7152
Rab3c	similar to RAB3C, member RAS oncogene family; RAB3C, member RAS oncogene family	0,1909
Rab9	RAB9, member RAS oncogene family; predicted gene 9181	25,247
Rac2	RAS-related C3 botulinum substrate 2	2,4082
Rad17	RAD17 homolog (S. pombe)	51
Rad23a	RAD23a homolog (S. cerevisiae)	12,2
Rad23b	RAD23b homolog (S. cerevisiae)	6,4
Rad50	RAD50 homolog (S. cerevisiae)	8,5
Rad51	RAD51 homolog (S. cerevisiae)	9,4
Rad52	RAD52 homolog (S. cerevisiae)	6,4
Ralb	v-ral simian leukemia viral oncogene homolog B (ras related)	0,5401
Rap1a	predicted gene 9392; similar to Raichu404X; RAS-related protein-1a	1,9481
Rap1gap	Rap1 GTPase-activating protein	0,2269
Rap2a	RAS related protein 2a	0,527
Rarb	retinoic acid receptor, beta	5,7101
Rarg	retinoic acid receptor, gamma	6,6905
Rasa1	RAS p21 protein activator 1	0,4801

Rassf3	Ras association (RalGDS/AF-6) domain family member 3	0,8467
Rassf8	Ras association (RalGDS/AF-6) domain family (N-terminal) member 8	0,6142
Rb1	retinoblastoma 1	5,095
Rbm6	RNA binding motif protein 6	3
Rdx	radixin	0,0896
Reg3b	regenerating islet-derived 3 beta	0,0868
Reg3g	regenerating islet-derived 3 gamma	0,1087
Rfc3	replication factor C (activator 1) 3	12,5
Rfc4	replication factor C (activator 1) 4	1,3
Rfpl4	ret finger protein-like 4	5,0893
Rgs17	regulator of G-protein signaling 17	0,2645
Rhag	Rhesus blood group-associated A glycoprotein	0,1789
Rhebl1	Ras homolog enriched in brain like 1	0,9474
Rhoa	ras homolog gene family, member A; similar to aplysia ras-related homolog A2; predicted gene 12844	1,2412
Rhob	ras homolog gene family, member B	2,4677
Rhoh	ras homolog gene family, member H	3,4187
Rhot1	ras homolog gene family, member T1	0,1163
Rims2	regulating synaptic membrane exocytosis 2	0,1947
Ripk1	receptor (TNFRSF)-interacting serine-threonine kinase 1	2,8601
Rnd1	Rho family GTPase 1	0,4963
Rnd3	Rho family GTPase 3	0,5729
Rnf169	ring finger protein 169	2,4671
Rpl10a	predicted gene 13573; predicted gene 15451; ribosomal protein L10A; predicted gene 7695; similar to ribosomal protein L10a	0,1189
Rpl34	ribosomal protein L34; predicted gene 10154; similar to ribosomal protein L34; predicted gene 7800; predicted gene 4705	1,7329
Rpn2	ribophorin II	1,6654
Rps23	predicted gene 8624; predicted gene 9701; predicted gene 8467; predicted gene 15450; ribosomal protein S23; similar to yeast ribosomal protein S28 homologue; predicted gene 5148; similar to ribosomal protein S23; predicted gene 10054	0,6451
Rps4x	predicted gene 4833; predicted gene 9616; predicted gene 13680; predicted gene 4859; predicted gene 8729; predicted gene 8231; ribosomal protein S4, X-linked	0,1664
Rps6ka5	ribosomal protein S6 kinase, polypeptide 5	1,8935
Rraga	Ras-related GTP binding A	2,5569
Rras2	related RAS viral (r-ras) oncogene homolog 2	0,3162
Rrp9	RRP9, small subunit (SSU) processome component, homolog (yeast)	3,951
Rsph1	radial spoke head 1 homolog (Chlamydomonas)	0,0862
Rspo3	R-spondin 3 homolog (Xenopus laevis)	4,2143
Rufy4	RUN and FYVE domain containing 4	7,2373
Ruvbl1	RuvB-like protein 1	7,7188
Rwdd4a	RWD domain containing 4A	9,5636
S100a10	S100 calcium binding protein A10 (calpactin)	0,0685
S100a11	predicted gene 7665; S100 calcium binding protein A11 (calgizzarin); predicted gene 5068	2,9679
S100a3	S100 calcium binding protein A3	0,108
S100a4	hippocampus abundant transcript-like 1; S100 calcium binding protein A4	1,3748
S100a7a	S100 calcium binding protein A7A	0,11
S100a8	S100 calcium binding protein A8 (calgranulin A)	0,2023
S100a9	S100 calcium binding protein A9 (calgranulin B)	0,8333
Sac3d1	SAC3 domain containing 1	0,9874
Scgb1a1	secretoglobin, family 1A, member 1 (uteroglobin)	0,1513

Scmh1	sex comb on midleg homolog 1	0,3795
Sel1l	sel-1 suppressor of lin-12-like (C. elegans)	0,1698
Sema3c	sema domain, immunoglobulin domain (Ig), short basic domain, secreted, (semaphorin) 3C	0,4286
Serpinb2	serine (or cysteine) peptidase inhibitor, clade B, member 2	0,8012
Serpinb3a	serine (or cysteine) peptidase inhibitor, clade B (ovalbumin), member 3A	0,6003
Serpinb3d	serine (or cysteine) peptidase inhibitor, clade B (ovalbumin), member 3D	0,6478
Serpinb5	serine (or cysteine) peptidase inhibitor, clade B, member 5	1,8758
Serpini2	serine (or cysteine) peptidase inhibitor, clade I, member 2	9,1447
Sfrp1	secreted frizzled-related protein 1	3,625
Sfrp4	secreted frizzled-related protein 4	0,1287
Sgk1	serum/glucocorticoid regulated kinase 1	0,1081
Sh2b1	SH2B adaptor protein 1	0,652
Sh2d3c	SH2 domain containing 3C	0,5741
Sharpin	SHANK-associated RH domain interacting protein	0,817
Shbg	sex hormone binding globulin	0,5541
Shfm1	split hand/foot malformation (ectrodactyly) type 1	1,1494
Sirt5	sirtuin 5 (silent mating type information regulation 2 homolog) 5 (S. cerevisiae)	0,401
Sirt6	sirtuin 6 (silent mating type information regulation 2, homolog) 6 (S. cerevisiae)	0,4305
Skp2	S-phase kinase-associated protein 2 (p45)	1,0202
Slc11a2	solute carrier family 11 (proton-coupled divalent metal ion transporters), member 2	0,5713
Slc17a3	solute carrier family 17 (sodium phosphate), member 3	0,6059
Slc25a4	solute carrier family 25 (mitochondrial carrier, adenine nucleotide translocator), member 4	1,1587
Slc25a44	solute carrier family 25, member 44	1,8889
Slc39a6	solute carrier family 39 (metal ion transporter), member 6	1,9706
Slc39a9	solute carrier family 39 (zinc transporter), member 9	2,7157
Slc4a3	solute carrier family 4 (anion exchanger), member 3	2,9034
Slc6a11	solute carrier family 6 (neurotransmitter transporter, GABA), member 11	0,0626
Slc8a1	solute carrier family 8 (sodium/calcium exchanger), member 1	0,4889
Sln	sarcolipin	0,2281
Smad4	similar to MAD homolog 4 (Drosophila); MAD homolog 4 (Drosophila)	1,2246
Smarca2	SWI/SNF related, matrix associated, actin dependent regulator of chromatin, subfamily a, member 2	1,2141
Smarca4	SWI/SNF related, matrix associated, actin dependent regulator of chromatin, subfamily a, member 4	1,3187
Sncg	synuclein, gamma	2,2734
Sntb1	syntrophin, basic 1	2,1308
Snx2	sorting nexin 2	0,183
Sox13	SRY-box containing gene 13	1,1758
Sox14	SRY-box containing gene 14	1,6799
Sox15	SRY-box containing gene 16; SRY-box containing gene 15	0,1613
Sox30	SRY-box containing gene 30	0,1754
Sox4	SRY-box containing gene 19; SRY-box containing gene 4	0,1623
Sox8	SRY-box containing gene 8	0,1776
Sp2	Sp2 transcription factor	0,3282
Sparc	secreted acidic cysteine rich glycoprotein; similar to Secreted acidic cysteine rich glycoprotein	3,2469
Spata1	spermatogenesis associated 1	0,7048
Sphk1	sphingosine kinase 1	1,052
Spock1	sparc/osteonectin, cwcv and kazal-like domains proteoglycan 1	0,3553
Spz1	spermatogenic leucine zipper 1	0,8033

Src	Rous sarcoma oncogene	3,2166
Sspn	sarcospan	0,8889
Sst	somatostatin	0,9356
Sstr1	somatostatin receptor 1	1,7895
Sstr2	somatostatin receptor 2	0,0475
Sstr3	somatostatin receptor 3	0,0522
St6galnac1	similar to Alpha-N-acetylgalactosaminide alpha-2,6-sialyltransferase 1 (GalNAc alpha-2,6-sialyltransferase I) (ST6GalNAc I) (Sialyltransferase 7A); predicted gene 11735; ST6 (alpha-N-acetyl-neuraminyl-2,3-beta-galactosyl-1,3)-N-acetylgalactosaminide alpha-2,6-sialyltransferase 1	1,125
St6galnac2	ST6 (alpha-N-acetyl-neuraminyl-2,3-beta-galactosyl-1,3)-N-acetylgalactosaminide alpha-2,6-sialyltransferase 2	1,1013
Stag3	stromal antigen 3	8,0505
Stat1	signal transducer and activator of transcription 1	1,0149
Stc1	stanniocalcin 1	1,1092
Stc2	stanniocalcin 2	7,0957
Stfa3	cDNA sequence BC100530; stefin A3	0,067
Stk17b	serine/threonine kinase 17b (apoptosis-inducing)	9,7063
Stk32b	serine/threonine kinase 32B; predicted gene 3080	13,8932
Strap	serine/threonine kinase receptor associated protein	15,7396
Stx5a	syntaxin 5A	0,7327
Sult1a1	sulfotransferase family 1A, phenol-preferring, member 1	17,057
Sult1b1	sulfotransferase family 1B, member 1	18,6582
Sult1e1	sulfotransferase family 1E, member 1	19,9176
Sult2a1	RIKEN cDNA C730007P19 gene; similar to androgen-repressible liver protein SMP-2; sulfotransferase family 2A, dehydroepiandrosterone (DHEA)-preferring, member 1	2,272
Sult5a1	sulfotransferase family 5A, member 1	6,5656
Sv2b	synaptic vesicle glycoprotein 2 b	0,3335
Syne2	synaptic nuclear envelope 2	0,3127
Syt1	synaptotagmin I	0,4575
Tap1	transporter 1, ATP-binding cassette, sub-family B (MDR/TAP)	0,2124
Tars2	threonyl-tRNA synthetase 2, mitochondrial (putative)	1,2556
Taz	tafazzin	5,2377
Tceb2	predicted gene 11401; similar to transcription elongation factor B (SIII), polypeptide 2; predicted gene 8971; transcription elongation factor B (SIII), polypeptide 2	2,1441
Tcf21	transcription factor 21	0,0598
Tcf4	transcription factor 4	0,1321
Tcfap2a	transcription factor AP-2, alpha	0,183
Terf1	telomeric repeat binding factor 1	5,9107
Tert	telomerase reverse transcriptase	5,3396
Tf	tufted	2,358
Tff1	trefoil factor 1; predicted gene 3090	0,2464
Tfrc	transferrin receptor	0,212
Tgfa	transforming growth factor alpha	0,9336
Tgfb3	transforming growth factor, beta 3	1,1613
Tgfbr2	transforming growth factor, beta receptor II	2,3096
Thbs2	thrombospondin 2	1,8749
Timp1	tissue inhibitor of metalloproteinase 1	7,2479
Timp4	tissue inhibitor of metalloproteinase 4	8,855
Tk2	thymidine kinase 2, mitochondrial	2,1759
Tm4sf1	transmembrane 4 superfamily member 1	0,1343

Tmco1	transmembrane and coiled-coil domains 1	0,1555
Tmco3	transmembrane and coiled-coil domains 3	0,1676
Tmem2	transmembrane protein 2	0,1774
Tnc	tenascin C	10,0185
Tnfaip2	tumor necrosis factor, alpha-induced protein 2	0,0839
Tnfrsf10b	tumor necrosis factor receptor superfamily, member 10b	0,0271
Tnfrsf1a	tumor necrosis factor receptor superfamily, member 1a	0,2623
Tnfrsf4	tumor necrosis factor receptor superfamily, member 4	0,0665
Tnfrsf8	tumor necrosis factor receptor superfamily, member 8	0,0787
Tnfsf10	tumor necrosis factor (ligand) superfamily, member 10	5,0291
Tnfsf4	tumor necrosis factor (ligand) superfamily, member 4	5,5892
Tnip2	TNFAIP3 interacting protein 2	11,9887
Top2a	topoisomerase (DNA) II alpha	14,5
Tpd52	similar to Tpd52 protein; tumor protein D52	0,2886
Tpd52l1	tumor protein D52-like 1	0,5093
Tpm4	tropomyosin 4; predicted gene 7809	1,7097
Traf4	TNF receptor associated factor 4	11,5768
Tram1	translocating chain-associating membrane protein 1	0,1215
Trdmt1	tRNA aspartic acid methyltransferase 1	0,6019
Trf	transferrin	0,1861
Triap1	TP53 regulated inhibitor of apoptosis 1	16,725
Trim31	tripartite motif-containing 31	0,2821
Trp73	transformation related protein 73	3,6
Tsg101	tumor susceptibility gene 101	0,7369
Tsga14	testis specific gene A14	0,3799
Ttc1	tetratricopeptide repeat domain 1	0,5338
Ttc4	tetratricopeptide repeat domain 4	0,8466
Ttk	Ttk protein kinase	1,7985
Tubb6	tubulin, beta 6	1,9901
Twf1	twinfilin, actin-binding protein, homolog 1 (Drosophila); predicted gene 4887	1,1608
Txn2	thioredoxin 2	1,019
Tyk2	tyrosine kinase 2	1,664
Tymp	thymidine phosphorylase	4,5642
Tyms	thymidylate synthase	4,653
Ubac1	ubiquitin associated domain containing 1	10,8997
Ube2b	ubiquitin-conjugating enzyme E2B, RAD6 homology (S. cerevisiae)	2
Ube2m	ubiquitin-conjugating enzyme E2M (UBC12 homolog, yeast)	2,1751
Uchl3	ubiquitin carboxyl-terminal esterase L3 (ubiquitin thiolesterase)	9,2171
Usp1	ubiquitin specific peptidase 1; predicted gene 5841	0,0461
Usp5	ubiquitin specific peptidase 5 (isopeptidase T)	1,046
Utp20	UTP20, small subunit (SSU) processome component, homolog (yeast)	2,579
Uxt	predicted gene 5808; ubiquitously expressed transcript; predicted gene 8242	0,186
Vapa	vesicle-associated membrane protein, associated protein A	0,0854
Vasn	vasorin	0,165
Vdr	vitamin D receptor	0,0904
Vegfa	vascular endothelial growth factor A	0,1072
Vegfc	vascular endothelial growth factor C	0,1224

Vim	vimentin	0,0877
Vipr1	vasoactive intestinal peptide receptor 1	0,1475
VPS54	vacuolar protein sorting 54 (yeast)	2,7346
Wdr62	similar to WD repeat domain 62; WD repeat domain 62	1,2531
Wdr69	WD repeat domain 69	0,6333
Wisp2	WNT1 inducible signaling pathway protein 2	0,9093
Wnt1	wingless-related MMTV integration site 1	5,56
Wnt10a	wingless related MMTV integration site 10a	0,6853
Wnt10b	wingless related MMTV integration site 10b	0,9489
Wnt11	wingless-related MMTV integration site 11	0,1537
Wnt2b	wingless related MMTV integration site 2b	0,0517
Wnt5a	wingless-related MMTV integration site 5A	0,1753
Wnt7a	wingless-related MMTV integration site 7A	0,4855
Wwc1	WW, C2 and coiled-coil domain containing 1	1,3655
Wwox	WW domain-containing oxidoreductase	0,922
Xpa	xeroderma pigmentosum, complementation group A	2,7
Xpc	xeroderma pigmentosum, complementation group C	4,9
Xpr1	xenotropic and polytropic retrovirus receptor 1	1,5774
Yes1	Yamaguchi sarcoma viral (v-yes) oncogene homolog 1	2,0808
Ylpm1	YLP motif containing 1	4,4361
Zbtb26	zinc finger and BTB domain containing 26	4,4843
Zc3h13	zinc finger CCCH type containing 13	7,7356
Zdhhc9	similar to zinc finger, DHHC domain containing 9; zinc finger, DHHC domain containing 9	0,067
Zfml	zinc finger, matrin-like	2,8414
Zfp217	zinc finger protein 217	0,465
Zfp345	zinc finger protein 345	1,9583
Zfp354a	zinc finger protein 354A	2,2243
Zfp36l2	zinc finger protein 36, C3H type-like 2	2,2295
Zfp566	zinc finger protein 566	2,4598
Zfp775	zinc finger protein 775	2,8116
Zmat3	zinc finger matrin type 3	11,4894

5.2 Table 2: short hairpin sequences for Batf, Lyn, Pdcd6, Bmp3, Stat3 and scrambled control

shRNA symbol	shRNA sequence
shBatf-1	CAGAGGCCTGGACAAGTAT
shBatf-2	GCAAACAGGACTCATCTGA
shLyn	CAGTAATACTGACCGAACTATT
shPdcd6	CGCTGTGCCGTTTGTTACACTA
shBmp3	CCGACAAGGTGTCGGAGCATAT
shStat3	CCACGTTGGTGTTTCATAA
scrambled control	CGCAGTTCGATATCTACTGAAA

5.3 Table 3: RT-PCR primers

Table is showing qPCR primers for lymphopoiesis and myelopoiesis related genes and single genes mentioned in our experiment. All of these lymphopoiesis and myelopoiesis related genes contain Batf binding sites in their promoter region (predicted by Genomatix software, www.genomatix.de).

Gene Symbol	RT-PCR primer: forward	RT-PCR primer: reverse
Ap3d1	ctttccccggcttaagga	ttaacagccgcagactgtacc
Bcl10	aaactggagcacctcaaagg	cggaattgcacctagagagg
Blm	cttggatgccagatgagga	tggctgagtgtcgctgtagt
Bmi1	aaaccagaccactcctgaaca	tcttcttctcttcatctcatttttga
Card11	tctccagagcgagtttcttctt	tgttttctgaccggctgac
Cd1d1	cccctatttgtccgtggtc	aggccactggcttctcttg
Cd28	ctggccctcatcagaacaat	ggcgactgctttaccaaaatc
Cd3e	aacacgtacttgtacctgaaagctc	gatgattatggctactgctgtca
Cd74	cttgtttgagatgagcaagaactc	tccatgtccagtggctcttt
Cd80	tcgtctttcacaagtgtcttcag	ttgccagtagattcggtcttc
Cdkn1a	tccacagcgatatccagaca	ggacatcaccaggattggac
Chrnb2	actctatggcgctgctgttc	tcctctgtgtcagtacccaaaa
Gimap5	ggaagagaatggaacaccttca	ggatcctcaggcagctagatt
Gpam	ggaaggtgctgctattcctg	tgggatactggggttgaaaa
H2-Aa	ctctgattctgggggtcct	accataggtgcctacgtggt
Hells	acccttttcaacaaccaaagc	ccattttcccaaagcatcc
Hprt1	tcctcctcagaccgctttt	cctggttcatcatcgctaatc
Hsp90aa1	gtctcgtgcgtgttcattca	cattaactgggcaatttctgc
Icosl	cgcaccatgcagctaaagt	aaacatggagcttcttccaaac
Il13	cctctgacccttaaggagcttat	cgttgcacaggggagtct
Il2	gctgttgatggacctacagga	ttcaattctgtggcctgctt
Il21	gacattcatcattgacctcgtg	tcacaggaagggcatttagc
Il2ra	tgtgctcacaatggagtataagg	ctcaggaggaggatgctgat
Il2rg	tgaataccaagggaacttttcg	gggaatctcgctgacgtg
Il4	acagcaccttatggctctctg	atggggtggcatcatgtagt
Impdh2	tcttacgtgccggacgac	cccaggaagaatgagaaaatcat
Inpp5d	cctctgtcgccaaagaagtt	agcttccacctttcccagat
Lig4	gaagaaatcgtgtcctgatgc	caaatcctccggtttgaact
Myd88	tggccttgttagaccgtga	aagtatttctggcagtcctcctc
Ptprc	gaggtgtctgatggtgcaag	tgtattccactaaagcctgatgaa
sart3	gtgagctcttccccctgac	catgctgatctcatcgtgga
Sash3	aggccttgtcagaggagatg	aggctgcagtctggagatgt
Stat5a	tgcaggcagatgtgaagttag	gcggtggaggctgttactt
Stat5b	cgattcgggctctgtaggt	tacaaggcctgcatctggt

Tac1	aagcctcagcagttctttgg	tctggccatgtccataaaga
Tgfbr2	ggctctggtactctgggaaa	aatgggggctcgtaatcct
Thy1	gaaaactgcgggcttcag	ccaagagttccgacttggat
Tnfrsf13c	ttcagaaggagtccagcaaga	gcgctgtctgcatcttcttt
Tnfsf13b	aacagacgcgctttccag	caggaggagctgagaggtctac
Xrcc4	tgcataaattgctaaatgaagtcc	ttgtcagaacacggattttcc
Zap70	cagaccgacggcaagttc	catagaccagggacagtgcat
Adora2b	gagctccatctttagcctcttg	tgtcccagtgaccaaacctt
Adora3	ctgtagggcttccaaagctg	aatcagtatacaaatgatcagaatgga
Btk	ggccatcaagatgatcagaga	gcttctcatgggaaagattca
Casp1	cccactgctgatagggtgac	gcataggtacataagaatgaactgga
Cnr2	cagctcttgggacctacgtg	tgtcccagaagactgggtgt
Cx3cr1	aagttcccttcccatctgct	caaaattctctagatccagttcagg
Fcer1a	tgtgtacttgaatgtaacgcaaga	ggactaagaccatgtcagcagat
Fcer1g	ccttttggtggaacaagcag	gggtaaggacaataccatacaaaaa
Fcgr3	caagcctgtcaccatcactg	gaggcacatcactagggagaa
Foxf1a	agcatctccacgcactcc	tgtgagtgataccgagggatg
Lat	ctgtgcctagcaaccctgac	cgtaatcttcacacgactccac
Lat2	aggagccctcaccctcag	ctccagctcggcactcat
Mlf1	ttccaggcctcaactcaaac	tctcattgcttttctggtttctt
Ndrg1	ttcatcagcgcctacaacag	agtgtgggttccaggcatt
Nod2	tgtggagtcaccgcaaaac	tcctctgtgcctggaactct
Pld2	gagtttgcggaagcactgtt	tcatcacagacagggtctcg
Ptpre	cacagactatatcaacgcatcctt	cctgtgtggccatgaagtag
Rhoh	tggtgatgagacttggcatt	cgtggcctcaggttctca
Slc11a1	gccatctctactaccccaagg	atggccagctcaatggtc
Snca	aagaagagtctgttcgctgga	aaagatgtatttttgctccacactt
Tlr4	ggactctgatcatggcactg	ctgatccatgcattggtaggt
Trpv1	caacaagaaggggcttacacc	tctggagaatgtaggccaagac
Vamp7	gaccttcgcccctcagtc	aatggccatgacttcaatctg
Ywhaz	cttcctgcagccagaagc	ggtttcctccaatcactagcc
Batf	agaaagccgacacccttca	cggagagctgcgttctgt
Bmp3	tctcccaagtcatttgatgct	gcgtgatttgatggtttcaa
Lyn	ttcgaagactcaaccagttcc	aaggccaccacaatgtcac
Pdcd6	agaccagagcttcctgtgga	ttgtctgaaatcactccactcc
Stat3	ggaaataacggtgaaggtgct	catgtcaaacgtgagcgact
human Batf	acacagaaggccgacacc	cttgatctccttgcgtagagc
p16 (Cdkn2a)	gggttttcttggtgaagttcg	ttgcccatcatcatcacct

5.4 Table 4: Ratio of enrichment in G3 mTerc$^{-/-}$ to mTerc$^{+/+}$ for DNA damage related genes which are compiled by using Gene Ontology software. All of these genes are involved in DNA damage pathway.

Gene Symbol	Gene Description	Ratio of enrichment in G3 mTerc-/- to mTerc+/+
Acta1	actin, alpha 1, skeletal muscle	3,5
Apc	similar to adenomatosis polyposis coli; adenomatosis polyposis coli	6,3
Atm	ataxia telangiectasia mutated homolog (human)	10,2
Atr	ataxia telangiectasia and Rad3 related	6,5
Bax	BCL2-associated X protein	2,5
Bcl2	predicted gene 3655; B-cell leukemia/lymphoma 2	8,2
Brca1	breast cancer 1	28
Brca2	breast cancer 2	30
Casp2	caspase 2	10,2
Casp3	caspase 3	1,4
Ccna2	cyclin A2	2,4
Ccnd1	cyclin D1	1,3
CD44	CD44 antigen	5,6
Cdc6	cell division cycle 6 homolog (S. cerevisiae); predicted gene 9430; similar to cell division cycle 6 homolog	14,4
Cdc7	cell division cycle 7 (S. cerevisiae)	1,26
Cdk2	cyclin-dependent kinase 2	8,2
Cebpg	CCAAT/enhancer binding protein (C/EBP), gamma	1,2
Chek1	checkpoint kinase 1 homolog (S. pombe)	1,4
Chek2	CHK2 checkpoint homolog (S. pombe)	2,1
Eef1a1	elongation factor 1 alpha 1	2,3
Ep300	E1A binding protein p300	6,5
Ercc1	excision repair cross-complementing rodent repair deficiency, complementation group 1	2,6
Ercc3	excision repair cross-complementing rodent repair deficiency, complementation group 3	0,91
Ercc4	excision repair cross-complementing rodent repair deficiency, complementation group 4	8,3
Ercc5	excision repair cross-complementing rodent repair deficiency, complementation group 5	6,3
Ercc6	excision repair cross-complementing rodent repair deficiency, complementation group 6	1,8
Exo1	exonuclease 1	2,1
Fgf10	fibroblast growth factor 10	10,2
Gadd45a	growth arrest and DNA-damage-inducible 45 alpha	13,2
Gadd45g	growth arrest and DNA-damage-inducible 45 gamma	9,8
Grb2	growth factor receptor bound protein 2; predicted gene 12791	2,3
Hat1	histone aminotransferase 1	22
Hmgb1	(Amphoterin) (Heparin-binding protein p30); predicted gene 7468; predicted gene 8554	15,4
Lyn	Yamaguchi sarcoma viral (v-yes-1) oncogene homolog	94

Mapk12	mitogen-activated protein kinase 12	5,6
Mcm10	minichromosome maintenance deficient 10 (S. cerevisiae)	23,1
Mcm3	minichromosome maintenance deficient 3 (S. cerevisiae)	2,5
Mcm7	minichromosome maintenance deficient 7 (S. cerevisiae)	2,2
Nupr1	nuclear protein 1	6,9
Parp1	poly (ADP-ribose) polymerase family, member 1	7,4
Pcna	proliferating cell nuclear antigen; similar to proliferating cell nuclear antigen (DNA polymerase delta auxiliary protein)	0,78
Polb	polymerase (DNA directed), beta	6,4
Polr2b	polymerase (RNA) II (DNA directed) polypeptide B	3
Prkdc	protein kinase, DNA activated, catalytic polypeptide	6,8
Psmb8	proteasome (prosome, macropain) subunit, beta type 8 (large multifunctional peptidase 7)	3,4
Rad17	RAD17 homolog (S. pombe)	51
Rad23a	RAD23a homolog (S. cerevisiae)	12,2
Rad23b	RAD23b homolog (S. cerevisiae)	6,4
Rad50	RAD50 homolog (S. cerevisiae)	8,5
Rad51	RAD51 homolog (S. cerevisiae)	9,4
Rad52	RAD52 homolog (S. cerevisiae)	6,4
Rfc3	replication factor C (activator 1) 3	12,5
Rfc4	replication factor C (activator 1) 4	1,3
Top2a	topoisomerase (DNA) II alpha	14,5
Trp73	transformation related protein 73	3,6
Ube2b	ubiquitin-conjugating enzyme E2B, RAD6 homology (S. cerevisiae)	2
Wnt1	wingless-related MMTV integration site 1	5,56
Xpa	xeroderma pigmentosum, complementation group A	2,7
Xpc	xeroderma pigmentosum, complementation group C	4,9

6. Reference

Akala, O.O., Park, I.K., Qian, D., Pihalja, M., Becker, M.W., and Clarke, M.F. (2008). Long-term haematopoietic reconstitution by Trp53-/-p16Ink4a-/-p19Arf-/- multipotent progenitors. Nature 453, 228-232.

Allman D., Miller J.P. (2003). Common lymphoid progenitors, early B-lineage precursors, and IL-7: characterizing the trophic and instructive signals underlying early B cell development. Immunol Res 27,131-140.

Allsopp R.C., Morin G.B., DePinho R.A., Harley C.B., Weissman I.L. (2003). Telomerase is required to slow telomere shortening and extend replicative lifespan of HSCs during serial transplantation. Blood 102,517-520.

Andrew D., Aspinall R. (2001). Il-7 and not stem cell factor reverses both the increase in apoptosis and the decline in thymopoiesis seen in aged mice. J Immunol 166,1524-1530.

Arinobu, Y., Mizuno, S., Chong, Y., Shigematsu, H., Iino, T., Iwasaki, H., Graf, T., Mayfield, R., Chan, S., Kastne,r P., at al. (2007). Reciprocal activation of GATA-1 and PU.1 marks initial specification of hematopoietic stem cells into myeloerythroid and myelolymphoid lineages. Cell Stem Cell 1, 416-427.

Aw D., Silva A.B., Maddick M., von Zglinicki T., Palmer D.B. (2008). Architectural changes in the thymus of aging mice. Aging Cell 7,158-167.

Aw D., Silva A.B., Palmer D.B. (2010) The effect of age on the phenotype and function of developing thymocytes. J Comp Pathol 142 Suppl 1,S45-S59.

Beausejour, C.M., and Campisi, J. (2006). Ageing: balancing regeneration and cancer. Nature 443, 404-405.

Beerman, I., Bhattachary,a D., Zandi, S., Sigvardsson, M., Weissman, I.L., Bryder, D., and Rossi, D.J. (2010). Functionally distinct hematopoietic stem cells modulate hematopoietic lineage potential during aging by a mechanism of clonal expansion. Proc Natl Acad Sci U S A. 107, 5465-5470.

Bell, J.J., and Bhandoola, A. (2010). There's many a CLP on the path to B. Blood 115, 2562-2563.

Betz, B.C., Jordan-Williams, K.L., Wang, C., Kang, S.G., Liao, J., Logan, M.R., Kim, C.H., and Taparowsky, E.J. (2010). Batf coordinates multiple aspects of B and T cell function required for normal antibody responses. J Exp Med. 207, 933-942.

Bilousova G., Marusyk A., Porter C.C., Cardiff R.D., DeGregori J. (2005). Impaired DNA replication within progenitor cell pools promotes leukemogenesis. PLoS Biol 3,e401.

Blasco, M.A., Lee, H.W., Hande, M.P., Samper, E., Lansdorp, P.M., DePinho, R.A., and Greider, C.W. (1997). Telomere shortening and tumor formation by mouse cells lacking telomerase RNA. Cell 91, 25-34.

Bodnar A.G., Ouellette M., Frolkis M., Holt S.E., Chiu C.P., Morin G.B., Harley C.B., Shay J.W., Lichtsteiner S., Wright W.E. (1998). Extension of life-span by introduction of telomerase into normal human cells. Science 279,349-352.

Bric, A., Miething, C., Bialucha, C.U., Scuoppo, C., Zender, L., Krasnitz, A., Xuan, Z., Zuber, J., Wigler, M., Hicks, J., et al. (2009). Functional identification of tumor-suppressor genes through an in vivo RNA interference screen in a mouse lymphoma model. Cancer Cell 16, 324-335.

Brown J.P., Wei W., Sedivy J.M. (1997). Bypass of senescence after disruption of p21CIP1/WAF1 gene in normal diploid human fibroblasts. Science 277,831-834.

Challen, G.A., Boles, N.C., Chambers, S.M., and Goodell, M.A. (2010). Distinct hematopoietic stem cell subtypes are differentially regulated by TGF-beta1. Cell Stem Cell 6, 265-278.

Chambers S.M., Shaw C.A., Gatza C., Fisk J.C., Donehower L.A., Goodell M.A. (2007) Aging hematopoietic stem cells decline in function and exhibit epigenetic dysregulation. PLoS Biol 5,e201.

Chin, L., Artandi, S.E., Shen, Q., Tam, A., Lee, S.L., Gottlieb, G.J., Greider, C.W., and DePinho, R.A. (1999). p53 deficiency rescues the adverse effects of telomere loss and cooperates with telomere dysfunction to accelerate carcinogenesis. Cell 97, 527-538.

Cho, R.H., Sieburg, H.B., and Muller-Sieburg, C.E. (2008). A new mechanism for the aging of hematopoietic stem cells: aging changes the clonal composition of the stem cell compartment but not individual stem cells. Blood 111, 5553-5561.

Choudhury, A.R., Ju, Z., Djojosubroto, M.W., Schienke, A., Lechel, A., Schaetzlein, S., Jiang, H., Stepczynska, A., Wang, C., Buer, J., et al. (2007). Cdkn1a deletion improves stem cell function and lifespan of mice with dysfunctional telomeres without accelerating cancer formation. Nat Genet. 39, 99-105.

Cordenonsi, M., Dupont, S., Maretto, S., Insinga, A., Imbriano, C., and Piccolo, S. (2003). Links between tumor suppressors: p53 is required for TGF-beta gene responses by cooperating with Smads. Cell 113, 301-314.

d'Adda di Fagagna, F., Reaper, P.M., Clay-Farrace, L., Fiegler, H., Carr, P., von Zglinicki, T., Saretzki, G., Carter, N.P., and Jackson, S.P. (2003). A DNA damage checkpoint response in telomere-initiated senescence. Nature 426, 194-198.

Dickins, R.A., Hemann, M.T., Zilfou, J.T, Simpson, D.R, Ibarra, I., Hannon, G.J., and Lowe, SW. (2005). Probing tumor phenotypes using stable and regulated synthetic microRNA precursors. Nat Genet 37, 1289-1295.
Dorsey, M.J., Tae, H.J., Sollenberger, K.G., Mascarenhas, N.T., Johansen, L.M., and Taparowsky, E.J. (1995). B-ATF: a novel human bZIP protein that associates with members of the AP-1 transcription factor family. Oncogene 11, 2255-2265.

Douek D.C., McFarland R.D., Keiser P.H., Gage E.A., Massey J.M., Haynes B.F.,

Polis M.A., Haase A.T., Feinberg M.B., Sullivan J.L., et al. (1998). Changes in thymic function with age and during the treatment of HIV infection. Nature 396,690-695.

Dykstra B., Kent D., Bowie M., McCaffrey L., Hamilton M., Lyons K., Lee S.J., Brinkman R., Eaves C. (2007) Long-term propagation of distinct hematopoietic differentiation programs in vivo. Cell Stem Cell 1,218-229.

Ema H., Morita Y., Yamazaki S., Matsubara A., Seita J., Tadokoro Y., Kondo H., Takano H., Nakauchi H. (2006) Adult mouse hematopoietic stem cells: purification and single-cell assays. Nat Protoc. 1, 2979-2987.

Eshraghi P., Rudolph K.L. (2011). Lineage-specific pleiotropy in immune aging. Blood 117,3250-3251.

Geiger H., Van Zant G. (2002). The aging of lympho-hematopoietic stem cells. Nat Immunol 3,329-333.

Geiger H., Rudolph K.L.(2009). Aging in the lympho-hematopoietic stem cell compartment. Trends Immunol 30,360-365.

Henry C.J., Marusyk A., Zaberezhnyy V., Adane B., DeGregori J. (2010). Declining lymphoid progenitor fitness promotes aging-associated leukemogenesis. Proc Natl Acad Sci U S A 107,21713-21718.

Hess, J., Angel, P., and Schorpp-Kistner, M. (2004). AP-1 subunits: quarrel and harmony among siblings. J Cell Sci. 117, 5965-5973.

Hildinger, M., Schilz, A., Eckert, H.G., Bohn, W., Fehse, B., Zander, A., Ostertag, W., and Baum, C. (1999). Bicistronic retroviral vectors for combining myeloprotection with cell-surface marking. Gene Ther. 6, 1222-1230.

Hoeijmakers, J.H. (2009). DNA damage, aging, and cancer. N Engl J Med. 361, 1475-1485.

Hope, K.J., Cellot, S., Ting, S.B., MacRae, T., Mayotte, N., Iscove, N.N., Sauvageau, G. (2010). An RNAi screen identifies Msi2 and Prox1 as having opposite roles in the regulation of hematopoietic stem cell activity. Cell Stem Cell 7, 101-13.

Inomata, K., Aoto, T., Binh, N.T., Okamoto, N., Tanimura, S., Wakayama, T., Iseki, S., Hara, E., Masunaga, T., Shimizu, H., et al. (2009). Genotoxic stress abrogates renewal of melanocyte stem cells by triggering their differentiation. Cell 137, 1088-1099.

Ito K., Hirao A., Arai F., Matsuoka S., Takubo K., Hamaguchi I., Nomiyama K., Hosokawa K., Sakurada K., Nakagata N., et al. (2004). Regulation of oxidative stress by ATM is required for self-renewal of haematopoietic stem cells. Nature 431,997-1002.

Janzen, V., Forkert, R., Fleming, H.E., Saito, Y., Waring, M.T., Dombkowski, D.M., Cheng, T., DePinho, R.A., Sharpless, N.E., and Scadden, D.T. (2006). Stem-cell

ageing modified by the cyclin-dependent kinase inhibitor p16INK4a. Nature 443, 421-426.

Kastan, M.B., Radin, A.I., Kuerbitz, S.J., Onyekwere, O., Wolkow, C.A., Civin, C.I., Stone, K.D., Woo, T., Ravindranath, Y., and Craig, R.W. (1991). Levels of p53 protein increase with maturation in human hematopoietic cells. Cancer Res. 51, 4279-4286.

Kollman, C., Howe, C.W., Anasetti, C., Antin, J.H., Davies, S.M., Filipovich, A.H., Hegland, J., Kamani, N., Kernan, N.A., King, R., et al. (2001). Donor characteristics as risk factors in recipients after transplantation of bone marrow from unrelated donors: the effect of donor age. Blood 98, 2043-2051.

Kim, M., Moon, H.B., and Spangrude, G.J. (2003). Major age-related changes of mouse hematopoietic stem/progenitor cells. Ann N Y Acad Sci. 996, 195-208.

Kondo, M., Weissman, I.L., and Akashi, K. (1997). Identification of clonogenic common lymphoid progenitors in mouse bone marrow. Cell 91, 661–672.

Kuerbitz, S.J., Plunkett, B.S., Walsh, W.V., and Kastan, M.B. (1992). Wild-type p53 is a cell cycle checkpoint determinant following irradiation. Proc Natl Acad Sci U S A. 89, 7491-7495.

Lacroix, M., Caramel, J., Goguet-Rubio, P., Linares, L.K., Estrach, S., Hatchi, E., Rodier, G., Lledo, G., de Bettignies, C., Thépot, A., et al. (2010). Transcription factor E4F1 is essential for epidermal stem cell maintenance and skin homeostasis. Proc Natl Acad Sci U S A. 107, 21076-21081.

Lee, H.W., Blasco, M.A., Gottlieb, G.J., Horner, J.W., Greider, C.W., and DePinho, R.A. (1998). Essential role of mouse telomerase in highly proliferative organs. Nature 392, 569-574.

Liao, J., Humphrey, S.E., Poston, S., and Taparowsky, E.J. (2011). Batf promotes growth arrest and terminal differentiation of mouse myeloid leukemia cells. Mol Cancer Res. 9, 350-363.

Lieber M.R., Karanjawala Z.E. (2004). Ageing, repetitive genomes and DNA damage. Nat Rev Mol Cell Bio 5,69-75.

Linton, P.J., and Dorshkind, K. (2004). Age-related changes in lymphocyte development and function. Nat Immunol. 5, 133-139.

Liu J., Cao L., Chen J., Song S., Lee I.H., Quijano C., Liu H., Keyvanfar K., Chen H., Cao L.Y., et al. (2009). Bmi1 regulates mitochondrial function and the DNA damage response pathway. Nature 459,387-392.

Liu, Y., Johnson, S.M., Fedoriw, Y., Rogers, A.B., Yuan, H., Krishnamurthy, J., and Sharpless, N.E. (2011). Expression of p16INK4a prevents cancer and promotes aging in lymphocytes. Blood 117, 3257-3267.

Mackall C.L., Gress R.E. (1997). Thymic aging and T-cell regeneration. Immunol

Rev 160,91-102.

Majeti R., Park C.Y., Weissman I.L. (2007). Identification of a hierarchy of multipotent hematopoietic progenitors in human cord blood. Cell Stem Cell 1,635-645.

Min H., Montecino-Rodriguez E., Dorshkind K. (2006). Effects of aging on the common lymphoid progenitor to pro-B cell transition. J Immunol 176,1007-12.

Mitchell W.A., Lang P.O., Aspinall R. (2010). Tracing thymic output in older individuals. Clin Exp Immunol 161,497-503.

Mohrin, M., Bourke, E., Alexander, D., Warr, M.R., Barry-Holson, K., Le Beau, M.M., Morrison, C.G., and Passegué, E. (2010). Hematopoietic stem cell quiescence promotes error-prone DNA repair and mutagenesis. Cell Stem Cell 7, 174-185.

Molofsky, A.V., Slutsky, S.G., Joseph, N.M., He, S., Pardal, R., Krishnamurthy, J., Sharpless, N.E., and Morrison, S.J. (2006). Increasing p16INK4a expression decreases forebrain progenitors and neurogenesis during ageing. Nature 443, 448-452.

Morita, Y., Ema, H., and Nakauchi, H. (2010). Heterogeneity and hierarchy within the most primitive hematopoietic stem cell compartment. J Exp Med. 207, 1173-1182.

Morrison, S.J., Wandycz, A.M., Akashi, K., Globerson, A., and Weissman, I.L. (1996). The aging of hematopoietic stem cells. Nat Med. 2, 1011-1016.

Nalapareddy K., Jiang H., Guachalla Gutierrez L.M., Rudolph K.L. (2008). Determining the influence of telomere dysfunction and DNA damage on stem and progenitor cell aging: what markers can we use? Exp Gerontol 43,998-1004.

Nijnik A., Woodbine L., Marchetti C., Dawson S., Lambe T., Liu C., Rodrigues N.P., Crockford T.L., Cabuy E., Vindigni A. et al. (2007). DNA repair is limiting for haematopoietic stem cells during ageing. Nature 447,686-690.

Nishino, J., Kim, I., Chada, K., and Morrison, S.J. (2008). Hmga2 promotes neural stem cell self-renewal in young but not old mice by reducing p16Ink4a and p19Arf Expression. Cell 135, 227-239.

Ohyashiki, J.H., Ohyashiki, K., Fujimura, T., Kawakubo, K., Shimamoto, T., Iwabuchi, A., and Toyama, K. (1994). Telomere shortening associated with disease evolution patterns in myelodysplastic syndromes. Cancer Res. 54, 3557-3560.

Omatsu Y., Sugiyama T., Kohara H., Kondoh G., Fujii N., Kohno K., Nagasawa T. (2010). The essential functions of adipo-osteogenic progenitors as the hematopoietic stem and progenitor cell niche. Immunity 33,387-399.

Pelicci, P.G. (2004). Do tumor-suppressive mechanisms contribute to organism aging by inducing stem cell senescence? J Clin Invest. 113, 4-7.

Rando, TA. (2006). Stem cells, ageing and the quest for immortality. Nature 441, 1080-1086.

Roeder I., Horn K., Sieburg H.B., Cho R., Muller-Sieburg C., Loeffler M. (2008) Characterization and quantification of clonal heterogeneity among hematopoietic stem cells: a model-based approach. Blood 112,4874-4883.

Rose, M.R, and Graves, J.L. Jr. (1989). What evolutionary biology can do for gerontology. J Gerontol. 44, B27-29.

Rossi, D.J., Bryder, D., Zahn, J.M., Ahlenius, H., Sonu, R., Wagers, A.J., and Weissman, I.L. (2005). Cell intrinsic alterations underlie hematopoietic stem cell aging. Proc Natl Acad Sci U S A. 102, 9194-9199.

Rossi, D.J., Bryder, D., Seita, J., Nussenzweig, A., Hoeijmakers, J., and Weissman, I.L. (2007). Deficiencies in DNA damage repair limit the function of haematopoietic stem cells with age. Nature 447, 725-729.

Rossi, D.J., Jamieson, C.H., and Weissman, I.L. (2008). Stems cells and the pathways to aging and cancer. Cell 132, 681-696.

Rübe, C.E., Fricke, A., Widmann, T.A., Fürst, T., Madry, H., Pfreundschuh, M., and Rübe, C. (2011). Accumulation of DNA Damage in Hematopoietic Stem and Progenitor Cells during Human Aging. PLoS One 6, e17487.

Schaetzlein, S., Kodandaramireddy, N.R., Ju, Z., Lechel, A., Stepczynska, A., Lilli, D.R., Clark, A.B., Rudolph, C., Kuhnel, F., Wei, K., et al. (2007). Exonuclease-1 deletion impairs DNA damage signaling and prolongs lifespan of telomere-dysfunctional mice. Cell 130, 863-877.

Schambach, A., Galla, M., Modlich, U., Will, E., Chandra, S., Reeves, L., Colbert, M., Williams, D.A., von Kalle, C., and Baum, C. (2006). Lentiviral vectors pseudotyped with murine ecotropic envelope: increased biosafety and convenience in preclinical research. Exp Hematol. 34, 588-592.

Schambach, A., Wodrich, H., Hildinger, M., Bohne, J., Kräusslich, H.G., and Baum, C. (2000). Context dependence of different modules for posttranscriptional enhancement of gene expression from retroviral vectors. Mol Ther. 2, 435-445.

Schlenner, S.M., Madan, V., Busch, K., Tietz, A., Läufle, C., Costa, C., Blum, C., Fehling, H.J., and Rodewald, H.R. (2010). Fate mapping reveals separate origins of T cells and myeloid lineages in the thymus. Immunity 32, 426-436.

Schraml, B.U., Hildner, K., Ise, W., Lee, W.L., Smith, W.A., Solomon, B., Sahota, G., Sim, J., Mukasa, R., Cemerski, S., et al. (2009). The AP-1 transcription factor Batf controls T(H)17 differentiation. Nature 460, 405-409.

Senga, T., Iwamoto, T., Humphrey, S.E., Yokota, T., Taparowsky, E.J., and Hamaguchi, M. (2002). Stat3-dependent induction of BATF in M1 mouse myeloid leukemia cells. Oncogene 21, 8186-8191.

Sharpless, N.E., and Depinho, R.A. (2007). How stem cells age and why this makes us grow old. Nat Rev Mol Cell Biol. 8, 703-713.

Sieburg H.B., Cho R.H., Dykstra B., Uchida N., Eaves C.J., Muller-Sieburg C.E. (2006). The hematopoietic stem compartment consists of a limited number of discrete stem cell subsets. Blood 107,2311-2316.

Signer, R.A., Montecino-Rodriguez, E., Witte, O.N., and Dorshkind, K. (2008). Aging and cancer resistance in lymphoid progenitors are linked processes conferred by p16Ink4a and Arf. Genes Dev. 22, 3115-3120.

Silva, J.M., Li, M.Z., Chang, K., Ge, W., Golding, M.C., Rickles, R.J,. Siolas, D., Hu, G., Paddison, P.J., Schlabach, M.R., et al. (2005). Second-generation shRNA libraries covering the mouse and human genomes. Nat Genet. 37, 1281-1288.

Song Z., Ju Z., Rudolph K.L. (2009). Cell intrinsic and extrinsic mechanisms of stem cell aging depend on telomere status. Exp Gerontol 44,75-82.

Song Z., Wang J., Guachalla L.M., Terszowski G., Rodewald H.R., Ju Z., Rudolph K.L. (2010). Alterations of the systemic environment are the primary cause of impaired B and T lymphopoiesis in telomere-dysfunctional mice. Blood 115,1481-1489.

Sudo, K., Ema, H., Morita, Y., and Nakauchi, H. (2000). Age-associated characteristics of murine hematopoietic stem cells. J Exp Med. 192, 1273-1280.

Sullivan, D.M., Latham, M.D., and Ross, W.E. (1987). Proliferation-dependent topoisomerase II content as a determinant of antineoplastic drug action in human, mouse, and Chinese hamster ovary cells. Cancer Res. 47, 3973-3979.

Takai, H., Smogorzewska, A., and de Lange, T. (2003). DNA damage foci at dysfunctional telomeres. Curr Biol. 13, 1549-1556.

Takubo, K., Goda, N., Yamada, W., Iriuchishima, H., Ikeda, E., Kubota, Y., Shima, H., Johnson, R.S., Hirao, A., Suematsu, M., et al. (2010). Regulation of the HIF-1alpha level is essential for hematopoietic stem cells. Cell Stem Cell 7, 391-402.

Tefferi, A., and Vardiman, J.W. (2009). Myelodysplastic syndromes. N Engl J Med. 361, 1872-1885.

Tian, S.S., Lamb, P., Seidel, H.M., Stein, R.B., and Rosen, J. (1994). Rapid activation of the STAT3 transcription factor by granulocyte colony-stimulating factor. Blood 84, 1760-1764.

Topley, G.I., Okuyama, R., Gonzales, J.G., Conti, C., and Dotto, G.P. (1999). p21(WAF1/Cip1) functions as a suppressor of malignant skin tumor formation and a determinant of keratinocyte stem-cell potential. Proc Natl Acad Sci U S A. 96, 9089-9094.

Urbánek, P., Wang, Z.Q., Fetka, I., Wagner, E.F., and Busslinger, M. (1994). Complete block of early B cell differentiation and altered patterning of the posterior

midbrain in mice lacking Pax5/BSAP. Cell 79, 901-912.

Van der Put E., Sherwood E.M., Blomberg B.B., Riley R.L. (2003). Aged mice exhibit distinct B cell precursor phenotypes differing in activation, proliferation and apoptosis. Exp Gerontol 38,1137-1147.

Warren L.A., Rossi D.J. (2009). Stem cells and aging in the hematopoietic system. Mech Ageing Dev 130,46-53.

Weiskopf, D., Weinberger, B., and Grubeck-Loebenstein, B. (2009). The aging of the immune system. Transpl Int. 22, 1041-1050.

Wilson, A., Laurenti, E., Oser, G., van der Wath, R.C, Blanco-Bose, W., Jaworski, M., Offner, S., Dunant, C.F., Eshkind, L., Bockamp, E., et al. (2008). Hematopoietic stem cells reversibly switch from dormancy to self-renewal during homeostasis and repair. Cell 135, 1118-1129.

Wright, W.E., and Shay, J.W. (1992). Telomere positional effects and the regulation of cellular senescence. Trends Genet. 8, 193-197.

Zender, L., Xue, W., Zuber, J., Semighini, C.P., Krasnitz, A., Ma, B., Zender, P., Kubicka, S., Luk, J.M., Schirmacher, P., et al. (2008). An oncogenomics-based in vivo RNAi screen identifies tumor suppressors in liver cancer. Cell 135, 852-864.

Zhong, Z., Wen, Z., and Darnell, J.E. Jr. (1994). Stat3: a STAT family member activated by tyrosine phosphorylation in response to epidermal growth factor and interleukin-6. Science 264, 95-98.

Zou Y., Sfeir A., Gryaznov S.M., Shay J.W., Wright W.E. (2004). Does a sentinel or a subset of short telomeres determine replicative senescence? Mol Biol Cell 15,3709-3718.

For reasons of privacy the CV in the electronic version has been removed.